

The Dynamic Impact of Ancillary Service Provision on Wind Turbine Operation, Loading and Wake

Narender Singh

Doctoral dissertation submitted to obtain the academic degree of
Doctor of Electromechanical Engineering

Supervisors

Prof. Lieven Vandevelde, PhD - Prof. Jeroen De Koning, PhD
Department of Electromechanical, Systems and Metal Engineering
Faculty of Engineering and Architecture, Ghent University

December 2023



**The Dynamic Impact of Ancillary Service Provision on Wind Turbine
Operation, Loading and Wake**

Narender Singh

Doctoral dissertation submitted to obtain the academic degree of
Doctor of Electromechanical Engineering

Supervisors

Prof. Lieven Vandevelde, PhD - Prof. Jeroen De Koning, PhD
Department of Electromechanical, Systems and Metal Engineering
Faculty of Engineering and Architecture, Ghent University

December 2023



ISBN 978-94-6355-778-8

NUR 959, 961

Wettelijk depot: D/2023/10.500/110

Members of the Examination Board

Chair

Prof. Sabine Wittevrongel, PhD, Ghent University

Other members entitled to vote

Prof. Bashir Bakhshideh Zad, PhD, Université de Mons

Prof. Frederik De Belie, PhD, Ghent University

Prof. Wim De Waele, PhD, Ghent University

Hossein Hooshyar, PhD, New York Power Authority, USA

Prof. Kurt Stockman, PhD, Ghent University

Supervisors

Prof. Lieven Vandeveldel, PhD, Ghent University

Prof. Jeroen De Kooning, PhD, Ghent University

Acknowledgements

I extend my heartfelt gratitude to every individual who has generously shared their expertise, offered guidance, or provided unwavering encouragement during the course of my doctoral studies. Whether through insightful discussions, constructive feedback, or simply being a source of motivation, your contributions have been crucial in providing me with direction and motivation when needed.

Firstly, I would like to thank my promoters, prof. Lieven Vandeveldel and prof. Jeroen De Kooning. Thank you, Lieven, for giving me the opportunity to work on BEOBIND and be a part of the energy transition initiative. Your solid knowledge of the fundamentals has often offered me a simple and robust solution to my problems. Jeroen, you have polished my work with your guidance. I have learnt a lot from you. I don't know what a better supervision would look like, this worked perfectly for me.

I had the pleasure of sharing the office with many different colleagues. I want to thank all these current and former colleagues- Anne, Anna, Arash, Daan, Francisco, Iman, Jens, Joannes, Kaveh, Milad, Mitko, Nezhmin, Nienke, Saleh, Samie, Sajid, Sara, Siavash, Siebe and Yentl.

I want to thank the administrative and technical personnel Ingrid, Nic, Tony and Vincent. I appreciate your assistance. Marilyn thank you for helping out since I joined EELAB up until getting the thesis printed.

I am fortunate to have ended up in the beautiful city of Ghent. The people I have met here and the friendships that I have built during this time will last a lifetime.

The acknowledgements will not be complete without mentioning my family members- Seema, Mohinder, Anuradha, Jyoti, Karan, Rashi, Aaru and Navya. Sanne, thank you for standing by me and sharing these moments with me. You took care of everything these past months while I was busy with work.

Reflecting on this incredible journey, it's evident that the path to earning a PhD isn't a smooth sail. It requires the ability to deal with uncertainties and setbacks. The unusual circumstances that COVID brought, did not

make it easier. However, this pursuit of a Doctor of Philosophy has been a profound learning experience, the lessons learned during these years are invaluable.

Narender Singh
Ghent, November 2023

Table of Contents

Acknowledgements	i
Table of contents	vi
List of figures	ix
List of tables	xi
Samenvatting	xiii
Summary	xvii
Abbreviations	xxi
1 Wind Energy: A Comprehensive Overview	1
1.1 Introduction	2
1.2 Wind energy growth and evolution	5
1.2.1 Wind energy today	5
1.3 Ancillary services: an overview	9
1.3.1 Frequency measure	9
1.3.1.1 Frequency containment reserve	13
1.3.1.2 Fast frequency reserve	14
1.3.2 Voltage control and reactive power management	15
1.3.3 Operational management and reconstruction of supply	16
1.4 Wind energy's role in ancillary services	16
1.5 Objectives	18
1.6 Thesis outline	20
References	23

2	Wind turbine capability to provide ancillary services	27
2.1	Introduction	29
2.2	Models	31
2.2.1	Wind turbine	33
2.2.2	Generator	38
2.3	Control	38
2.3.1	Torque control	39
2.3.2	Pitch control	41
2.4	Tests	41
2.5	Conclusion	43
	References	49
3	Dynamic Wake Analysis of a Wind Turbine Providing Frequency Support Services	55
3.1	Introduction	57
3.2	Model description	58
3.2.1	Wake model	58
3.3	Ancillary services	58
3.4	Data	59
3.4.1	Frequency data	59
3.4.2	Wind field	60
3.4.2.1	Constant wind field	61
3.4.2.2	Turbulent wind field	61
3.5	Control	61
3.5.1	FCR control	61
3.5.2	FFR control	62
3.6	Results and discussion	63
3.6.1	Case I: FCR provision with oscillating grid frequency	65
3.6.2	Case II: FCR provision with realistic grid frequency	66
3.6.3	Case III: FCR provision in turbulent wind	69
3.6.4	Case IV: FFR provision of Types A, B and C	71
3.7	Conclusion	73
	References	78
4	Wind Turbine Main Bearing Lifetime	81
4.1	Introduction	83
4.2	Models and data	84
4.2.1	Main bearing	85
4.2.2	Torque control	86
4.2.3	Wind field design and data processing	86

4.3	Methodology	87
4.3.1	Dynamic equivalent force	88
4.3.2	Lifetime	89
4.4	Results and discussion	90
4.5	Conclusion	93
	References	96
5	Prediction-based Wind Turbine Operation for Active Participation in the Day-Ahead and Reserve Markets	99
5.1	Introduction	101
5.2	Model	101
5.3	Wind profile design and prediction	102
5.4	Control and operation strategy	102
5.4.1	Control system	102
5.4.2	Operation strategy	104
5.4.2.1	Operation strategy 1	105
5.4.2.2	Operation strategy 2	105
5.4.2.3	Operation strategy 3	105
5.5	Results	107
5.5.1	Illustrative example	107
5.5.2	Out-of-sample analysis	108
5.6	Conclusion	109
	References	110
6	Wind Turbine Load Aware Operation	113
6.1	Introduction	115
6.2	Models and data	116
6.3	Methodology	116
6.3.1	Load calculation	118
6.3.1.1	Bearing load	118
6.3.1.2	Blade load	119
6.3.1.3	Shaft load	120
6.3.1.4	Tower load	120
6.3.1.5	Equivalent load metric	121
6.3.2	Optimisation	121
6.3.3	Revenue calculation	123
6.4	Results and discussion	124
6.5	Conclusion	129
	References	132

- 7 Conclusions & future work** **135**
- 7.1 Conclusions 136
- 7.2 Future work 138
 - 7.2.1 Wind turbine ageing 138
 - 7.2.2 Wind farm load informed reserve dispatch 140
- References 141

- Author bibliography** **143**
- 143

List of Figures

1.1	World primary energy consumption by source 1965-2022 [3]	2
1.2	World CO ₂ emissions [4]	3
1.3	Change in global surface temperature rise [5]	4
1.4	Timeline of wind energy evolution	6
1.5	Total installed wind capacity 2000-2022	7
1.6	Expected new wind energy installations 2020-2030 [14]	8
1.7	Share of electricity production from wind [3]	9
1.8	Wind energy investment in Europe 2013-2022 [15]	10
1.9	Expected LCOE changes in the median scenario in percentage terms relative to 2019 baseline values [16]	11
1.10	Power system frequency response [17]	13
1.11	ENSTSO-E defined balancing services [18]	13
1.12	Frequency-Power relationship as per 200 mHz symmetrical service	14
1.13	FFR framework	15
1.14	Thesis outline	18
2.1	Type 4 wind turbine [33]	31
2.2	FAST modules block diagram [37]	32
2.3	Simulink environment	33
2.4	NREL 5 MW wind turbine monopile structure [41]	36
2.5	Power curve of a 5 MW wind turbine	37
2.6	C _p -TSR curve of 5 MW wind turbine	37
2.7	Power coefficient of simulated cases	38
2.8	Reference axis in PMSG	39
2.9	Equivalent scheme of a PMSG in the rotating reference frame	39
2.10	Field oriented control of the PMSG	40
2.11	Pitch control of the wind turbine blades	41
2.12	Turbulence intensity level for type A, B, C wind	45
2.13	Output power plots for different turbulence test	46
2.14	Overlaid output power plots for different turbulence test	47

2.15	Probability density function and normal distribution plots for wind type A, B, C and steady wind	48
3.1	Wake schematic	59
3.2	Frequency with sinusoidal ripples	60
3.3	Frequency data extreme event	60
3.4	u-component of wind speed (m/s)	62
3.5	v-component of wind speed (m/s)	63
3.6	w-component of wind speed (m/s)	64
3.7	Generator PLC and FCR power	64
3.8	Wind speed at different points behind the rotor for 7 m/s simulations	67
3.9	Wind speed at different points behind the rotor for 12 m/s simulations	67
3.10	Magnitude of wake oscillations with period varying grid frequency for 7 m/s simulations	68
3.11	Magnitude of wake oscillations with period varying grid frequency for 12 m/s simulations	68
3.12	Grid frequency and influenced outputs with changing control action for a wind speed of 7 m/s	69
3.13	Grid frequency and influenced outputs with changing control action for a wind speed of 12 m/s	70
3.14	Case III: FCR provision in turbulent wind	71
3.15	FFR power output and frequency	73
3.16	FFR Type A service	74
3.17	FFR Type B service	74
3.18	FFR Type C service	75
3.19	Wind speed behind the rotor at 3 different points	75
3.20	Wind speed at different heights behind the rotor	76
4.1	Main bearing position	85
4.2	Control design for 20% FCR	87
4.3	Control design for 40% FCR	87
4.4	Wind speed percentage occurrences	88
4.5	Power reference for No FCR and 20% deloaded cases	91
4.6	Power reference for 20% FCR and 40% FCR cases	92
4.7	Dynamic forces acting on the wind turbine main bearing	94
4.8	Bearing life versus β for different basic dynamic load rating values	95

5.1	Train and test datasets for ANFIS model (60-min).	103
5.2	Controller performance	104
5.3	Operation strategies	106
5.4	Power outputs and reserve margin	108
6.1	Wind profile used for the simulations	116
6.2	Methodology	117
6.3	Forces acting on the wind turbine	119
6.4	Forces acting of different wind turbine components	125
6.5	Reserve market bid versus Loading	126
6.6	Variation in $R_{m_{bid}}$ with respect to α	130
6.7	Variation in R with respect to α	130
7.1	Power curve of a 5 MW wind turbine with years	139
7.2	Reserve market bid versus Loading	139

List of Tables

1.1	Type of FFR services	16
2.1	Wind turbine properties	34
2.2	Blade structural Properties	35
2.3	Nacelle and Hub Properties	35
2.4	Tower properties	36
2.5	Generator properties	39
2.6	Time series test for service type 200 mHz	44
4.1	Bearing life in years	93
5.1	Revenue (€)	109
6.1	Normalised loading associated with the changing $R_{m_{bid}}$ [MW]	127
6.2	Revenues as a function of α	129

Samenvatting

Over de hele wereld ondergaan energiesystemen veranderingen die ongekend zijn in de geschiedenis van het elektriciteitsnet. Het energiesysteem heeft vanaf het begin sterk gesteund op conventionele energiebronnen zoals steenkool en olie. De reden hiervoor is de beschikbaarheid en eenvoud van deze bronnen. De groeiende vraag naar elektriciteit en de uitputting van fossiele brandstoffen heeft de behoefte aan alternatieven aangewakkerd. De negatieve milieu-impact van het gebruik van deze bronnen is duidelijk zichtbaar. De dominantie van fossiele brandstoffen in de energiesector heeft geleid tot onvoorziene schade aan het klimaat. Dergelijke brandstoffen zijn de belangrijkste oorzaak van de opwarming van de aarde. Het gebruik ervan leidt tot de uitstoot van enorme hoeveelheden schadelijke broeikasgassen, zoals koolstofdioxide (CO₂). Deze broeikasgassen zijn verantwoordelijk voor het vasthouden van een grote hoeveelheid warmte in de atmosfeer van de aarde, wat leidt tot rampzalige gevolgen zoals droogte, veranderende neerslagpatronen en stijgende temperaturen.

Gezien het feit dat het voortgezette gebruik van conventionele energiebronnen kan leiden tot onherstelbare schade aan het milieu, evolueert de wereld richting een energietransitie. Energie transitie verwijst naar de verschuiving van conventionele vervuilende energiebronnen naar schone en duurzamere alternatieven. Het doel is om klimaatverandering te bestrijden door de uitstoot van broeikasgassen te verminderen en milieuschade te beperken of mogelijk te verminderen. Een onvervangbaar instrument voor deze overgang is een grotere afhankelijkheid van hernieuwbare energie. Hernieuwbare energiebronnen hebben het potentieel om het energiesysteem te transformeren en duurzamer te maken. Enkele van de belangrijkste hernieuwbare energiebronnen zijn wind, zon, waterkracht, getijdenenergie, geothermie en biomassa. De energie die uit dergelijke bronnen wordt gegenereerd, wordt onttrokken aan natuurlijke processen die minder of geen impact hebben op het milieu. Het genereren van energie uit hernieuwbare bronnen stoot geen broeikasgassen uit en vervuult de atmosfeer niet zoals fossiele brandstoffen dat doen. De talloze voordelen van hernieuw-

bare energie omvatten een verbeterde gezondheid door minder luchtvervuiling, een schoon en duurzaam energiesysteem, energiezekerheid, enz. Deze voordelen hebben geleid tot een prominente rol voor hernieuwbare energie in de afgelopen decennia. Met elk jaar neemt het aandeel van hernieuwbare energie in de energiemix toe, wat leidt tot een pad naar een duurzamer energiesysteem.

Van alle hernieuwbare energiebronnen is windenergie één van de meest veelbelovende. Windenergie werkt volgens het principe van het omzetten van de kinetische energie in de wind tot bruikbare elektrische energie. Zodra windturbines in gebruik zijn genomen, produceren zij geen broeikasgassen, waardoor ze een ideale en betrouwbare alternatieve energiebron zijn voor de energietransitie. De overvloedige en onuitputtelijke aard ervan maakt het een geschikte vorm van energieopwekking over de hele wereld. Ten gevolge van de technologische ontwikkelingen van de voorbije decennia is windenergie toegankelijker geworden en wordt ze nu gebruikt uitbreide energiesystemen, maar ook in afgelegen eiland-netwerken. Ondanks al haar voordelen komt de naadloze integratie van windenergie in het energiesysteem niet zonder uitdagingen.

De wind is voortdurend in beweging, waardoor windenergie van nature intermitterend is. De productie van energie uit wind is niet constant en er zijn schommelingen aanwezig, afhankelijk van de geografische locatie, luchtdruk, enz. De intermitterende aard van windenergie vormt een uitdaging voor de transmissienetbeheerder of Transmission System Operator (TSO), aangezien de exacte energieproductie onvoorspelbaar is. De vooruitgang in technologie, zoals energie-opslagsystemen, is te hulp gekomen en biedt betrouwbaarheid aan windenergiesystemen (WES). Het nauwkeurig voorspellen van de wind is cruciaal voor de betrouwbaarheid van windenergie. Methoden voor windvoorspelling zijn voortdurend in ontwikkeling. Big data-analyse en op kunstmatige intelligentie (AI) gebaseerde modellen zijn nu in staat om de windsnelheid op een korte termijn met een hoge nauwkeurigheid te voorspellen.

Deze ontwikkelingen op het gebied van windenergie hebben windenergieproducenten (Wind Power Producers of WPP's) in staat gesteld actief deel te nemen aan netondersteunende diensten zoals primaire reserve. Actieve primaire-reservediensten zoals 'Frequency Containment Reserve' (FCR) en 'Fast Frequency Reserve' (FFR) kunnen aanzienlijk profiteren van de deelname van windparken. In feite is in energiesystemen met een hoog percentage windenergie, de levering van primaire reserve een noodzaak. Er is echter beperkt onderzoek gedaan naar het effect van primaire

reservevoorziening door windturbines op de toestand, de omgeving en de opbrengst van WPP's. Deze thesis behandelt deze kwesties.

De primaire reserve FCR, vereist een snelle aanpassing van het vermogen op basis van de veranderingen in de netfrequentie. Dit is een uitdagende taak, aangezien de vereiste reactietijd binnen enkele seconden ligt. Daarom is de eerste taak voor het onderzoekswerk in deze thesis de ontwikkeling van een efficiënt controlesysteem. Om de effectiviteit van de besturing te valideren, wordt deze vervolgens gevalideerd met behulp van de pre-kwalificatietest vastgelegd door de Belgische TSO Elia.

Zogeeffekten zijn een bekend fenomeen in windparken. Een windturbine die zich bevindt in het zog van een operationele windturbine ervaart een lagere, verstoorde windsnelheid, wat leidt tot een afname van de energieproductie van de eerstgenoemde. Daarom worden windparken ontworpen met minimale interferentie. Veel landen, zoals België, hebben echter windparken met een hoge capaciteitsdichtheid, waardoor het zogeffect blijft bestaan. Bovendien is het effect van het leveren van FCR op het zog achter een windturbine niet bestudeerd. Om deze reden heeft dit onderzoek tot doel dergelijke zogeffecten te bestuderen. Het dynamische gedrag van het zog wordt bestudeerd voor een reeks scenario's met variërende netfrequentie en windprofielen.

Vanwege de besturingsactie in verband met de levering van FCR wordt verwacht dat er variaties optreden in de belastingen op verschillende delen van de windturbine. De belangrijkste belastingen op windturbinecomponenten zoals het hoofdlager, bladen, as en toren worden bestudeerd. Deze belastingen worden vervolgens gecombineerd met behulp van een methodologie om de algehele belasting op een windturbine te kwantificeren. De belastingresultaten worden gebruikt in een optimalisatie-algoritme om optimale reserve- en energiemarktbiedingen te genereren, zodat er een evenwicht wordt gecreëerd tussen de belasting van de windturbine en de omzet van de WPP.

Een ander aspect dat in deze thesis wordt gepresenteerd, is een optimale besturingsstrategie van windturbines. Een optimale strategie wordt ontwikkeld die ervoor zorgt dat het vermogen wordt gereguleerd om te voldoen aan de gecontracteerde biedingen voor energie- en reserve-markten, rekening houdend met de werkelijke variaties in de wind.

Kernwoorden: *Netondersteunende diensten, Primaire reserve, Snelle frequentierespons, Frequentie regeling, Zogeffect, Windenergie, Levensduuranalyse van windturbinecomponenten, Belasting van windturbines*

Summary

Power systems around the world are witnessing changes that are unprecedented in the history of the electricity grid. The power system from the very beginning has heavily relied upon conventional energy sources such as coal and oil. The reason being the abundance and acceptable efficiency of these sources. The growing demand of electricity and constantly depleting dispatchable sources of energy kindled the need for alternatives. The negative environmental impact of the usage of these sources is evident. The dominance of fossil fuels in the energy industry led to unforeseen detriment to the climate. Such fuels are the main driver of global warming. Their usage release vast amount of harmful greenhouse gases (GHG) such as carbon dioxide (CO₂). These GHG are responsible for trapping a great amount of heat in the earth's atmosphere leading to disastrous outcomes, droughts, changed rainfall patterns and higher temperatures, to name a few.

Considering the fact that the continued usage of conventional energy sources can result in an irreparable damage to the environment, the world is moving towards an energy transition. Energy transition refers to the shift from conventional polluting energy sources to clean and more sustainable alternatives. The aim is to combat the climate change by reducing GHG and confine or possibly reduce the environmental damage. An irreplaceable tool for this transition is more reliance on renewable energy. Renewable energy sources have the potential to transform the energy system by making it more sustainable. Some of the prime renewable energy sources are wind, solar, hydro, tidal, geothermal and biomass. The energy generated from such sources are tapped from natural processes that have lesser or no impact on the environment. Generating energy from renewable sources does not emit GHG and pollute the atmosphere like fossil fuels. The numerous benefits of renewable energy include improved health due to less air pollution, clean and sustainable energy system, energy security, etc. These advantages have led to a prominence of renewable energy in the past decades. With each passing year the share of renewable energy in the energy mix is increasing, leading a pathway to a more sustainable power system.

Amongst the renewable energy sources, wind energy has the promise of providing an efficient mode of clean energy. Wind energy works on the principle of converting kinetic energy available in the wind to usable electrical energy. At the power production stage, modern wind turbines do not produce any GHG, making them an ideal and reliable alternative for the energy transition. Its abundant and inexhaustible nature makes it a suitable form of energy generation across the world. As a result, with time and improved technologies, wind energy has become more accessible and is now used in international grids as well as small ill-connected island networks. Despite all its benefits, the seamless inclusion of wind energy into the power system does not come without challenges.

Wind is constantly varying, making wind energy intermittent in nature. The production of energy from wind is not constant and fluctuations are seen depending on the geographical location, air pressure, etc. The intermittent nature of wind energy poses challenges for the Transmission System Operator (TSO), as the exact energy production is unpredictable. The advances in technology such as energy storage systems have come to aid, providing reliability to wind energy systems (WES). The accurate forecasting of wind is crucial for the reliability of wind energy. Wind forecasting methods are continuously evolving. Big data analysis and artificial intelligence (AI) based models are now able to predict the short term wind forecast with a high accuracy.

These developments in the area of wind energy have equipped wind power producers (WPPs) to actively participate in ancillary services such as primary reserve. Active primary reserve services such as frequency containment reserve (FCR) and fast frequency reserve (FFR) can greatly benefit from the participation of wind farms. In fact, in the power systems with high penetration of wind energy, such provision of primary reserve is a necessity. However, there has been limited research in the area of the effect of primary reserve provision by wind turbines on the health, surroundings and WPP's revenue. This dissertation addresses these issues.

The primary reserve service, FCR requires a fast adjustment in the power output based on the changes in the grid frequency. This is a challenging task as the required response time is within seconds. Therefore, for the research work presented in this dissertation the first task is to develop a fast acting control system. To validate the effectiveness of the control, it is then validated using the pre-qualification established by the Belgian TSO Elia.

Wake effects are a well known phenomenon in wind farms. A wind

turbine located in the wake trail of an operational wind turbine experiences a lower, disturbed wind speed causing a decrease in the former's energy production. Due to this, wind farms are designed such that the interference is minimal. However, many countries such as Belgium have wind farms that have a high capacity density, prevailing the effect of wake. Moreover, the effect of providing FCR on the wake trail behind a wind turbine is not studied. For this purpose, this research aims to study such wake behaviours. The dynamic behaviour of wake is studied for a range of scenarios with varying grid frequency and wind profiles.

Due to the control action related to the provision of FCR, a variation in the loads on different parts of the wind turbine is expected. The major loads on wind turbine components such as main bearing, blades, shaft and tower are studied. These loads are then combined using a methodology to quantify the overall load on a wind turbine. The loading results are used in an optimisation algorithm to generate optimal reserve and energy market bids such that a balance between wind turbine loading and the WPP's revenue is created.

Another aspect presented in this dissertation is related to optimal control strategies of wind turbines. For this objective optimal strategies for WPPs are developed that ensure the power output regulation to meet the energy and reserve market contracted bids while considering the real-time wind variations.

Keywords: *Ancillary services, Primary reserve, Fast frequency reserve, Frequency containment reserve, Wake effect, Wind energy, Wind turbine component lifetime analysis, Wind turbine loading*

Abbreviations

A

AC	Alternating current
AEP	Annual energy production
aFRR	automatic Frequency Restoration Reserve
AGC	Automatic generation control
AI	Artificial intelligence
ANFIS	Adaptive Neuro-Fuzzy Inference System

B

BEM	Blade element momentum
BRP	Balancing responsible party
BSP	Balancing service provider

C

CIPU	Contract for the Injection of Production Units
CO ₂	Carbon dioxide

D

DER	Distributed energy resources
DFIG	Doubly fed induction generator
DSO	Distribution system operator
DTC	Direct torque control

E

EFS	Enhanced frequency response
EIS	Energy imbalance settlement
ENTSO-E	European association for the cooperation of TSOs for electricity
EU	European Union

F

FAT	Full activation time
FCR	Frequency containment reserve
FFR	Fast frequency reserve
FOC	Field oriented control
FPEAPR	Fast post-fault active power recovery
FSP	Flexibility service provider

G

GHG	Greenhouse gas
GW	Giga Watt
GWEC	Global Wind Energy Council
GSC	Gird-side converter

I

IEA	International energy agency
IPCC	Intergovernmental Panel on Climate Change

J

JERM Joint day-ahead energy and reserve market

L

LCOE Levelized cost of energy

LRC Long-range consumer

M

mFRR manual Frequency Restoration Reserve

MILP Mixed-integer linear programming

MPC Model predictive control

MPPT Maximum power point tracking

MSC Machine-side converter

N

NAPCC National Action Plan on Climate Change

NCTF National Climate Task Force

NDC Nationally Determined Contribution

NREL National Renewable Energy Laboratory

O

OC3 Offshore Code Comparison Collaboration

P

PLC	Power limiting control
PI	Proportional Integral
PMSG	Permanent magnet synchronous generator
PWM	Pulse width modulated

R

RES	Renewable energy sources
RMS	Root mean square
RoCoF	Rate of change of frequency
RPM	Rotations per minute
RR	Replacement reserve

S

SIR	Synchronous inertial response
SMC	Sliding model control

T

TIL	Turbulence intensity level
TSO	Transmission system operator
TSR	Tip speed ratio

U

UC	Unit commitment
US	United States

W

WES	Wind energy systems
-----	---------------------

Y

YoY	Year-on-year
-----	--------------

1

Wind Energy: A Comprehensive Overview

This chapter provides a background, literature review, objectives and the thesis outline of the research presented in this dissertation. Section 1.1 presents an overview of the environmental scenario and the role of renewable energy. Section 1.2 gives an outlook on the growth and evolution of wind energy from its first use to the present day. In Section 1.3, an overview of main ancillary services is given. The role of wind energy in ancillary services provision is explained Section 1.4. Section 1.5 allows the readers to understand the objectives of this dissertation. In Section 1.6 the outline of the dissertation is given.

1.1 Introduction

The global energy landscape is undergoing an extensive transformation. The key reasons for the transformation being the negative environmental impact and exhaustive nature of the conventional energy sources. As a result, the "alternative fuels" which are renewable in nature have gained a recognition as the major contributors to the energy mix and are poised to become the majority mode of energy production in the future [1]. Although, to the day, fossil fuels remain the cornerstone of our energy systems, a fast paced change in the emergence of renewable energy resources has been witnessed in the past decade. Figure 1.1 shows the world primary energy consumption by source from 1965-2022 [2]. Fossil fuels have dominated the energy mix, and continue to do so till date. However, coal and oil, that as combined energy resources formed almost 80 % of the energy mix in 1965 are reduced to 58.3 % in 2022. This is partly due the prominence of renewable energy. In 2022 solar and wind energy combined account for more than 5 % of the world's energy consumption. Wind energy which had a negligible percentage share in the power mix up until the early 2000's, is now emerging as one of the fastest growing mode of energy generation.

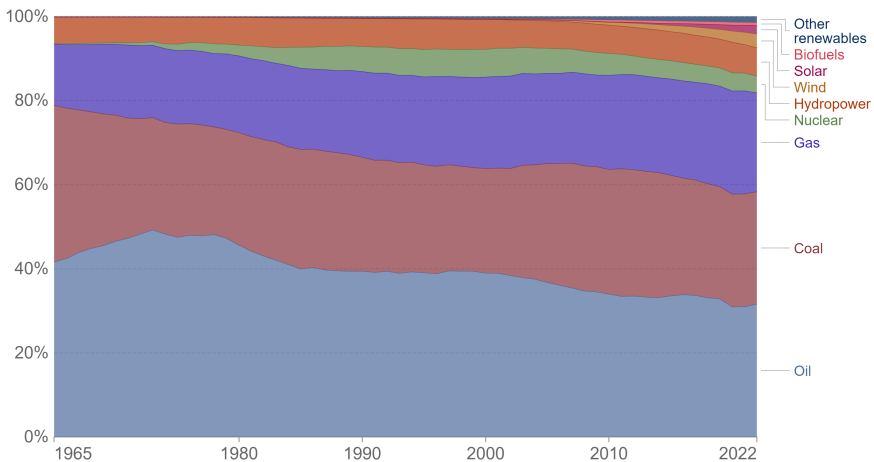


Figure 1.1: World primary energy consumption by source 1965-2022 [3]

This significant shift is lead by the cognizance of enormous increase in greenhouse gases emission post industrialisation. Figure 1.2 shows the increase in CO₂ emissions over the years [4]. The global emission of carbon dioxide from fossil fuels has reached a record 37.5 billion tonnes in 2022. If the trend continues, the global temperature is expected to rise by 1.5° above pre-industrial temperatures within nine years. The use of coal

as an energy source is the major contributor of CO₂ emissions. In 2021 coal accounted for over 40 % of the overall growth in CO₂, with an all time high of 15.3 billion tonnes emission [5]. The Intergovernmental Panel on Climate Change (IPCC) has reported an increase in surface temperature of 1.1° above 1850-1900 in 2011-2020. The observed warming is caused by human activities. The warming is dominated by greenhouse gases such as CO₂ and methane [6]. Figure 1.3 presents the change in global surface temperature 1850-2020. The increasing trend of global temperature can be clearly observed.

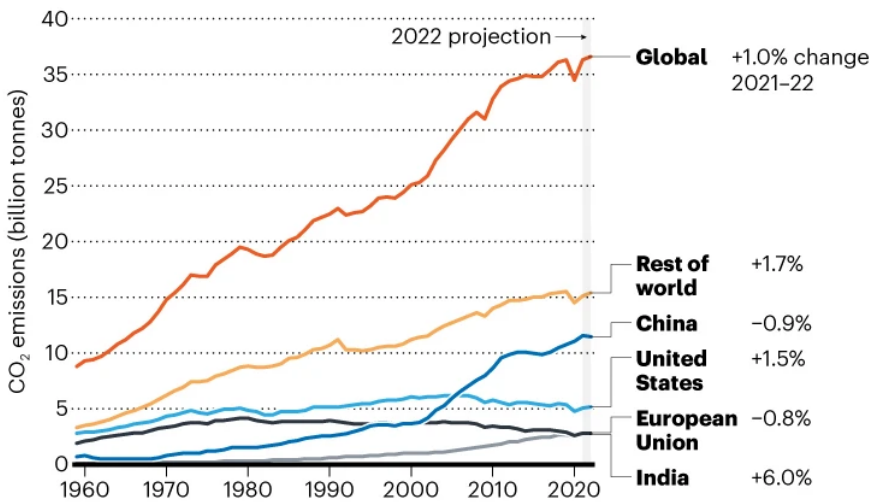


Figure 1.2: World CO₂ emissions [4]

With the clear evidence of global warming from research and data studies, many countries in the world are actively implementing plans to ensure the curtailment of the rising global temperatures. The European green deal has set an ambitious roadmap to introduce 40 % new renewable energy and to reduce the emissions by at least 55 % below 1990 level by 2030, and become climate neutral by 2050 [7]. As per the Nationally Determined Contributions (NDCs) under the Paris agreement, countries have self defined national climate pledges detailing their action plans to contribute in meeting the global goal to pursue the temperature rise below 1.5 ° [8]. India's National Action Plan on Climate Change (NAPCC) has extensive guidelines for sustainable energy production, enhanced energy efficiency and strategic steps for climate change prevention [9]. In the United States (U.S.), the National Climate Task Force (NCTF) is formed with the goal of reducing

U.S. greenhouse gas emissions 50-52 % below 2005 levels by 2030, 100 % carbon-pollution free electricity by 2035 and achieving net-zero emissions by 2050 [10].

The fundamental idea at the core of each of these plans is to increase the share of renewable energy sources. Renewable energy resources have the inherent ability to generate power without depleting the finite fossil resources or releasing harmful greenhouse gases. These energy sources, including wind, solar, hydro power, geothermal, tidal energy, etc. are vital for establishing a sustainable power system. Among these sources, wind energy stands out as one of the most promising option for sustainable energy development. Wind energy, harnessed from the kinetic energy present in the wind is one of the most efficient methods to harness renewable energy. Although GHG are emitted during the production of wind turbine components, the transport and the installations, the numbers are much lower compared to the conventional power production methods. The carbon footprint of coal and natural gas are 90 and 40 times more than that of wind energy, respectively [11]. Furthermore wind energy is a resource that ensures long term and reliable solutions for global energy demands. For its importance

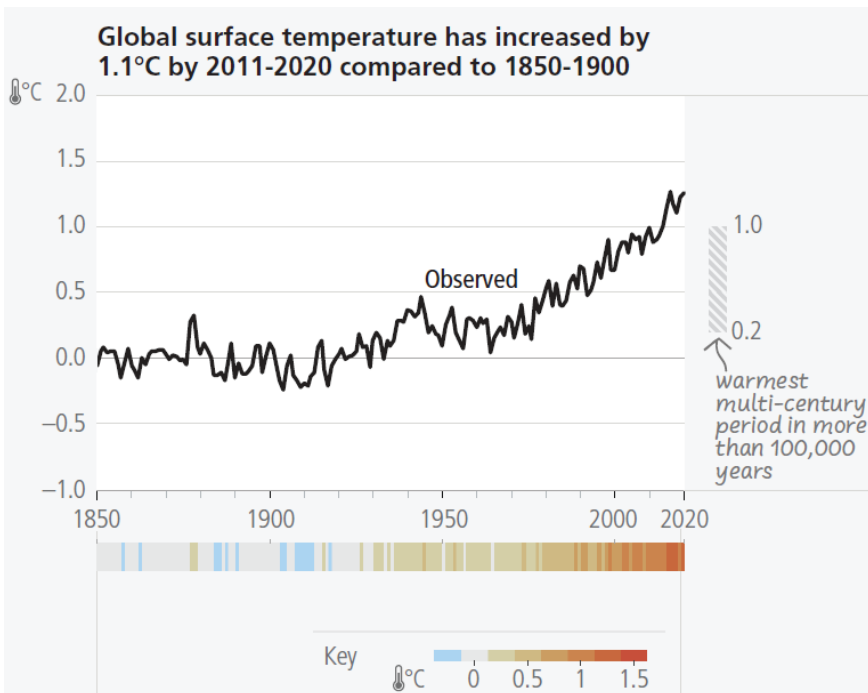


Figure 1.3: Change in global surface temperature rise [5]

in energy transition, further research and development are necessary to integrate wind energy into the power systems.

1.2 Wind energy growth and evolution

From being used as wind mills to grind grains to becoming multi-megawatt power generating machines, wind energy has come a long way. Figure 1.4 presents a timeline of wind energy evolution over the years [12]. The first use of wind energy can be traced back to the 1st century AD when a Greek engineer Heron of Alexandria invented the first wind powered machine in the form of an organ [13]. During the 7th century AD in the Sistan region of Iran, Panemone windmills were being used to grind corn and flour in addition to being used to pump water. By 1000 AD, windmills in China were used to pump sea water to make salt in China and Sicily. It was not until 1887, that the first wind turbine was used to produce electricity. This invention of James Blyth in 1887, a small scale wind turbine was the first known example of electricity being generated from a wind turbine. The first half of the 20th century brought many advancements in the wind energy technology. It was during this time period that wind energy began to be used on a mass scale. In 1941, the first MW scale wind turbine was connected to the grid. The later part of the 20th century established wind energy as one of the most promising source of renewable energy. The wind turbines had expanded from land to the oceans in the form of offshore wind energy. By 2012, 30 % of the electricity demand in Denmark was met with wind energy. In 2022 the global wind power installed capacity stands at a staggering 906 GW. World's largest wind turbine MySE 16-20 is functional as of 2023.

1.2.1 Wind energy today

Many countries around the world are moving towards renewable energy sources in order to meet their green energy targets and reduce the greenhouse gases emissions. This has led to a substantial growth in wind energy over the past decades. Figure 1.5 presents the total installed capacity and year-on-year (YoY) growth of wind energy from 2000-2022. During the past two decades, the installed capacity of wind energy has experienced a remarkable growth. This growth can be clearly observed in Figure 1.5. Where in 2000 the installed capacity was only 16.94 GW, by the beginning of 2011 it had already crossed 200 GW and with more than a fourfold increase since 2011, the wind turbine capacity by 2022 had reached over 900 GW. This progression is a clear indication of the power system trend

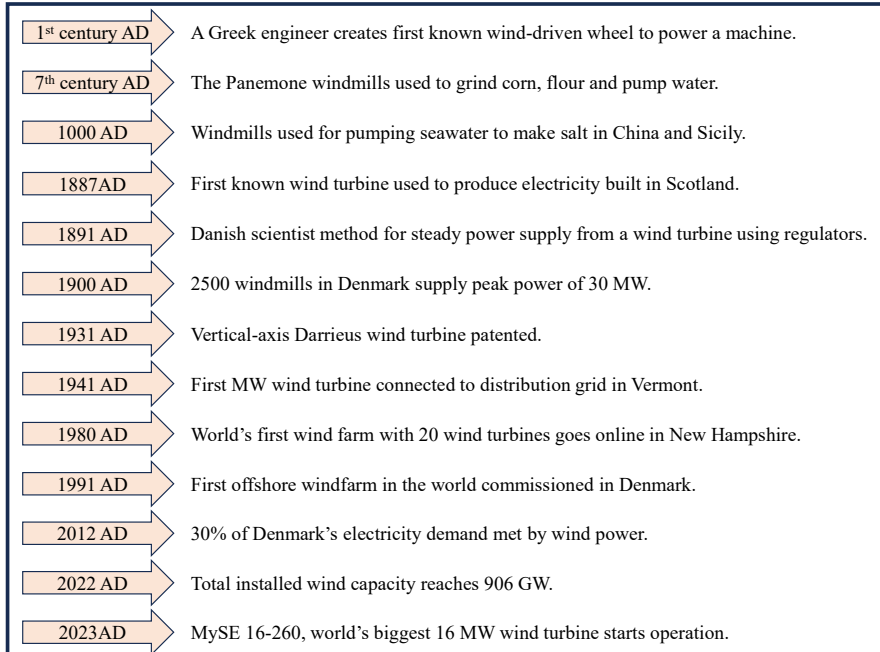


Figure 1.4: Timeline of wind energy evolution

moving towards a power mix with a significant portion of energy coming from wind.

According to the Global Wind Energy Council (GWEC) report, the 1 TW mark of global wind energy installations will be reached somewhere in 2023 [14]. The forecast for total wind energy for 2023-2030 has been increased by 143 GW (13 % YoY), mainly due to the energy system reforms in Europe that focus on replacing fossil fuels with renewable energy to achieve energy security. Additionally, India, U.S. and China's commitment to expand the renewable energy will play a substantial role in this growth. Figure 1.6 shows the new wind capacity, projected new wind capacity based on current growth rates, annual capacity gap to meet net zero by 2050 scenarios and cumulative wind capacity to meet net zero by 2050 scenarios. According to the trends, it is expected that 2 GW global installed capacity milestone will be reached before 2030. However, with the current trends only 68 % of the wind power required by 2030 to stay on track for a net-zero emission by 2050 will be reached. A global collective effort is required to meet the high targets. To this end many countries strive to increase their share of wind energy. Figure 1.7 shows the share of electricity

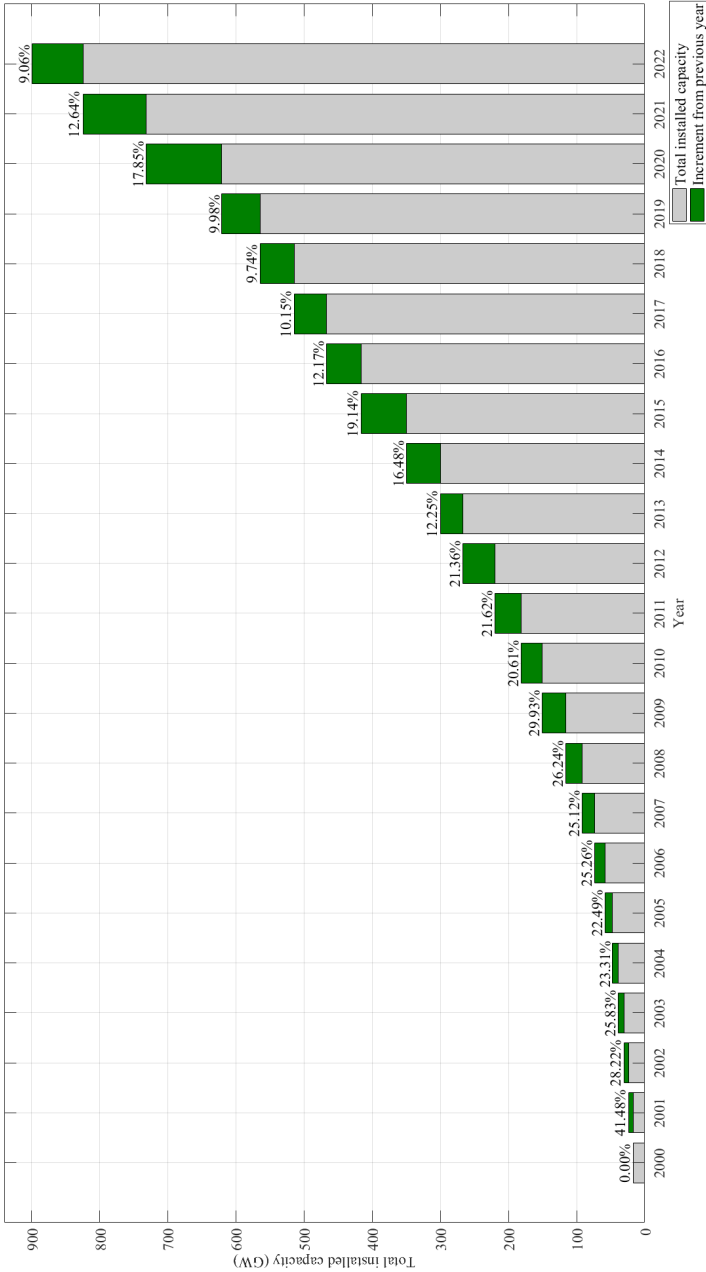


Figure 1.5: Total installed wind capacity 2000-2022

production from wind energy for Europe, North America, Asia, Africa and the World [3]. In 2022, the global share of electricity production from wind had reached 7.5 %. This significant share has increased by almost 3 % in the last 5 years, where it stood at 4.54 % in 2017. The share of electricity production from wind for North America, Asia and Africa was 8.86 %, 5.6 % and 2.68 % respectively. Europe emerged as the leader with a 10.95 % share of its electricity production coming from wind energy. This feat achieved by Europe is certainly powered by the substantial investment in wind energy. Figure 1.8 shows the wind energy investment in Europe from 2000-2022. Only in the last three years an investment of over 100 €bn has been made [15]. These investments in wind energy also bring out breakthrough research and innovations that make wind energy more economic. The Levelized cost of energy (LCOE), the ratio of the costs involved in building and operating of a system to the total value of electrical energy produced over its lifetime, for wind energy systems has been continuously on a downward slope. Figure 1.9 show the expected decline in the LCOE of onshore, fixed bottom and floating offshore wind turbines [16]. The study predicts a 37 % to 49 % decline in wind energy costs by 2050. The cost decline is attributed to the present and expected continued advancements in wind energy technologies. In such a scenario, wind power has the potential to emerge as a major player in the global energy market.

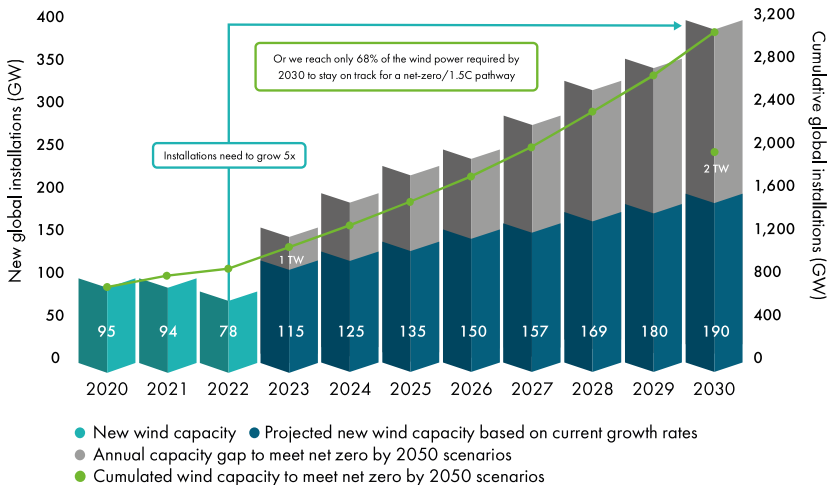


Figure 1.6: Expected new wind energy installations 2020-2030 [14]

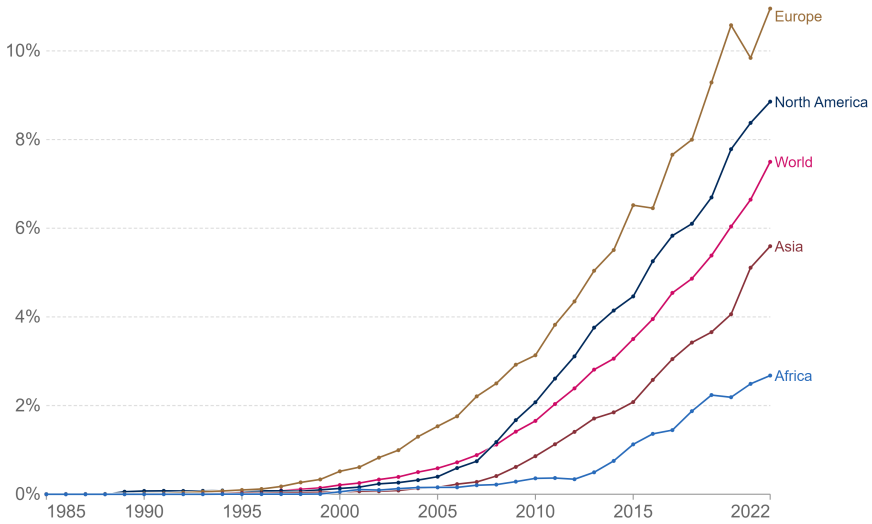


Figure 1.7: Share of electricity production from wind [3]

1.3 Ancillary services: an overview

Ancillary services, in the context of power systems, are a set of support functions and capabilities that are essential for maintaining the reliability, stability, and overall operational integrity of the electric grid. These services are supplementary to the basic generation and delivery of electricity and play a crucial role in ensuring that the power system operates smoothly under various conditions. Ancillary services are crucial for reliable performance of the power system. These services are related to the control of frequency, voltage and power load, and are generally controlled by TSOs and distribution system operators (DSOs). Power system ancillary services are broadly divided into four categories as follows:

1.3.1 Frequency measure

Frequency is a critical parameter in a power system. Deviations from the nominal frequency can impact the stability and reliability of the system. In principle, the frequency of a power system must always remain close to 50 Hz (60 Hz in North America and some other countries). However, in practice the grid frequency is not static. Therefore, a deviation of 200 mHz is the defined range of acceptable deviation in the European power system. Any further deviation from this range can result in blackouts or even the collapse of the power system. Inertial response and controlled frequency

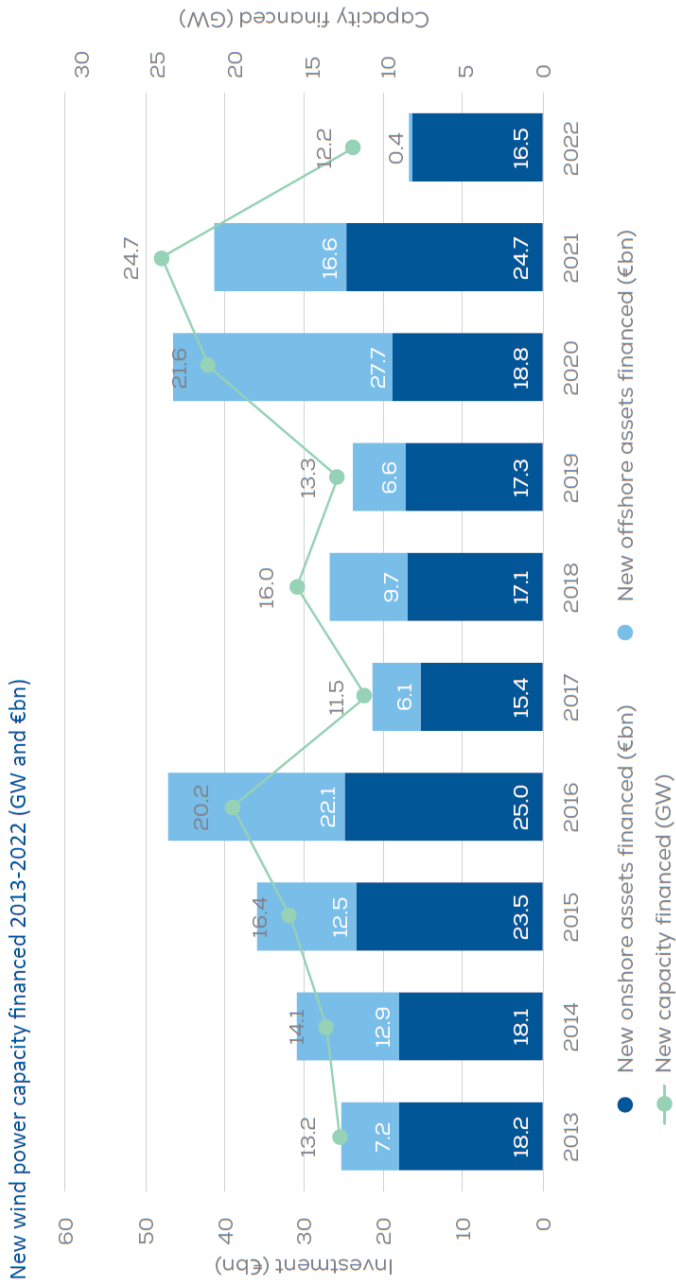


Figure 1.8: Wind energy investment in Europe 2013-2022 [15]

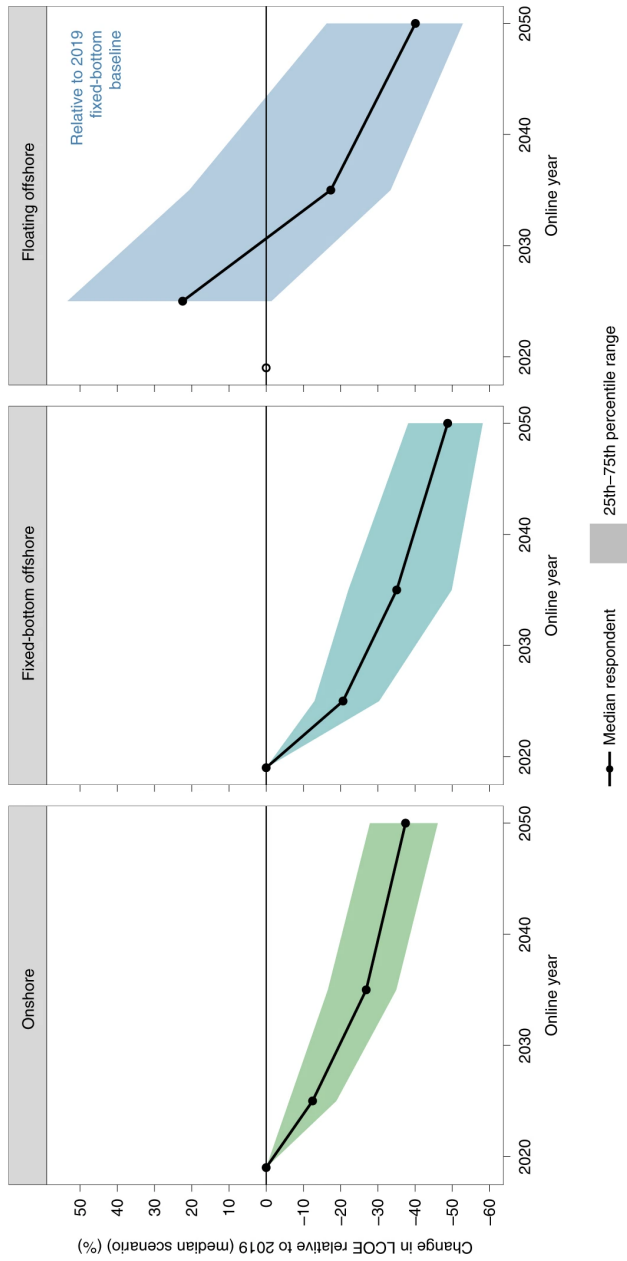


Figure 1.9: Expected LCOE changes in the median scenario in percentage terms relative to 2019 baseline values [16]

response are the two main power system responses to maintain the grid frequency, as shown in Figure 1.10. Inertial response is the inherent rotational inertia of the rotating masses in the power system, such as generators and turbines. When there is a sudden change in the balance between the mechanical power of directly coupled machines and the electrical power, the system frequency deviates from its nominal value. In such a scenario, the inertial response is the initial, automatic reaction of the rotating masses to counteract this deviation. Rotating masses, due to their inertia, resist changes in speed. When a sudden increase in load occurs, the kinetic energy stored in these rotating masses helps limit the rate of change of frequency (RoCoF) until other control mechanisms can respond. The control mechanisms that follow the inertial response are primary, secondary and tertiary frequency control. These controlled frequency responses involve the use of various control mechanisms and devices to actively manage and stabilize the system frequency. Methods such as automatic generation control (AGC) and governor control are used to adjust the power outputs of generators.

The TSO is responsible for maintaining this balance of supply and demand so that the frequency is as close to 50 Hz as possible. Figure 1.11 shows the frequency balancing services as defined by the ENTSO-E. Primary reserve or frequency containment reserve (FCR) exists in different forms and shapes in power systems across the world. FCR is a service to maintain the frequency within a specified frequency deviation band, by balancing the mechanical power and the electrical power. The responsible parties must react and completely adjust the power upward or downward based on the contracted FCR within the full activation time (FAT) of 30 s. Another faster version of primary reserve frequency measure is fast frequency reserve (FFR). This service requires the delivery of contracted reserve by increasing or decreasing generation within a time frame of 2 sec. The short activation time makes FFR one of the most challenging services, especially for power generators without an inherent system inertia directly coupled to the grid, such as wind turbines or photovoltaics.

Secondary reserve or automatic Frequency Restoration Reserve (aFRR) works for the same purpose of grid frequency restoration. However, it has a longer FAT than FCR. The parties responsible for delivering aFRR, flexibility service providers (FSPs) or balancing service provider (BSPs) must activate the full contracted reserve within 5 minutes. The role of aFRR is to gradually take over and free the FCR. Tertiary reserve or manual Frequency Restoration Reserve (mFRR) helps in restoring the grid frequency in the case of longer deviations. mFRR are fully deployable after 12.5 min and have a minimum duration period of 5 min. Unlike the automatic ser-

vices FCR and aFRR, mFRR is activated manually by the TSO. Replacement Reserve (RR) are additional frequency support services subjective to individual TSOs. The two main frequency support services implemented in the studies, FCR and FFR, are described in the following subsections.

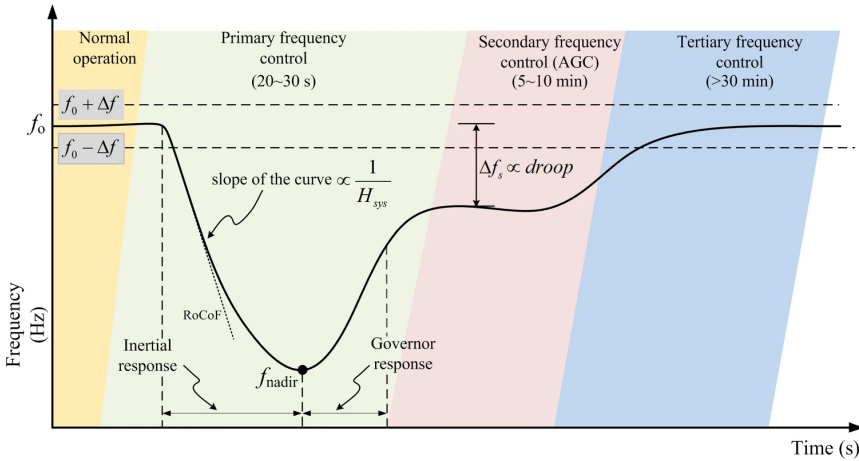


Figure 1.10: Power system frequency response [17]

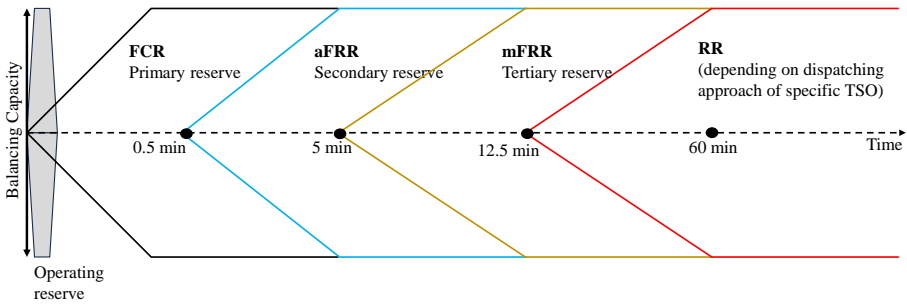


Figure 1.11: ENSTSO-E defined balancing services [18]

1.3.1.1 Frequency containment reserve

The Belgian TSO Elia procures grid frequency balancing services through two different frameworks based on the generation capacity of the production units. These contracts are the Contract for the Injection of Production Units (CIPU) and non-CIPU. For harmonisation of FCR products and FCR procurement rules on the European level, from July 2020 on, only the 200

mHz symmetrical service are continued [19]. Due to this reason, the FCR tests presented in this work are conducted for a 200 mHz symmetrical service. In this type of service, a proportional frequency support within the range of 49.8-50.2 Hz of grid frequency is required from the participating production unit.

The relation between the reference power and the grid frequency for a 200 mHz symmetrical service can be seen in Figure 1.12. In this representation, the wind turbine operates at a base power P_{base} . With the change in grid frequency, the reference power follows a linear slope between P_{min} and P_{max} . The service is obligated between the bounds of 49.8 Hz – 50.2 Hz. However unlikely, if the frequency drops or increases beyond this range, the power supply should be maintained at a constant, on upper or lower limit respectively. A frequency response deadband of 10 mHz centred at nominal frequency (50 Hz) is present to reduce excessive controller activities and turbine mechanical wear for normal power system frequency variations.

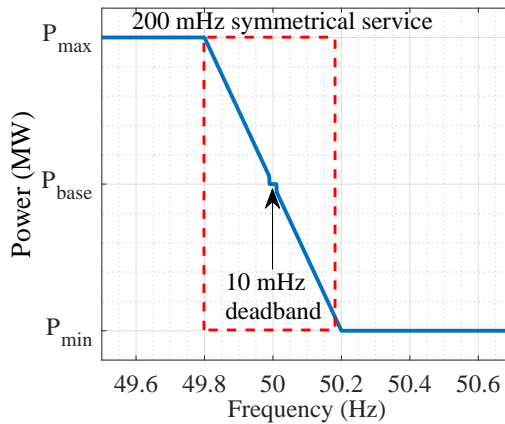


Figure 1.12: Frequency-Power relationship as per 200 mHz symmetrical service

1.3.1.2 Fast frequency reserve

The fast frequency reserve service has been adopted by different countries and therefore exists in various forms and manners. For the tests presented in this research, FFR as defined for the Nordic synchronous area was chosen [20]. All the generation units intending to participate in the FFR market must pass a prequalification process to ensure their ability to deliver FFR when ordered by the TSO. A crucial part of this prequalification process is a prequalification test. The specified support durations are, ‘long support duration FFR’ (at least 30 s) and ‘short support duration FFR’ (at least

5 s). There are 3 different combinations of FFR services available that can be freely chosen by the production units. These services presented in Table 1.1 differ in activation level and the required maximum activation level. The participants are free to choose from the type of service they intend to provide beforehand. Figure 1.13 is a graphical representation of the FFR service. The activation instant at $t = 0$ s is the moment when the FFR reserve is activated. Depending on the type of service chosen by the production unit, an upper time limit ranging from 0.7 s to 1.3 s is given during which the full activation should be completed. The activation level should be sustained for the minimum support duration based on the choice of long duration or short duration support. At the end of the support duration the production units are given a recovery time of 15 minutes, after which the production units must be fully prepared for a new support cycle. During the support duration a maximum overshoot equivalent to 35% of the prequalified FFR capacity is permissible.

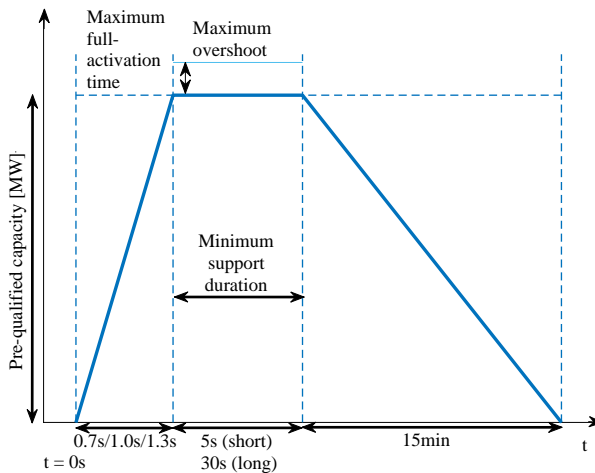


Figure 1.13: FFR framework

1.3.2 Voltage control and reactive power management

Voltage control and reactive power management are important aspects for the reliability of the power system. The power network equipment as well as the consumer equipment are designed for a specified range of supply voltages. Therefore, the power system voltage should be maintained and kept within acceptable limits. The reactive power management helps minimise variations in voltage, enhancing the stability of AC systems. By

Table 1.1: Type of FFR services

Type	Activation level [Hz]	Maximum full activation time [s]
A	49.7	1.3
B	49.6	1.0
C	49.5	0.7

improving the stability of the power system, it prevents the need for load shedding and averts system collapse. This, in turn, enhances overall system security and reliability. Voltage control in an alternating current (AC) power system involves managing the balance between locally injected or absorbed reactive power to support and stabilize voltages, particularly in inductive grids, thereby influencing the overall stability of the system [21].

1.3.3 Operational management and reconstruction of supply

The operational management of the power system comprises of controlling and monitoring the operations of the grid. Grid congestion management is one such operation where the TSO reviews the net supply and demand of the following day. The information is then used to analyse proper management of the grid by using tools such as load flow calculations. In case of a black out, reconstruction of supply is needed. The power plants that are autonomously operable without the need of external energy supply are used to re-energise the grid.

Amongst these ancillary services, frequency related ancillary services are the most challenging from the perspective of control design. These primary reserve services such as FCR and FFR require an activation within a very short time period ranging from 2-5 sec. Therefore, the scope of this study lies around the implementation and effects of providing such services by the means of a wind turbine.

1.4 Wind energy's role in ancillary services

Ancillary services are typically provided by the traditional non renewable power plants. However, wind power has the capability to be a reliable ancillary services provider. The increased participation of wind energy in the ancillary services market is beneficial for the power system as well as the WPPs. The energy transition towards a more sustainable power system re-

quires increased wind energy production. The ability of the wind farms to provide ancillary services make their integration in the power system easier and more reliable. On the other hand, a limited or no participation of wind farms in the ancillary services market will lead to a lost revenue stream for the WPPs. Moreover, low participation of wind turbines in the ancillary market will eventually limit the amount of wind power, since the ancillary services are needed to stabilise the grid and must then be provided by other energy sources.

The high penetration of the power system with renewable energy sources such as wind energy poses some challenges. The main challenges are the intermittency and reduced inertia of the power system. Conventional power plants respond to the variation in grid frequency by their inertial response and primary reserve. Inertial response is the natural reaction to the changes in the grid frequency in the form of increased or decreased speed of the operating turbine. The stored kinetic energy is used to compensate and balance out the grid frequency. On the other hand, primary reserve is activated using control, to proportionally vary the power output based on the changes in the grid frequency. Since, the wind turbines are decoupled from the grid through power electronics, they do not offer a natural inertia to the grid. However, the wind turbines using advanced control systems are capable of providing primary reserve. The existing studies point to the possibility and current implementations of wind energy for ancillary services provision [22], [23], [24], [25]. Torque control techniques based on the RoCoF and frequency deviation can be utilised using a reference power based on the grid frequency [26], [27], [28]. Such techniques enable the wind power producer (WPP) to enable frequency regulations in line with the rapid changes in the grid frequency by the means of adjusting the reference power. These implementations are necessary for a wider market participation of wind energy in electricity markets. Moreover, the active participation of wind farms in the ancillary services market is becoming a norm in regulatory frameworks. In [29] and [30], a review of European grid codes for wind farms are presented. These grid codes imply active power control and frequency deviation from wind farms. The review of international grid codes for wind power integration are presented in [31] and [32]. These modern grid codes require WPPs to contribute towards grid disturbances and network stability by the means of ancillary services provision. Similar trends have been observed in India and China [33], [34].

1.5 Objectives

The transition of the power system towards a sustainable energy production system has led to a significant penetration of wind energy into the power mix. Wind energy over the past decades has become the fastest growing mode of renewable energy. For a reliable and robust energy system, ancillary services provision from wind energy is a requirement. In the light of current and perceivable future trend of accelerated wind energy participation in both energy and reserve markets, the research work presented in this dissertation aims to study the ability of wind turbines to provide FCR, and then analyse its effects on the wind turbine's loads, wake effect and revenue of the WPP. The four main objectives of this as shown in Figure 1.14, are as follows:

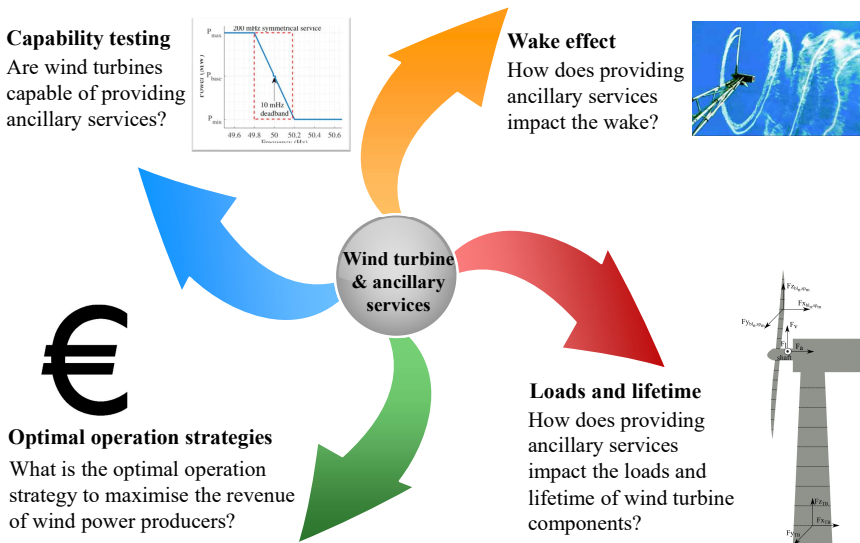


Figure 1.14: Thesis outline

1. Capability testing

The first objective of this research work is to develop a control system that is capable of following grid frequency based reference power and providing FCR. The control system should be able to adjust the reference power within seconds. For validation purpose, the control system is tested with the Belgian TSO pre-qualification test that is mandatory for any FCR provider to pass.

2. **Wake effect**

The wake effect is the trail of disturbed air produced by an operational wind turbine. The wake effect is known to reduce the wind speed in the affected area. As a result the nearby wind turbines or wind farms may receive a reduced wind. The control actions performed to provide primary reserve services such as FCR can potentially alter the wake effect. In this line the second objective of this research is to study the impact of FCR provision on the wake of a wind turbine.

3. **Loads and lifetime**

As the third objective of this research, the loads and lifetime of an FCR providing wind turbine is studied. Firstly, a crucial wind turbine component, its main bearing is studied under dynamically varying load conditions caused due to providing a range of FCR services. Secondly, a methodology is developed to accumulate all the major loads on the wind turbine and use them as a single unit in order to analyse them based on FCR provision. Additionally, this loading term is also used to optimise the reserve market participation of a wind turbine by the means of an optimisation methodology.

4. **Optimal operation strategies**

The fourth objective of this research is to develop a control strategy that allows the WPP to regulate output power to provide the contracted FCR while considering real-time variations in the wind speed.

1.6 Thesis outline

This dissertation is organised as follows:

Chapter 2 *Wind turbine capability to provide ancillary services*

Chapter 2 presents the first step in the research presented in this dissertation. A control system is developed in order to adjust the power output of the wind turbine according to the grid frequency. Detailed models of a direct-drive wind turbine with a PMSG are used to perform the simulation tests. The models and control system are validated against Belgian TSO established pre-qualification test to examine the feasibility of providing FCR from a wind turbine. The tests are performed for a range of wind scenarios, ranging from steady wind to a high turbulence scenario. The results obtained through the simulations prove the capability of wind turbines to provide primary frequency control. The developed control system is able to perform with a low error, not exceeding 0.22 % for the most turbulent wind scenario.

The control system presented in Chapter 2 is further used and developed in the following Chapters to perform studies related to wake effects, component lifetime, wind turbine loading and optimal operation strategies.

Chapter 3 *Dynamic Wake Analysis of a Wind Turbine Providing Frequency Support Services*

Chapter 3 presents a study of wake effect analysis associated with a frequency support service providing wind turbine. The control actions performed for quick activation and deactivation of power reserve margin, to provide frequency support services have an impact on the dynamic behaviour of the wind turbine's wake. To study these changes in the wake effect, the control system developed in Chapter 2 is used. The frequency support services FCR and FFR are tested for a range of grid frequency designs including both synthetic and actual grid frequencies. Jensen wake model is used to study the wake behaviour for steady and turbulent wind scenarios. The findings from this study indicate a clear impact of frequency support services provision from a wind turbine on its wake.

The findings from this study motivated an exploration of the impact of frequency support services on other aspects of a wind turbine such as the loads and lifetime of the components. These areas are explored in the following chapters.

Chapter 4 *Wind Turbine Component Lifetime*

Chapter 4 explores the study of loads and the lifetime of the main bearing

in a wind turbine under dynamically varying conditions resulting from the provision of FCR. The main bearing of a wind turbine is a crucial component and experiences heavy forces during the operation. When a wind turbine provides FCR to support the grid frequency, the forces acting upon the main bearing are also expected to exhibit more dynamic variations. These forces have a direct impact on the lifetime of the main bearing. Simulations are performed for a range of FCR margin, to study the changing behaviour of dynamical forces acting on the main bearing with respect to the amount of FCR provided. Based on the outputs from these simulations and using 2 years of LiDAR wind data, the lifetime of the main bearing of the wind turbine is calculated and compared for different cases. Through this study, a clear impact of providing FCR on the lifetime of the main bearing of the wind turbine is observed.

The evident impact of FCR provision on the wake and the loads of the wind turbine main bearing is presented in Chapter 3 and Chapter 4, respectively. The economic implications of FCR provision, design of optimal operation strategies and the overall load aware operation of wind turbine are the topics that require due diligence for a well rounded study on ancillary services provision from wind turbines. These areas are covered in the following chapters.

Chapter 5 *Prediction-based Wind Turbine Operation for Active Participation in the Day-Ahead and Reserve Markets*

Chapter 5 presents an effective control system design that allows WPP to regulate their power output by meeting the contracted reserve power demand. The control system presented in Chapter 2 is upgraded to account for real-time wind variations. A machine-learning algorithm based on the Adaptive Neuro-Fuzzy Inference System (ANFIS) is used to predict the wind speed of the following instances, to be used as input to the control system. Wind profiles with different turbulence intensity are used to simulate a practical case study. Three different operation strategies including, conventional, ideal and the proposed strategy are tested. The effectiveness of the proposed control strategy is evaluated based on the WPP's profit.

Thus far in this dissertations, the topics of wind turbine control, wake, main bearing lifetime and optimal control strategies are covered. A conclusive study in the following chapter builds up on the previous chapters to develop a load-aware operation strategy for wind turbine participation in energy and reserve market.

Chapter 6 *Wind Turbine Load Aware Operation*

In Chapters 6 a load aware optimisation method of wind turbine bidding

in joint energy and reserve market (JERM) is presented. In Chapter 4, it was established that the provision of ancillary services impact the load and lifetime of the wind turbine main bearing. To further the scope of the study, the major loads on a wind turbine components including the blades, the shaft, the tower and the main bearing are calculated under different reserve market participation scenarios. The calculated loads are then used as input into an optimisation problem that generates energy and reserve market bid for profit maximisation of the WPP while taking into account the wind turbine loading.

The findings of the study indicate that when considering the wind turbine loading in power scheduling, the reserve bid is a crucial factor. The proposed novel method, unlike the traditional scheduling models that overlook the wind turbine loading and its hidden costs, implicitly accounts for the costs associated with the wind turbine physical health. The method provides WPPs to always have a trade-off option to create a balance between the physical load on the wind turbine and the monetary benefit.

Chapter 7 *Conclusions & Future Work*

Chapter 7 summarises the research. Conclusions are derived and potential future works are presented.

References

- [1] S. Rudnik, "Selected issues concerning transposition to the Polish Legal Order of the directive 2014/94/EU of the 22 October 2014 on the deployment of Alternative Fuels Infrastructure" AUTOBUSY – Technika, Eksploatacja, Systemy Transportowe, 2018. doi:10.24136/atest.2018.207
- [2] Energy Institute, "Statistical Review of World Energy", Online, [Accessed: Aug. 2023], <https://www.energyinst.org/statistical-review>
- [3] H. Ritchie, M. Roser and P. Rosado, "CO and Greenhouse Gas, Our World in data", 2020, <https://ourworldindata.org/co2-and-greenhouse-gas-emissions>.
- [4] "Record-breaking carbon emissions, and more — this week's best science graphics," Nature, 2022. doi:10.1038/d41586-022-03721-5
- [5] "Global Energy Review: CO2 Emissions in 2021.," IEA, 2021. <https://www.iea.org/reports/global-energy-review-co2-emissionsin-2021-2>.
- [6] H. Lee and J. Romero, "Climate Change 2023: Synthesis Report. Contribution of Working Groups I, II and III to the Sixth Assessment Report of the Intergovernmental Panel on Climate Change," 2023.
- [7] E.U. "European Commission, Directorate-General for Research and Innovation. European Green Deal: research & innovation call. Publications Office of the European Union, 2021.
- [8] UNFCCC, Secretariat, "Nationally Determined Contributions under the Paris Agreement. Synthesis report by the secretariat", 2021.
- [9] "NAPCC – national action plan on climate change," The Palgrave Encyclopedia of Urban and Regional Futures, 2022. doi:10.1007/978-3-030-87745-3_300442
- [10] "United States Department of State. U.S. Climate Action Report 2010". Global Publishing Services, Washington, June 2010.
- [11] "How Wind Can Help Us Breathe Easier". Wind Energy Technologies Office. <https://www.energy.gov/eere/wind/articles/how-wind-can-help-us-breathe-easier>

- [12] Z. Shahan, "History of wind turbines".[Accessed: September 2023] <https://www.renewableenergyworld.com/storage/grid-scale/history-of-wind-turbines>, 2014.
- [13] E. Papadopoulos, "Heron of Alexandria (c. 10–85 AD)," *History of Mechanism and Machine Science*, doi:10.1007/978-1-4020-6366-4_9
- [14] GWEC, "Global wind report, 2023." <https://gwec.net/globalwindreport2023/>
- [15] Wind Europe. *Financing and Investment Trends: The European Wind Industry in 2022*. Technical report, March 2023.
- [16] R. Wiser et al., "Expert elicitation survey predicts 37% to 49% declines in wind energy costs by 2050," *Nature Energy*, 2021. doi:10.1038/s41560-021-00810-z
- [17] R. Rajan and F. M. Fernandez, "Small-signal stability analysis and frequency regulation strategy for photovoltaic sources in Interconnected Power System," *Electrical Engineering*. 3005–3021, 2021. doi:10.1007/s00202-021-01293-7
- [18] Next Kraftwerke, *What are Balancing Services?*, <https://www.next-kraftwerke.com/knowledge/balancing-services> [Accessed: September 2023]
- [19] Elia, *General Framework For Frequency Containment Reserve Service By CIPU Technical Units*. 2019.
- [20] ENTSO-E. *Technical Requirements for Fast Frequency Reserve Provision in the Nordic Synchronous Area – External document*. <https://www.statnett.no/> [Accessed: September 2023]
- [21] B. Kirby and E. Hirst, *Ancillary service details: Voltage Control*, 1997. doi:10.2172/607488
- [22] A. B. Attya, J. L. Dominguez-Garcia, and O. Anaya-Lara, "A review on frequency support provision by wind power plants: Current and future challenges," *Renewable and Sustainable Energy Reviews*, 2018. doi:10.1016/j.rser.2017.06.016
- [23] P. Sonkar and O. Rahi, "Contribution of wind power plants in grid frequency regulation: Current perspective and future challenges," *Wind Engineering*, 2020. doi:10.1177/0309524x19892899

- [24] Z. Wang, K. P. Wong, S. S. Choi, D. Gan, and Y. Zong, "An overview of codes and control strategies for frequency regulation in wind power generation," *Smart Power Distribution Systems*, 2019. doi:10.1016/b978-0-12-812154-2.00001-8
- [25] H. Karbouj, Z. H. Rather, D. Flynn, and H. W. Qazi, "Non-synchronous fast frequency reserves in Renewable Energy Integrated Power Systems: A critical review," *International Journal of Electrical Power & Energy Systems*, 2019. doi:10.1016/j.ijepes.2018.09.046
- [26] M. Kayikci and J. V. Milanovic, "Dynamic contribution of DFIG-based wind plants to system frequency disturbances," *IEEE Transactions on Power Systems*, 2009. doi:10.1109/tpwrs.2009.2016062
- [27] P. Keung, P. Li, H. Banakar, and B. Ooi, "Kinetic energy of wind-turbine generators for system frequency support," *IEEE Transactions on Power Systems*, 2009. doi:10.1109/tpwrs.2008.2004827
- [28] N. W. Miller, K. Clark, and M. Shao, "Frequency responsive wind plant controls: Impacts on grid performance," 2011 IEEE Power and Energy Society General Meeting, 2011. doi:10.1109/pes.2011.6039137
- [29] E. Nycander and L. Söder, "Review of European Grid Codes for Wind Farms and Their Implications for Wind Power Curtailments," in 17th International Wind Integration Workshop Stockholm, Sweden | 17 – 19 October 2018.
- [30] M. Altin et al., "Overview of recent grid codes for Wind Power Integration," 2010 12th International Conference on Optimization of Electrical and Electronic Equipment, 2010. doi:10.1109/optim.2010.5510521
- [31] M. Mohseni and S. M. Islam, "Review of International Grid Codes for Wind Power Integration: Diversity, technology and a case for Global Standard," *Renewable and Sustainable Energy Reviews*, 2012. doi:10.1016/j.rser.2012.03.039
- [32] F. Díaz-González, M. Hau, A. Sumper, and O. Gomis-Bellmunt, "Participation of wind power plants in system frequency control: Review of grid code requirements and control methods," *Renewable and Sustainable Energy Reviews*, 2014. doi:10.1016/j.rser.2014.03.040

- [33] M. P. Bhawalkar, N. Gopalakrishnan, and Y. P. Nerkar, “A review of Indian grid codes for wind power generation,” *Journal of The Institution of Engineers (India): Series B*, 609–617, 2019. doi:10.1007/s40031-019-00407-x
- [34] [1] Y. Zhang, Z. Duan, and X. Liu, “Comparison of grid code requirements with wind turbine in China and Europe,” 2010 Asia-Pacific Power and Energy Engineering Conference, 2010. doi:10.1109/appeec.2010.5449434

2

Wind turbine capability to provide ancillary services

The global wind power capacity is on a constant rise. Many countries are moving towards renewable energy sources. Wind energy accounts for the biggest renewable energy resource in Europe. Despite all the benefits, wind energy tends to weaken the grid stability. One reason for this is the fact that most wind turbine generators are not directly coupled to the grid and do not provide ancillary services, such as primary frequency control, due to the lack of rotating inertia. In the context of this PhD study, developing and testing a control system that is capable of providing ancillary services is primary step on basis of which further studies are conducted. In this Chapter, detailed models of a direct-drive wind turbine with permanent magnet synchronous generator (PMSG) are presented. The models are used to test the feasibility of providing ancillary services by performing the pre-qualification test for primary frequency control, as established by the Belgian TSO. These tests are conducted for different wind profiles, each having a different level of turbulence.

The rest of this chapter is structured as follows: Section 2.1 presents an introduction to the study. Section 2.2 presents the

model and specifications of wind turbine and generator used for this study. In Section 2.3, the control system implemented to perform the tests is presented. The performed tests and results are presented in Section 2.4. Finally, the conclusion is drawn in Section 2.5. The content of this chapter has been published in [1].

2.1 Introduction

Participation in the reserve markets is strictly based on the ability of a production unit to increase or decrease the reserve power within a fixed span of time. Usually this time range is small, ranging from an instantaneous response to a few minutes. In order to qualify to participate in these markets, the production units need to prove their ability to efficiently provide these services by going through several tests. Providing these services is a challenge for production units that are fully converter-interfaced, such as a wind farm. A support from energy storage technologies such as supercapacitors, flywheels, batteries, etc., can be sought in such cases [2], [3]. These technologies can provide the desired active power output within 0.5-2 s [4]. However, many power system operators in Europe forbid the participation of energy storage power plants in the primary reserve market [5]. New control systems for wind turbines are potentially capable of a quick response to the changing grid frequency. Hence, this makes them an eligible candidate for frequency support ancillary services. Studies have shown the feasibility and methods of operating wind farms as FCR and FFR provider [6] - [12]. Regarding wind turbine control, several different techniques are available [13] - [15]. A generator control method that uses direct torque control (DTC) for an interior mounted magnet PMSG is presented in [16]. An improved direct torque control method for smooth power injection and short circuit protection is presented in [17]. These control strategies are widely used for variable-speed generation and for extracting the maximum power available in the wind. The conventional operation of a wind turbine is to use maximum power point tracking (MPPT) to extract maximum power or power limiting control (PLC) in case of wind speeds higher than the rated wind speed. However, the control system required for this study should not only operate in MPPT and PLC, but should also be able to follow the reference power signal that changes with the fast varying input grid frequency. The results from this research support the effectiveness of fast frequency reserve from wind turbine control on supporting active power disturbances in low-inertia power systems. An added advantage for wind farms in this scenario is that the FCR market in Europe is moving towards shorter procurement periods [18], [19]. Since the wind prediction is more reliable and accurate on short time scale, it is easier for wind farms to make a more confident bid in the FCR market.

The possibility of temporary power over-production in variable speed wind turbines is explored in [20]. In [21], an active control of wind turbines for ancillary services using pitch and control methods is explored. The study presented in [22], presents a wind turbine participation in the

ancillary service market by the means of rotational kinetic energy. A grid frequency stabilisation strategy using inertial control of the wind turbine incorporating energy storage systems is presented in [23]. The present studies are not only confined to frequency support services. In [24], a method of voltage control from a power plant is presented. The capability of wind farms to provide reactive power ancillary services is explained in [25] and [26]. Another study presented in [27] explores the coordination strategy of large wind farms for voltage support by the means of high converter capacity. An ancillary services provision method by the means of coordination between wind turbine and electrolysis systems is presented in [28]. The evolution of fast acting control systems for wind turbines has enabled the integration of wind farms into the ancillary services market [29]. In [1], a control system is presented that is capable of following the grid frequency with minimal error. An advanced converter control maintaining a transient frequency stability is presented in [6]. The study presented in [7], proposes a coordinated control strategy to efficiently utilise energy in permanent magnet synchronous generators (PMSG). A hybrid control strategy of frequency based power point tracking method is presented in [8]. In [30] control system capability for FCR and FFR is shown. A strategy incorporating wake control for optimised operation of wind farms providing FCR is proposed in [31]. These control techniques have made it possible for the wind turbines to have a deeper integration in ancillary services market. Crucial grid frequency services such as FCR and FFR can greatly benefit from these enhanced control capabilities of the wind turbines to swiftly respond to the grid frequency fluctuations. Grid services essential to maintain the grid stability such as synchronous inertial response (SIR), enhanced frequency response (EFR) and fast post-fault active power recovery (FPFAPR) can also benefit from increased wind energy participation in the ancillary services market [32].

This chapter introduces the various models and control designs used for the work presented in this dissertation. The different software packages used and the simulations performed in the multi-software environment are also explained. A model consisting of an offshore wind turbine coupled with a PMSG is presented. The system is controlled in a manner that the output power of the PMSG follows the reference power provided to it. This reference power can be dependent on the grid frequency. However, for the tests presented in this study, the reference power is based on a pre-qualification test set up by the Belgian TSO Elia for the power plants to be eligible as a FCR provider. This test requires the production unit to respond to the changing reference value within a short time span. The controller is designed to respond to these changes. The model is additionally

stress-tested by subjecting it to different intensity of wind levels. The wind profiles range from steady wind to highly turbulent winds.

2.2 Models

The wind energy conversion system used in this study is based on a Type-4 wind turbine as shown in Figure 2.1 [33]. A Type-4 wind turbine is a specific configuration in which the generator, a PMSG, is connected to the wind turbine without the use of a gearbox. This type of connection is known as a direct-drive connection. The generator of the variable speed wind energy conversion system is connected to the grid via the AC-DC-AC power converter, known as full back-to-back converter [34]. The generator is connected to the machine-side converter (MSC), whereas, the grid is connected to the grid-side converter (GSC). The generator operation is variable speed in order to optimise the aerodynamic operation. The generator control is operated using the MSC. The MSC regulates the active and the reactive power of the PMSG using abc to dq transformation [35]. The d- and q-axis currents control the active and the reactive power of the PMSG. The GSC works on grid following control and is capable of producing active and reactive power. The active output power injected into the grid is adjusted to balance the energy in the power converter by controlling the DC bus voltage. The reactive output power to the grid is usually controlled either at constant power factor, constant reactive power, or with some form of grid voltage control.

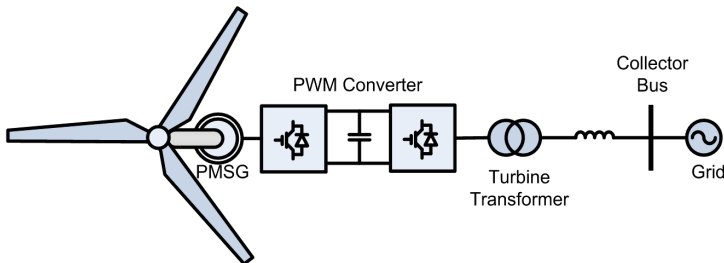


Figure 2.1: Type 4 wind turbine [33]

The simulations performed for the studies presented in this thesis are performed in FAST and Simulink. FAST is a high fidelity wind turbine simulator developed by the National Renewable Energy Laboratory (NREL). The work flow and various modules of FAST are shown in Figure 2.2. With the external conditions as the inputs, the applied loads are used for the

wind turbine dynamics calculations. The blade element momentum (BEM) method is implemented in the AeroDyn v15 module of FAST v8 [36]. Within AeroDyn there are four sub-models for rotor induction, blade air-foil aerodynamics, tower influence on the fluid local to the blade nodes and tower drag. The module calculates aerodynamic loads on the blades and the tower. Simulink has the ability to incorporate custom Fortran routines in a block called an S-Function. The FAST subroutines have been linked with a MATLAB standard gateway subroutine in order to use the FAST equations of motion in an S-Function that can be incorporated in a Simulink model. This introduces flexibility in wind turbine controls implementation during simulation. Generator torque control, nacelle yaw control, and pitch control modules can be designed in the Simulink environment and simulated while making use of the complete nonlinear aeroelastic wind turbine equations of motion available in FAST. The software-in-the-loop setup between FAST and Simulink is presented in Figure 2.3. The wind turbine block, as shown in Figure 2.3, contains the S-Function block with the FAST equations of motion. It also contains blocks that integrate the DOF accelerations to get velocities and displacements. Thus the equations of motion are formulated in the FAST S-function but solved using one of the Simulink solvers.

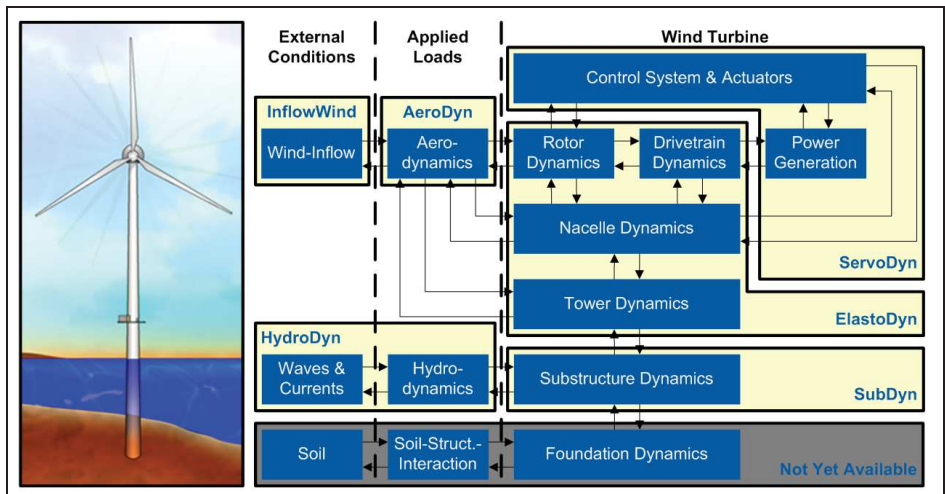


Figure 2.2: FAST modules block diagram [37]

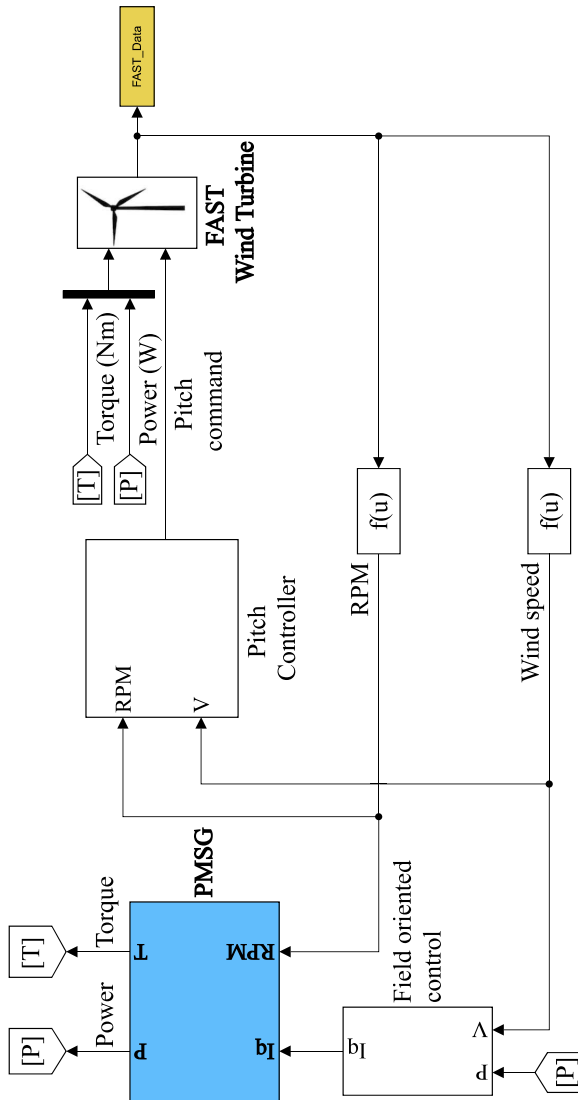


Figure 2.3: Simulink environment

2.2.1 Wind turbine

The wind turbine model used for the studies presented in this thesis, is a 5 MW reference wind turbine for offshore system development [38]. The wind turbine model uses broad design information from published documents of turbine manufacturers with a high correspondence with the RE-

power 5M machine. The model is developed in FAST. The structural model of the wind turbine is the Offshore Code Comparison Collaboration (OC3) monopile [39]. The main properties of this wind turbine are listed in Table 2.1.

Table 2.1: Wind turbine properties

Property	Specification
Power rating	5 MW
Rotor orientation & configuration	Upwind, 3 blades
Rotor and hub diameter	126 m and 3 m
Hub height	90 m
Cut-in, Rated and Cut-out wind speed	3.0 m/s, 11.4 m/s and 25.0 m/s
Cut-in and Rated rotor speeds	6.9 rpm, 12.1 rpm
Rated tip speed	80 m/s
Overhang, Shaft tilt, Precone	5 m, 5°, 2.5°

The wind turbine comprises three blades, and the blade's structural characteristics are drawn from the LM Glasfiber blade, as detailed in [40]. The structural properties of the blade are presented in Table 2.2. The distributed blade structural properties and their scaling for the overall mass, the nacelle's positioning, mass, and inertia about the yaw axis, as well as the hub's mass and inertia about the shaft, are integral components defining the turbine's mechanical framework. The nacelle and hub properties are detailed in Table 2.3. The properties related to the tower of the wind turbine are described in Table 2.4. Furthermore, a comprehensive Figure 2.4, shows the wind turbine tower at the depths of the mudline and the mean sea level.

The wind turbine of the defined type operates in 3 different regions. These regions, as presented in Figure 2.5, are based on the free-flow wind speed measured on the wind turbine rotor. It can be seen in Figure 2.5 that Region 1 corresponds to wind speeds below 3 m/s, i.e. below the cut-in speed of the wind turbine. There is no torque generated in Region 1 and no power is extracted, as the lift forces generated by the wind are insufficient. In Region 2, the wind turbine operates in MPPT mode. MPPT is a control technique for the optimisation of energy extraction from the wind. It op-

erates by continuously adjusting the turbine's rotor speed and blade pitch to find the ideal operating point where the turbine generates the maximum power from the available wind. By dynamically adapting to changing wind

Table 2.2: Blade structural Properties

Property	Value
Length (w.r.t. Root Along Preconed Axis)	61.5 m
Mass Scaling Factor	4.536%
Overall (Integrated) Mass	17,740 kg
Second Mass Moment of Inertia (w.r.t. Root)	11,776,047 kg·m ²
First Mass Moment of Inertia (w.r.t. Root)	363,231 kg·m
CM Location (w.r.t. Root along Preconed Axis)	20.475 m
Structural-Damping Ratio (All Modes)	0.477465%

Table 2.3: Nacelle and Hub Properties

Property	Value
Elevation of Yaw Bearing above Ground	87.6 m
Vertical Distance along Yaw Axis from Yaw Bearing to Shaft	1.96256 m
Distance along Shaft from Hub Center to Yaw Axis	5.01910 m
Distance along Shaft from Hub Center to Main Bearing	1.912 m
Hub Mass	56,780 kg
Hub Inertia about Low-Speed Shaft	115,926 kg m ²
Nacelle Mass	240,000 kg
Nacelle Inertia about Yaw Axis	2,607,890 kg m ²
Nacelle CM Location Downwind of Yaw Axis	1.9 m
Nacelle CM Location above Yaw Bearing	1.75 m
Equivalent Nacelle-Yaw-Actuator Linear-Spring Constant	9e9 Nm/rad
Equivalent Nacelle-Yaw-Actuator Linear-Damping Constant	1.9e7 Nm/(rad/s)
Nominal Nacelle-Yaw Rate	0.3°/s

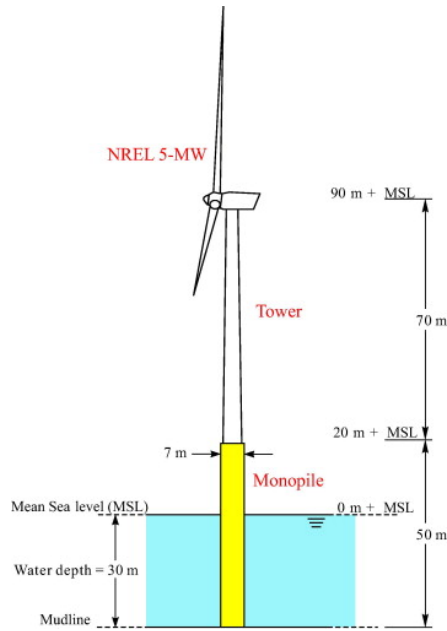


Figure 2.4: NREL 5 MW wind turbine monopile structure [41]

Table 2.4: Tower properties

Property	Value
Height above Ground	87.6 m
Overall (Integrated) Mass	347,460 kg
CM Location (w.r.t. Ground along Tower Centerline)	38.234 m
Structural-Damping Ratio (All Modes)	1%

conditions, MPPT ensures that the turbine operates at its peak efficiency, maximising energy production while safeguarding the turbine from potential damage due to overspeed or inefficient operation. This process enables wind turbines to harvest the most energy possible from varying wind conditions, enhancing their overall performance and power output. Region 2.5 is the linear transition between Regions 2 and 3. In Region 3, the wind speeds are higher than the nominal wind speed. In this region, the torque, speed and power are limited using control methods in order to avoid overloading of the drivetrain components. In case the wind speed exceeds 25 m/s, the

wind turbine is in the cut-out region and is shut down to prevent damage or failure.

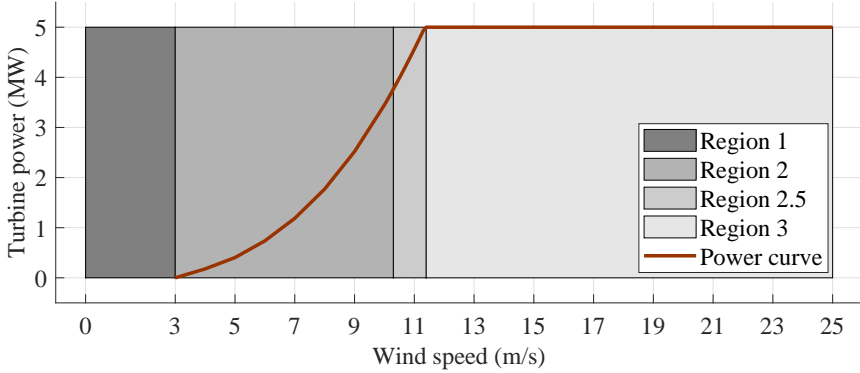


Figure 2.5: Power curve of a 5 MW wind turbine

Figure 2.6 shows the power coefficient C_p vs tip-speed ratio (TSR) curve of the turbine. This curve is obtained by simulating the turbine under different wind conditions ranging from 3 m/s to 25 m/s. The C_p and TSR values are averaged for each step in the steady state. The operation of the wind turbine follows this curve depending on the wind conditions and the reference power. In Figure 2.7, the C_p curve for one of the simulated cases is presented. The value of C_p during this test ranges between 0.49 and 0.26 based on the reference power variation for the duration of the test.

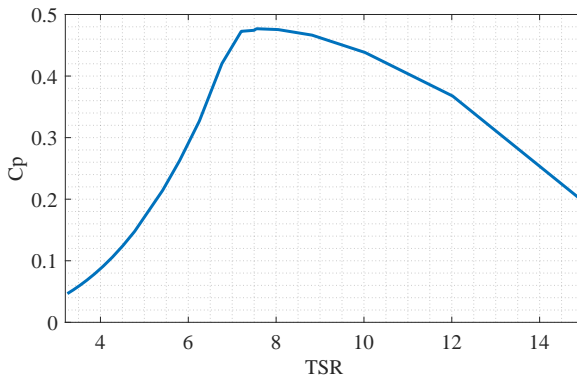


Figure 2.6: C_p -TSR curve of 5 MW wind turbine

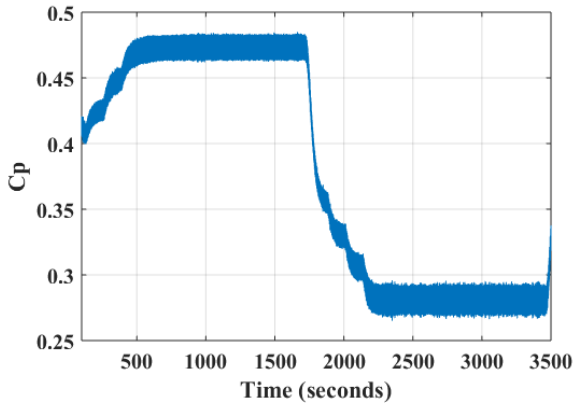


Figure 2.7: Power coefficient of simulated cases

2.2.2 Generator

Classical doubly fed induction generators (DFIG) have been dominant in wind energy. However, in recent times, direct-drive PMSG have gained more acceptability as a result of their reliable gearless functioning and high efficiency, especially at high power ratings. In its typical form, a PMSG has a stator with a three-phase winding and a rotor with permanent magnets. In gearless ‘direct-drive’ systems, the rotor consists of a high number of poles and is directly driven by the wind turbine. The stator winding observes a varying magnetic field which induces a back-emf. With this voltage, power can be delivered by the stator winding to the power-electronic converter. Figure 2.8 gives a schematic representation of a PMSG. The stator is represented by the windings a, b and c whereas the rotor is shown as a magnet with rotating d and q axis. The generator is modeled in the rotating dq reference frame. Figure 2.9 shows the equivalent scheme for the PMSG used in this thesis. R_s and R_c respectively represent the copper losses in the stator winding and the iron losses. L_q and L_d represent the d and q- axis inductance, respectively. Ω represents the rotor electrical speed in rad/sec. ψ_{RM} represents the rotor flux linkage. The generator parameters are listed in Table 2.5.

2.3 Control

There are two main control systems employed in the studies. These control systems associated with torque and pitch control of the wind turbine and PMSG are presented in the following subsections.

Table 2.5: Generator properties

Property	Specification
Rated power	5 MW
Rated speed	12.1 rpm
Efficiency	93%
Pole pairs	117
R_s	98.5 m Ω
L_q	5.86 mH

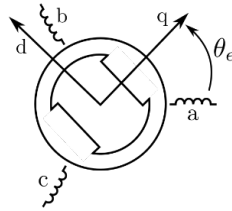


Figure 2.8: Reference axis in PMSG

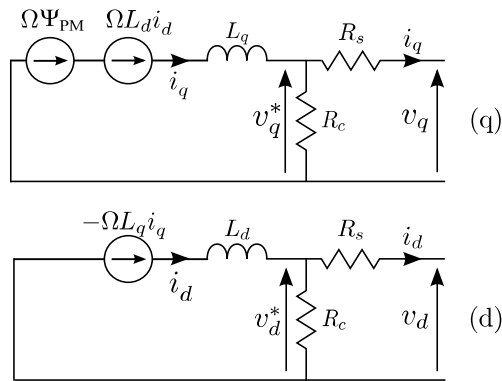


Figure 2.9: Equivalent scheme of a PMSG in the rotating reference frame

2.3.1 Torque control

The effectiveness of this study relies heavily on the accurate control of torque in the PMSG. To achieve this, Field Oriented Control (FOC) is employed. In addition to FOC, other control strategies such as model predic-

tive control (MPC) and sliding mode control (SMC) have been proposed for torque control in PMSG-based wind turbines. However, FOC remains one of the most popular control strategies due to its simplicity and robustness. FOC regulates the quadrature current component \hat{i}_q proportionally to the torque setpoint while keeping the direct current component \hat{i}_d at zero for field orientation. The torque control scheme is depicted in Figure 2.10, with the Proportional Integral (PI) controller's proportional and integral gains set at 0.0001. All symbols represent the numerical values of the quantities in SI units. At each time step, the PI controller generates a current signal based on a comparison between the reference power \hat{P} and actual power P . The reference power is determined by the grid frequency and the amount of contracted ancillary reserve. The PI controller's output is then converted to three-phase abc signals by using the inverse Park transformation, resulting in pulse width modulated (PWM) signals. The PI controller is configured to minimise the tracking error by minimising overshoot and settling time. Although the controller's performance varies with changing wind speeds and the rate of change of the reference power, it is capable of tracking the reference power with minimal error. It is worth noting that accurate torque control is crucial for PMSGs to operate efficiently and deliver maximum power output. Additionally, FOC has become increasingly popular due to its ability to precisely control torque and provide excellent dynamic performance.

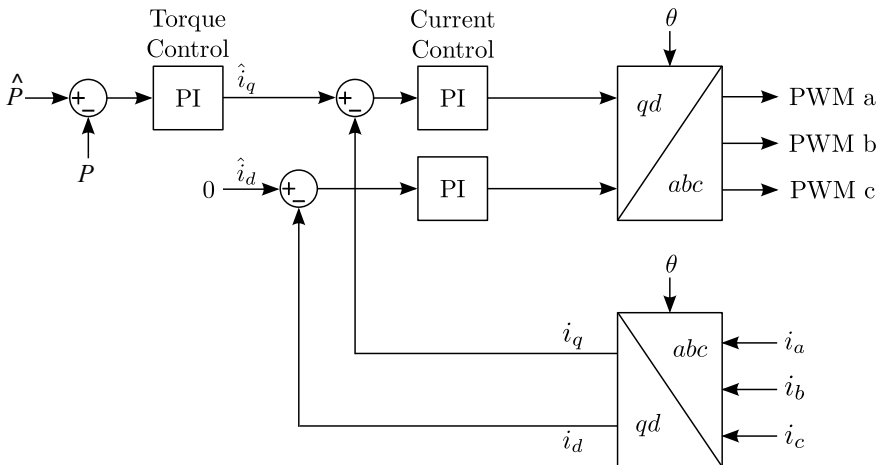


Figure 2.10: Field oriented control of the PMSG

2.3.2 Pitch control

The pitch control system developed in Simulink is integrated with the wind turbine model in FAST to ensure smooth operation. During each iteration of the simulation, the pitch control system transmits a pitch command to each of the three blades of the wind turbine. Figure 2.11 illustrates the block diagram of the pitch control system, which employs a proportional-integral (PI) controller with proportional and integral gains of 206.3 and 25, respectively. The PI controller continuously compares the reference rotor speed, Ω_{ref} , a preset parameter, with the actual rotor speed, Ω , at each time step. The gain scheduling technique utilises a dimensionless gain correction factor, G , defined as in (2.1) further in the text. The pitch angle, θ , plays a critical role in the gain scheduling process, and a tuning parameter, θ_d , is set to 0.055 radians to optimise its performance [41]. Furthermore, the pitch control system can dynamically adjust its parameters based on wind speed to maintain stable turbine operation, which is essential for maximising energy production.

$$G = \frac{1.6}{1 + \left(\frac{\theta}{2\theta_d}\right)} \quad (2.1)$$

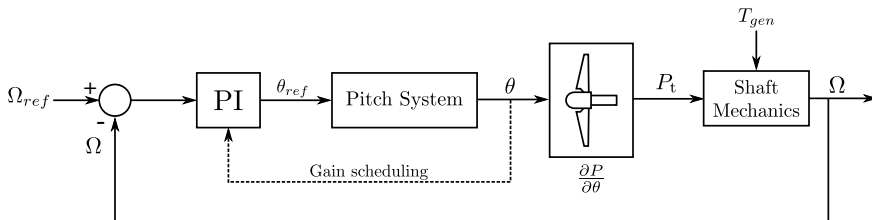


Figure 2.11: Pitch control of the wind turbine blades

2.4 Tests

The Belgian TSO Elia categorizes its grid frequency balancing services as:

- Frequency Containment Reserve (FCR)
- Automatic Frequency Restoration Reserve (AFRR)
- Manual Frequency Restoration Reserve (MFRR)

These names correspond to the classical terminology used for grid balancing services, i.e., Primary, Secondary and Tertiary reserve. The scope of this study lies within FCR, which is the primary frequency reserve. This service is contracted through two different frameworks setup by Elia, based on the generation capacity of the production units. These contracts are the Contract for the Injection of Production Units (CIPU) and non-CIPU. For a production unit to be eligible to provide FCR services, among other necessary conditions, it must qualify a pre-qualification test set up by Elia. On successful completion of this test, the production unit is eligible as an FCR provider for a duration of 5 years. Elia provides details of its synthetic frequency profile test in the public domain [18]. The focus of this test is on the 200 mHz type service which implies frequency support within the range of 49.8-50.2 Hz of grid frequency. The time series of the pre-qualification test, as provided by Elia, is enlisted in Table 2.6 and is followed to simulate this test in the developed model. In order for a wind turbine to be able to provide FCR it must run at a lower power output than its optimal operating point, i.e., the turbine must be curtailed. This is necessary since it allows the wind turbine to regulate the output power both downwards and upwards in order to provide a symmetric 200 mHz control. Since the used wind turbine model has a nominal power of 5 MW, the wind turbine is operated at 4 MW and ramps up and down within the range of 3-5 MW. This implies a non-CIPU contract of 1 MW for the symmetric 200 mHz type service. For all 4 wind types, the average wind speed is above the rated value. In this manner, the rated power can be achieved at all times. However, the power set point is set at 4 MW in order to provide a 1 MW primary reserve band. The function to generate the reference power is defined as in (2.2). P_{ref} is the reference power and P_{PQT} is the power signal of the pre-qualification test, which is time dependent, with values ranging from -1 MW to +1 MW based on the simulated test.

$$P_{ref} = 4 \text{ MW} + P_{PQT}(t) \quad (2.2)$$

This test was conducted for 4 different levels of wind:

- Wind type A (high turbulence)
- Wind type B (medium turbulence)
- Wind type C (low turbulence)
- Steady wind

The entire test has a duration of 3500 sec. Figure 2.12 shows a sample section of wind speed data between 500-550 seconds. The turbulence in-

tensity of the different wind types can be observed from the figure. These wind profiles are generated using TurbSim, a tool developed by NREL.

Figure 2.13 shows the output power from the tests conducted for different wind turbulence levels. The section of these results is panned in the interval between 600-800 seconds. The effect of increasing the wind turbulence level can be seen clearly. For the highest turbulence level (wind type A) a maximum variation in output power is observed, whereas, for steady wind, a more stable output power is achieved. Figure 2.14, shows the same results in an overlaid fashion. Figure 2.15 shows the probability density function for the controller error values for the different wind types. This figure is used to analyze the performance of the controller. It can be seen here that at high turbulence levels, the absolute mean error and standard deviation are the highest, i.e., 0.2241% and 0.3024 respectively. In lower turbulent wind tests, these values are expectedly lower.

2.5 Conclusion

To study the applicability of the developed control design in an actual power network, the tests simulated are based on a pre-qualification test set up by the Belgian TSO. The results obtained through the simulations prove the capability of wind turbines to provide primary frequency control with a band of 1 MW. The tests were conducted for various wind profiles, ranging from steady wind to a very high turbulence. The control design developed for the tests performed effectively for all the tests. One crucial factor in the simulations is the control algorithm. This discrete control design needs to be matched with the small time step of the model. Also the control output needs to be highly efficient. In order to test these properties of the controller, the model is subjected to different levels of turbulent winds. Although the error level increases with the increasing turbulence intensity, the controller still performs with low absolute error percentage never exceeding 0.2241%. With this research, a controller design has been developed specifically to analyze the pre-qualification of wind turbines as an FCR provider.

Table 2.6: Time series test for service type 200 mHz

Step	Δ sec	From t =	To t =	Step	Δ sec	From t =	To t =
Upward direction				Downward direction			
Ramp-up	8	0	8	Ramp down	8	0	8
Step up 1	120	8	128	Step down 1	120	8	128
Ramp up	8	128	136	Ramp down	8	128	136
Step up 2	120	136	256	Step down 2	120	136	256
Ramp up	8	256	264	Ramp down	8	256	264
Step up 3	120	264	384	Step down 3	120	264	384
Ramp up	8	384	392	Ramp down	8	384	392
Full power up	1320	392	1712	Full power down	1320	392	1712
Ramp down	30	1712	1742	Ramp up	30	1712	1742

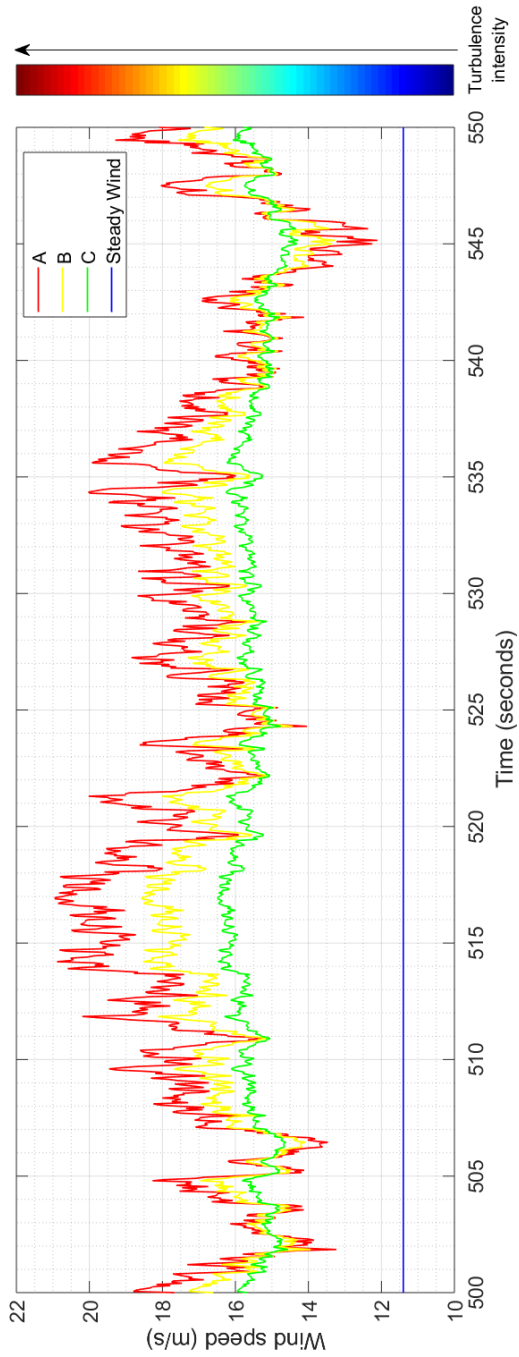


Figure 2.12: Turbulence intensity level for type A, B, C wind

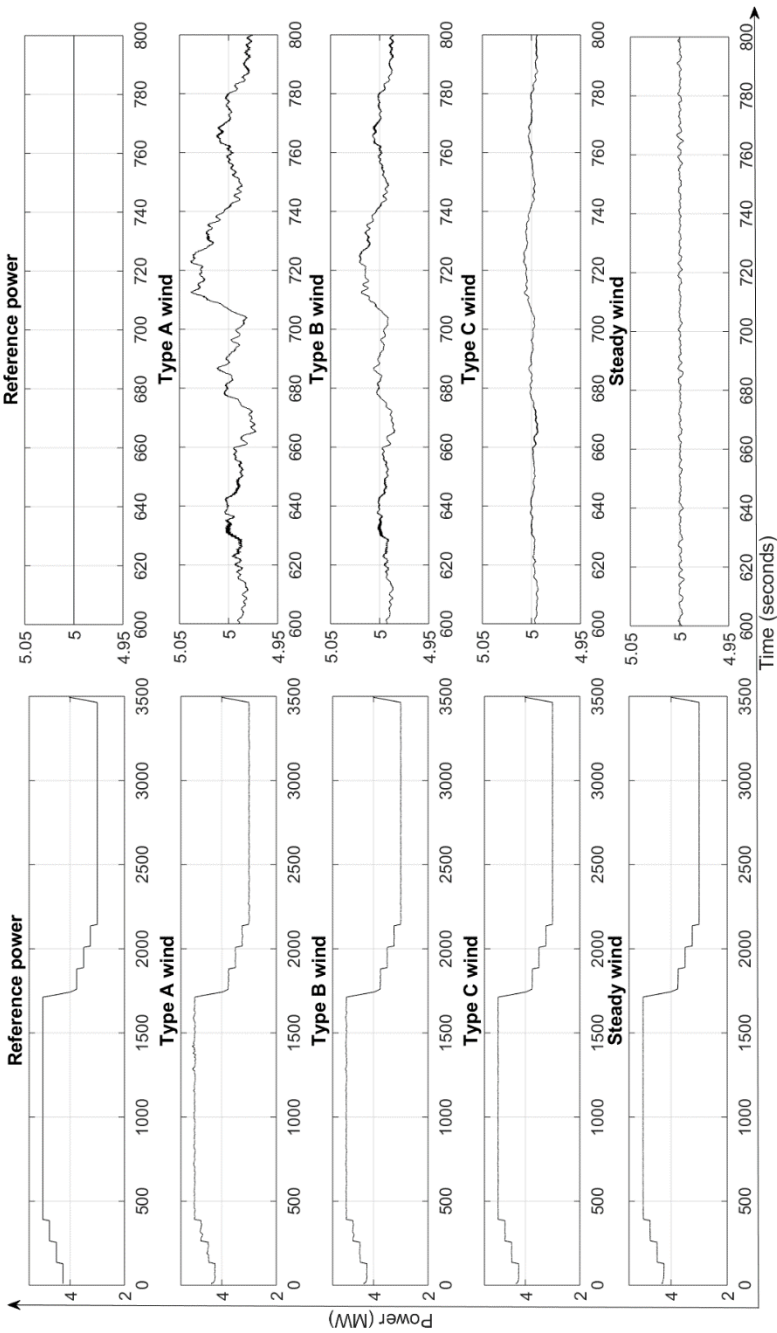


Figure 2.13: Output power plots for different turbulence test

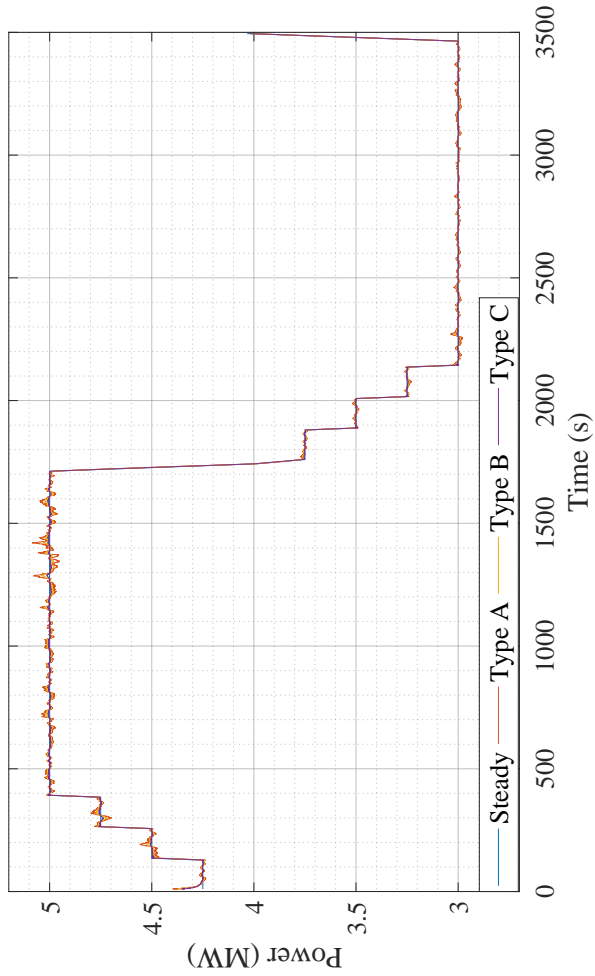


Figure 2.14: Overlaid output power plots for different turbulence test

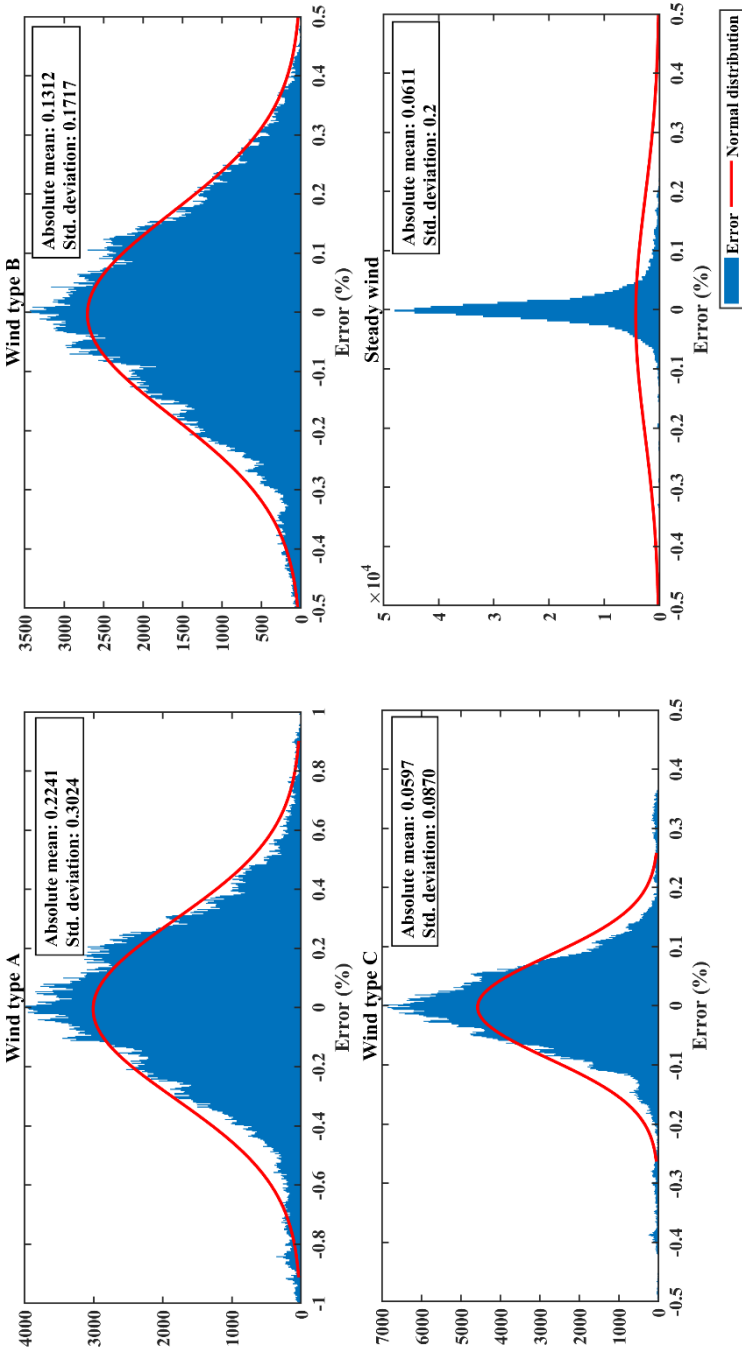


Figure 2.15: Probability density function and normal distribution plots for wind type A, B, C and steady wind

References

- [1] N. Singh, J. De Kooning, and L. Vandeveld, "Simulation of the primary frequency control pre-qualification test for a 5MW wind turbine," in 2020 IEEE/PES Transmission and Distribution Conference and Exposition (T&D), Chicago, IL, USA (virtual event), 2020, doi: 10.1109/td39804.2020.9299921
- [2] Q. Long; A. Celna; K. Das; P. Sørensen. Fast Frequency Support from Hybrid Wind Power Plants Using Supercapacitors. *Energies* 2021, 14, 3495. doi:10.3390/en14123495
- [3] B. Lian, A. Sims, D. Yu, C. Wang and R. W. Dunn, "Optimizing LiFePO₄ Battery Energy Storage Systems for Frequency Response in the UK System," in *IEEE Transactions on Sustainable Energy*, Jan. 2017, doi: 10.1109/TSTE.2016.2600274.
- [4] D. Fernandez-Muñoz, I. Guisandez, J. I. Perez-Diaz, M. Chazarra, A. Fernandez-Espina and F. Burke, "Fast Frequency Control Services in Europe," 2018 15th International Conference on the European Energy Market (EEM), 2018, doi: 10.1109/EEM.2018.8469973
- [5] ENTSO-E, "Survey on ancillary services procurement, balancing market design 2016," March, 2017, Available at: <https://www.entsoe.eu/publications/market-reports/> [Accessed: September 2023]
- [6] J. Daković, P. Ilak, T. Baškarad, M. Krpan and I. Kuzle, "Effectiveness of wind turbine fast frequency response control on electrically distanced active power disturbance mitigation," *Mediterranean Conference on Power Generation, Transmission, Distribution and Energy Conversion (MEDPOWER 2018)*, 2018, doi: 10.1049/cp.2018.1923.
- [7] H. Kim, J. Lee and G. Jang, Novel Coordinated Control Strategy of BESS and PMSG-WTG for Fast Frequency Response. *Appl. Sci.* 2021, 11, 3874. <https://doi.org/10.3390/app11093874>
- [8] Xilin Zhao, Zhenyu Lin, Bo Fu, Sili Gong, Research on frequency control method for micro-grid with a hybrid approach of FFR-OPPT and pitch angle of wind turbine, *International Journal of Electrical Power & Energy Systems*, Volume 127, 2021, 106670, ISSN 0142-0615, <https://doi.org/10.1016/j.ijepes.2020.106670>.

- [9] R. Heydari, M. Savaghebi and F. Blaabjerg, "Fast Frequency Control of Low-Inertia Hybrid Grid Utilizing Extended Virtual Synchronous Machine," 2020 11th Power Electronics, Drive Systems, and Technologies Conference (PEDSTC), 2020, doi: 10.1109/PEDSTC49159.2020.9088504.
- [10] E. Rakhshani, J. L. Rueda Torres, P. Palensky and M. d. van Meijden, "Determination of Maximum Wind Power Penetration Considering Wind Turbine Fast Frequency Response," 2019 IEEE Milan PowerTech, 2019, doi: 10.1109/PTC.2019.8810492.
- [11] N. Kayedpour, A. Ebneali Samani, J. De Kooning, L. Vandevelde, and G. Crevecoeur, "Model predictive control with a cascaded Hammerstein neural network of a wind turbine providing frequency containment reserve," IEEE Transactions on Energy Conversion, 2021, doi: 10.1109/tec.2021.3093010
- [12] N. Singh, J. D. M. De Kooning, and L. Vandevelde, 2020. Dynamic wake analysis of a wind turbine providing frequency containment reserve in high wind speeds. In: IET Renewable Power Generation, doi: 10.1049/rpg2.12455
- [13] S. Li, T. A. Haskew, R. P. Swatloski and W. Gathings, "Optimal and Direct-Current Vector Control of Direct-Driven PMSG Wind Turbines," in IEEE Transactions on Power Electronics, May 2012, doi: 10.1109/TPEL.2011.2174254.
- [14] X. Zeng, T. Liu, S. Wang, Y. Dong and Z. Chen, "Comprehensive Coordinated Control Strategy of PMSG-Based Wind Turbine for Providing Frequency Regulation Services," in IEEE Access, 2019. doi: 10.1109/ACCESS.2019.2915308.
- [15] Z. Zhang, Y. Zhao, W. Qiao and L. Qu, "A Discrete-Time Direct Torque Control for Direct-Drive PMSG-Based Wind Energy Conversion Systems," in IEEE Transactions on Industry Applications. 2015, doi: 10.1109/TIA.2015.2413760.
- [16] Y. Inoue, S. Morimoto and M. Sanada, "Control method for direct torque controlled PMSG in wind power generation system," 2009 IEEE International Electric Machines and Drives Conference, 2009, doi: 10.1109/IEMDC.2009.5075360.
- [17] N. Abdolghani, J. Milimonfared and G.B. Gharehpetian. "A Direct Torque Control Method for CSC Based PMSG Wind Energy Conversion Systems." Renewable Energy & Power Quality Journal (2012).

- [18] Elia, "General Framework for Frequency Containment Reserve Service by Non-CIPU resources". [online] Available at: <https://www.elia.be/>
- [19] J. Van de Vyver, J. De Kooning, B. Meersman, L. Vandeveldel, and T. Vandoorn, "Droop control as an alternative inertial response strategy for the synthetic inertia on wind turbines," *IEEE Transactions on Power Systems*, 2016, doi: 10.1109/tpwrs.2015.2417758
- [20] G. C. Tarnowski, P. C. Kjær, P. E. Sørensen and J. Østergaard, "Variable speed wind turbines capability for temporary over-production," 2009 IEEE Power & Energy Society General Meeting, Calgary, AB, Canada, 2009, doi: 10.1109/PES.2009.5275387.
- [21] J. Aho, P. Fleming and L. Y. Pao, "Active power control of wind turbines for ancillary services: A comparison of pitch and torque control methodologies," 2016 American Control Conference (ACC), Boston, MA, USA, 2016, doi: 10.1109/ACC.2016.7525114.
- [22] A. Žertek, G. Verbič and M. Pantoš, "Participation of DFIG wind turbines in frequency control ancillary service by optimized rotational kinetic energy," 2010 7th International Conference on the European Energy Market, Madrid, Spain, 2010, doi: 10.1109/EEM.2010.5558666.
- [23] C. Nikolakakos, U. Mushtaq, P. Palensky and M. Cvetković, "Improving Frequency Stability with Inertial and Primary Frequency Response via DFIG Wind Turbines equipped with Energy Storage System," 2020 IEEE PES Innovative Smart Grid Technologies Europe (ISGT-Europe), The Hague, the Netherlands, 2020, doi: 10.1109/ISGT-Europe47291.2020.9248807.
- [24] H. Karbouj and Z. H. Rather, "Voltage Control Ancillary Service From Wind Power Plant," in *IEEE Transactions on Sustainable Energy*, April 2019, doi: 10.1109/TSTE.2018.2846696.
- [25] N. R. Ullah, K. Bhattacharya and T. Thiringer, "Wind Farms as Reactive Power Ancillary Service Providers—Technical and Economic Issues," in *IEEE Transactions on Energy Conversion*, Sept. 2009, doi: 10.1109/TEC.2008.2008957.
- [26] E. Gatavi, A. Hellany, M. Nagrial and J. Rizk, "An integrated reactive power control strategy for improving low voltage ride-through capability," in *Chinese Journal of Electrical Engineering*, Dec. 2019, doi: 10.23919/CJEE.2019.000022.

- [27] Z. Dong, Z. Li, L. Du, Y. Liu and Z. Ding, "Coordination Strategy of Large-Scale DFIG-Based Wind Farm for Voltage Support With High Converter Capacity Utilization," in *IEEE Transactions on Sustainable Energy*, April 2021, doi: 10.1109/TSTE.2020.3047273.
- [28] X. Cheng et al., "A Coordinated Frequency Regulation and Bidding Method for Wind-Electrolysis Joint Systems Participating Within Ancillary Services Markets," in *IEEE Transactions on Sustainable Energy*, July 2023, doi: 10.1109/TSTE.2022.3233062.
- [29] S. A. Hosseini et al., "Impact Of Fast Wind Fluctuations On The Profit Of A Wind Power Producer Jointly Trading In Energy And Reserve Markets," *The 9th Renewable Power Generation Conference (RPG Dublin Online 2021)*, Online Conference, 2021, doi: 10.1049/icp.2021.1386.
- [30] N. Singh, J.D.M. De Kooning and L. Vandevelde: Dynamic wake analysis of a wind turbine providing frequency support services. *IET Renewable Power Generation* 16, 1853–1865 (2022). doi:10.1049/rpg2.12455
- [31] N. Kayedpour, J. D. M. De Kooning, A. E. Samani, F. Kayedpour, L. Vandevelde and G. Crevecoeur, "An Optimal Wind Farm Operation Strategy for the Provision of Frequency Containment Reserve Incorporating Active Wake Control," in *IEEE Transactions on Sustainable Energy*, 2023 (early access), doi: 10.1109/TSTE.2023.3288130.
- [32] Energy Storage Applications Summary, 2020. European Association for Storage of Energy. [online] Available at: <https://ease-storage.eu/wp-content/uploads/2020/06/ES-Applications-Summary.pdf> [Accessed 6 May 2022]
- [33] M. Singh et al., Simulation for wind turbine generators – with fast and MATLAB-Simulink modules, 2014. doi:10.2172/1130628
- [34] Z. Zhang, Z. Cui, Z. Zhang, R. Kennel and J. Rodríguez, "Advanced Control Strategies for Back-to-Back Power Converter PMSG Wind Turbine Systems," 2019 IEEE International Symposium on Predictive Control of Electrical Drives and Power Electronics (PRECEDE), Quanzhou, China, 2019, doi: 10.1109/PRECEDE.2019.8753366.
- [35] K. E. Okedu, "Improving the performance of PMSG wind turbines during grid fault considering different strategies of fault current limiters," *Frontiers in Energy Research*, vol. 10, 2022. doi:10.3389/fenrg.2022.909044

- [36] J. Jonkman. FAST (Version V8) [Software]. NREL. <https://www.nrel.gov/wind/nwtc/fastv8.html>
- [37] J. M. Jonkman, G. J. Hayman, B. J. Jonkman, R. R. Damiani, and R. E. Murray AeroDyn v15 User's Guide and Theory Manual, NREL. URL: <https://www.nrel.gov/wind/nwtc/assets/pdfs/aerodyn-manual.pdf>
- [38] J. Jonkman, S. Butterfield, W. Musial, and G. Scott, "Definition of a 5-MW Reference Wind Turbine for Offshore System Development," 2009.
- [39] Jonkman, J., Butterfield, S., Passon, P., Larsen, T., Camp, T., Nichols, J., Azcona, J., and Martinez, A., "Offshore Code Comparison Collaboration within IEA Wind Annex XXIII: Phase II Results Regarding Monopile Foundation Modeling," 2007 European Offshore Wind Conference & Exhibition, 4–6 December 2007, Berlin, Germany
- [40] Lindenburg, C., "Aeroelastic Modelling of the LMH64-5 Blade," DOWEC Dutch Offshore Wind Energy Converter 1997–2003 Petten, the Netherlands: Energy Research Center of the Netherlands, December 2002.
- [41] A. E. Samani, J. D. M. De Kooning, N. Kayedpour, N. Singh, and L. Vandeveld, "The Impact of Pitch-To-Stall and Pitch-To-Feather Control on the Structural Loads and the Pitch Mechanism of a Wind Turbine," *Energies*, Sep. 2020, doi: 10.3390/en13174503.

3

Dynamic Wake Analysis of a Wind Turbine Providing Frequency Support Services

The participation of wind farms in providing ancillary services is an asset for the power system and one way to maintain a strong grid with the increasing penetration of renewable energy sources. It can however be challenging for the wind farms to efficiently participate in grid frequency support services, especially for primary reserve services. The reason behind this is the requirement of quick activation and deactivation of power reserve margin for services such as FCR and FFR. A full activation of the contracted reserve is required within seconds of a grid frequency dip. A sudden change in wind turbine dynamics is expected to have an impact on the wake behind the wind turbine. For the study presented in this chapter fast acting wind turbine control system is developed based on the control design presented in Chapter 2. Additionally, the capability of developed wind turbines controllers to follow primary reserve services are also tested. FFR and FCR services are simulated for a range of frequency designs, these include both synthetic and actual grid frequencies. The synthetic frequency profiles are designed to replicate both fast and slow frequency varia-

tions in order to analyse the impact on wake behaviour. The simulations are performed for low and high wind speed including constant as well as turbulent winds.

The rest of this chapter is structured as follows: Section 3.1 presents a literature review of existing wake studies. Section 3.2 presents the wind turbine, generator and wake model used in this study. Section 3.3 presents a detailed description of the two ancillary services FCR and FFR, tested in this study. The data of grid frequency and different wind field data used in the study are presented in Section 3.4. The FCR, FFR and pitch control methods are described in Section 3.5. The results and discussion from the study are presented in Section 3.6. Finally, the conclusion is drawn in Section 3.7. The content of this chapter has been published in [1]

3.1 Introduction

In order to provide ancillary services with a wind turbine, its power output must vary more dynamically, especially when providing short-term grid balancing services such as inertial response, FCR and FFR. However, these dynamic power variations impact the wake effect, which in turn could impact neighbouring turbines. The study of wake effects is even more significant for wind farms with high capacity density. Countries like Belgium and Germany have higher capacity densities of offshore wind farms as compared to the European average. The reason for this high density in Belgium is the regulatory framework. Due to the limited space resources in the Belgian North Sea, the obligated policy demands the use of space granted as intensively as possible [2].

The wind farms located in close proximity generate wake effects that reduce the downwind wind speeds. Studies have shown that these effects can extend over 50 km resulting in economic losses for the wind farms owners [3]. Methods have been developed in order to minimise the impact of the wake and optimise the wind farm power output. These methods use algorithms developed to maximise the annual energy production (AEP) of wind farms [4]. One such approach utilises optimised yaw alignment that deflects wakes away from downstream turbines and wind farms [5]. Such measures have shown to improve the wind speed by up to 13%. Studies have been conducted to demonstrate the significance of wake effects in influencing the inertial response capacity of a wind farm [6]. However, a research gap is seen for studies on wake effects produced by wind turbines providing FCR and FFR.

To this end, the scope of this research lies in the study of dynamic wake behaviour of a wind turbine providing FCR and FFR. The study presented in this chapter uses a detailed wind turbine model to simulate FCR and FFR based control. The influence of the control strategy on the wake behind the turbine at several locations behind the wind turbine is observed. The model uses a conventional PI controller to generate blade pitch commands. The torque is controlled by a grid frequency following algorithm. A reference power is generated based on the frequency and the power output is adjusted accordingly. Different frequency profile designs have been used in the presented simulations.

The chapter is organised as follows: Section 3.2 presents the models used for the simulations in this study. The two ancillary services investigated in the study are discussed in Section 3.3. The frequency and wind inputs to the model are presented in Section 3.4. The different control systems used in this study are presented in Section 3.5. The tests performed and the results

from this study are presented in Section 3.6. Discussion and conclusions are drawn in Section 3.7.

3.2 Model description

The simulation setup consists of a wind turbine model in FAST, a generator model and the control system in MATLAB Simulink, as presented in Section 2.2. These models are interconnected for a co-simulation with loop communications at each time-step of the simulation. Additionally, the data is post-processed using a wake model as presented in the following sections.

3.2.1 Wake model

The Jensen wake model is one of the oldest and most popular models used in wake studies [7]. It is a simple model to analyse the wake effect. In its original form, it does not account for the wind turbine dynamics. However, for this study, a robust yet computationally simple wake model that accounts for wind turbine dynamics was required. Therefore a modified Jensen model, i.e., Jensen-Katic, is used in this study [8]. This model allows to incorporate the actual characteristics of the turbine, thus different control behaviours of the machine can be modelled. Figure 3.1 schematically shows the wake. The free flow ambient speed is denoted by U . The wake behind the turbine is assumed to have an initial diameter equal to the rotor diameter D . The wake diameter at a distance X is defined as D_w . The velocity deficit V at a given distance X depends on the thrust coefficient c_t , and is defined as:

$$V = U \left(1 - \frac{1 - \sqrt{1 - c_t}}{\left(1 + \frac{2kX}{D}\right)^2} \right) \quad (3.1)$$

3.3 Ancillary services

A range of different ancillary services are offered for production units by TSOs in different countries. In this research two kinds of primary reserve ancillary services, FCR and FFR, as presented in Section 1.3.1 are tested.

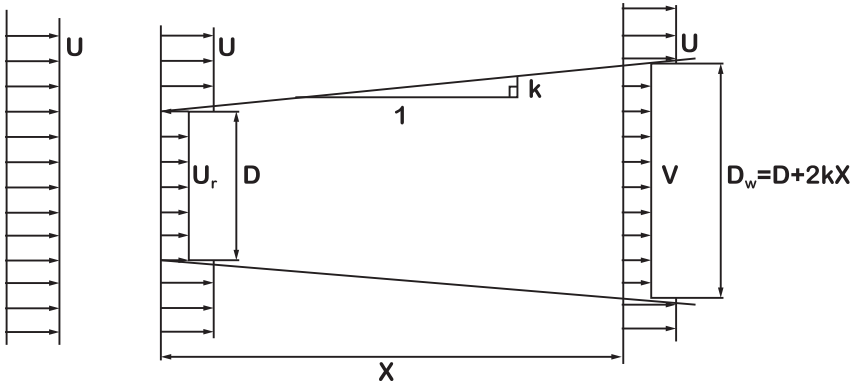


Figure 3.1: Wake schematic

3.4 Data

The simulations presented in this study require two essential datasets. The developed FCR and FFR based control models require a frequency input on every time step. Additionally, to be able to run a wind turbine model in FAST, a fitting wind field model is necessary.

3.4.1 Frequency data

The simulations performed for FCR services in this work are performed for different frequency profiles. These data form an important input for the controller as it determines the reference power for the frequency following controller. The first frequency dataset is an artificially generated frequency pattern with a sinusoidal ripple, with an amplitude of 0.2 Hz and 12 different periods of 1 s, 5 s, 10 s, 25 s, 50 s, 100 s, 150 s, 200 s, 250 s, 400 s, 500 s and 700 s respectively. Figure 3.2 shows a sample of these data. The frequency is sampled at the same rate as the time step of simulations. This artificial frequency is used to investigate the propagation of FCR dynamics in the wake. Moreover, by simulating the different scenarios with varying frequency of oscillation, the aim is to assess the varying magnitude of propagation in the wake.

The second frequency dataset is actual grid frequency dataset of the European synchronous grid. The frequency retrieved from the source is sampled every 0.5 seconds [9]. However, to adjust the frequency to the simulation time-step, the frequency data are interpolated. Figure 3.3 presents a section of frequency data used in the simulations. The frequency data are

from an extreme event that occurred on the 10th of January 2019, 21:02 CET. During this event, the continental European power system stretching across 26 countries witnessed the largest absolute frequency deviation since 2006 [10]. During this rare event, the frequency dropped to 49.8 Hz. The reason for choosing this event is to clearly observe the impact of changing grid frequency on a turbine providing FCR.

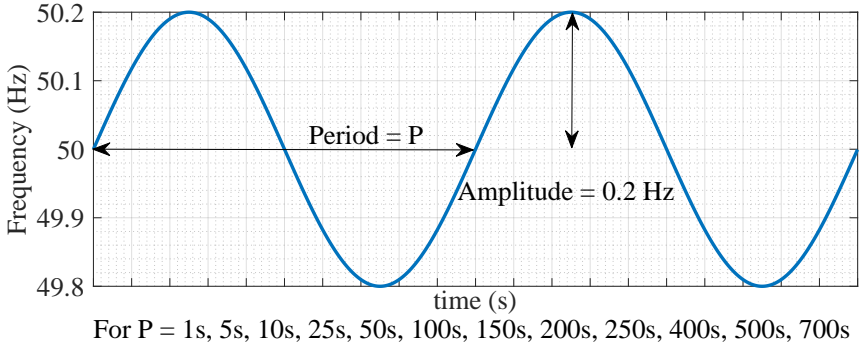


Figure 3.2: Frequency with sinusoidal ripples

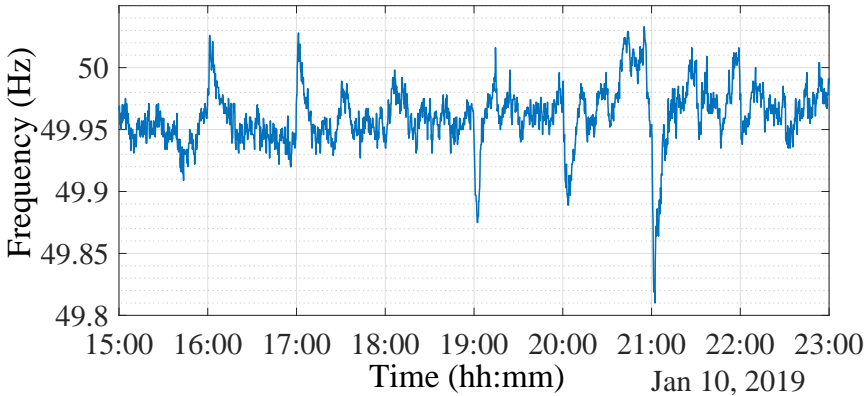


Figure 3.3: Frequency data extreme event

3.4.2 Wind field

In FAST, different wind profile input methods are available and can be used for analysis. For the simulations performed in this study two different wind profiles are used. These are presented in the following.

3.4.2.1 Constant wind field

In the simulations presented in this work, steady wind profiles of 7 m/s and 12 m/s are used. These wind speeds are chosen to study the behaviour of the wake in both low and high winds, respectively.

3.4.2.2 Turbulent wind field

A three-dimensional turbulent wind field is used to analyse the wake effect of a wind turbine providing frequency support. The TurbSim Risø smooth-terrain model (SMOOTH) based on [11] and [12] is used to generate the turbulent wind data. The wind field has a grid height and width of 160 m. The three components of the wind field are presented in Figure 3.4, Figure 3.5 and Figure 3.6. The inertial reference frame of these three components: The u-component is along the positive X-axis (downwind). The v-component is along positive Y-axis (to the left when looking along X). The w-component up, along positive Z-axis (opposite gravity.) The reference height of the wind field is chosen similar to the height of the wind turbine rotor hub at 90 m. The mean wind speed is 20 m/s and the turbulence intensity is 5%. The wind speed values within the simulated time ranges from 16.45 m/s to 23.1 m/s.

3.5 Control

The basic torque and pitch control strategy used for this study is as presented in Section 2.3. Specific control strategies regarding FCR and FFR services are presented in the following subsections.

3.5.1 FCR control

The maximum available power P_{max} that can be harnessed by the turbine is dependent on the wind speed and is defined by the power curve as presented in Figure 2.5. In order to provide an FCR reserve power P_{FCR} equivalent to 20% of P_{max} , the wind turbine is operated at a base power equal to 80% of P_{max} . The turbine ramps up and down within 60% to 100% of P_{max} based on the grid frequency. In this manner, there is enough capacity at all times to follow the grid frequency in the specified range. The control algorithm to generate the reference power based on the grid frequency is defined in Algorithm 1.

Figure 3.7 shows the generator power under PLC and FCR based controls. The generated power is plotted on the left y-axis and the grid fre-

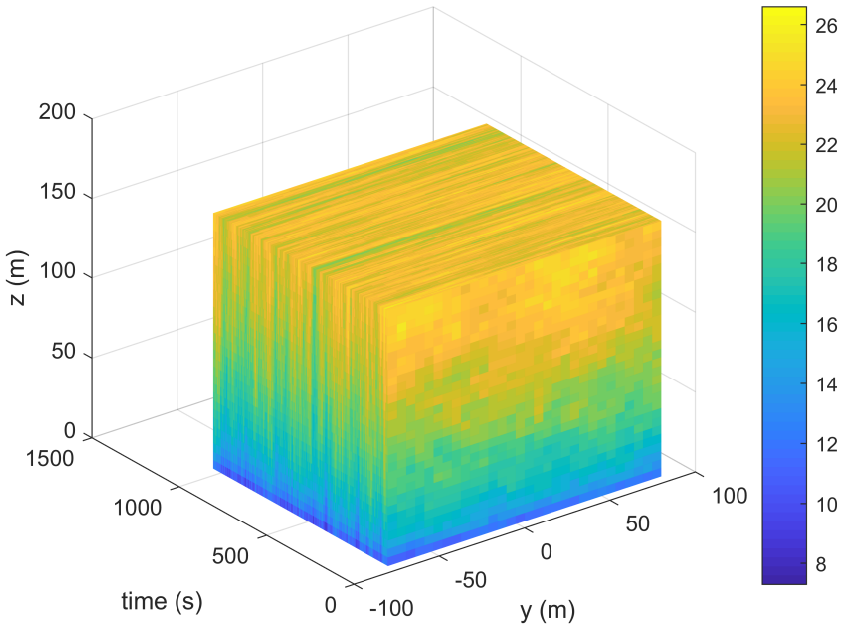


Figure 3.4: u -component of wind speed (m/s)

quency on the right y -axis. The case considered here has a steady wind speed input of 12 m/s. It can be seen that the power output under PLC control is constant at 5 MW, whereas, with FCR control, the generator power varies with the changing grid frequency. The effect of changing grid frequency can be seen on the power output. The controller works with a satisfactory tracking performance, following the reference power with low error.

3.5.2 FFR control

There are three different types of FFR services as presented in Table 1.1. These service require a fast response time to adjust the power output to the changing grid frequency. As a result, the controller presented in Section 3.5.1, in its current form is unable to follow these rapid variations in the reference power signal. Therefore, the simulations for FFR service are performed in FAST.Farm.

There is no control method in Fast.Farm that can include the effect of changing grid frequency on the power output of a wind turbine providing frequency support services. The sole control option is the torque control built within the program. For this reason, the control system in FAST.Farm

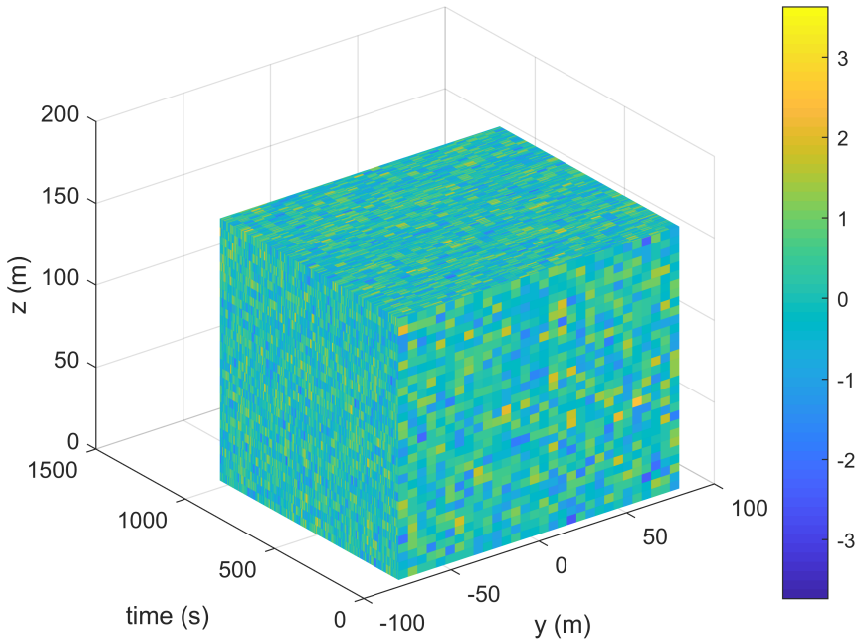


Figure 3.5: *v*-component of wind speed (m/s)

has been modified to operate the turbine with FFR based control. The operation is modified such that instead of providing a constant power, the power output is based on the changing input grid frequency. This control is defined in the following equations:

$$P_{ref} = P_{base} + P_{freq}(t) \quad (3.2)$$

where,

$$P_{freq} = (50.8 - f)P_{FCR} \quad (3.3)$$

Here, the reference power P_{ref} is calculated as the sum of base power P_{base} and a time varying term $P_{freq}(t)$. Furthermore, $P_{freq}(t)$ is defined by the changing grid frequency and the contracted FCR bid P_{FCR} .

3.6 Results and discussion

Using the aforementioned data, models and control systems, several tests are performed for different wind profiles and frequencies to analyse the dynamic impact of ancillary service provision on the turbine wake. This

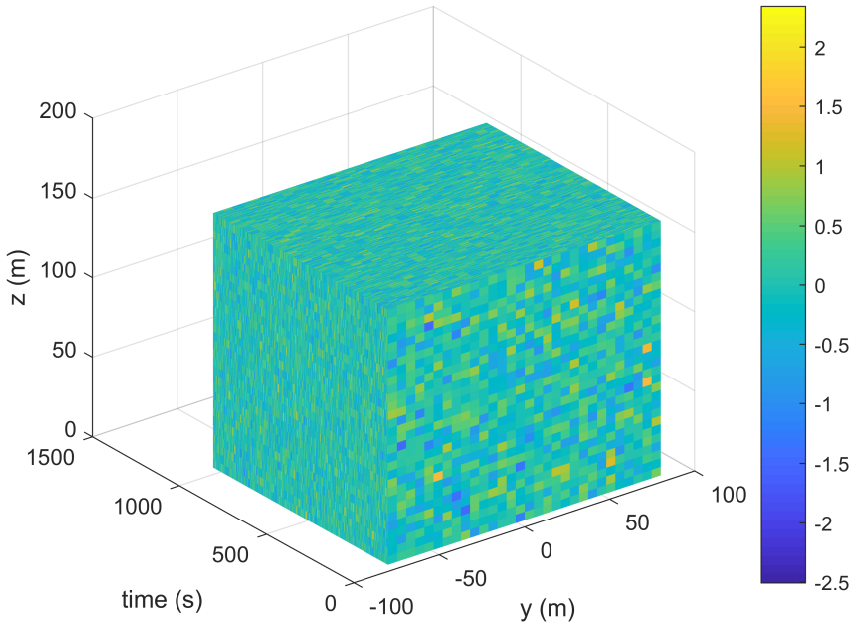


Figure 3.6: w -component of wind speed (m/s)

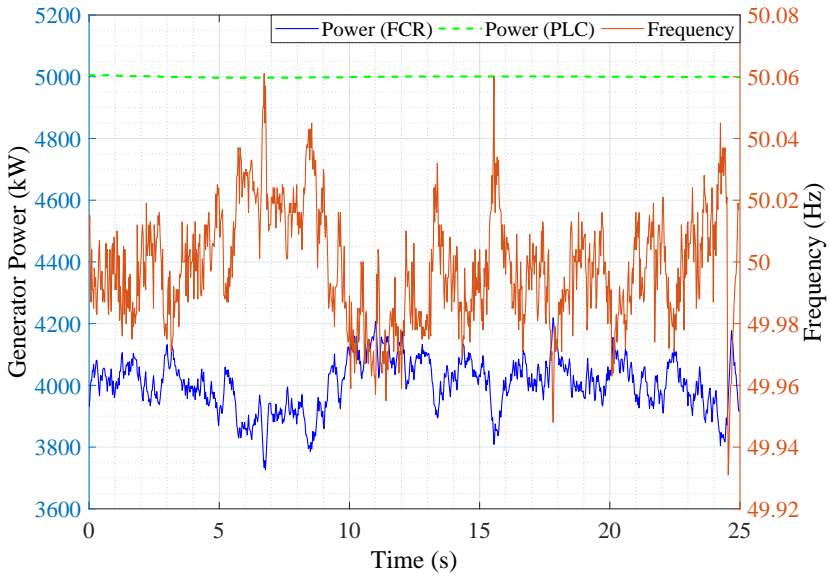


Figure 3.7: Generator PLC and FCR power

Algorithm 1 Reference power decision

Require: $P_{\max} \geq P_{\text{ref}}$
if $f \leq 49.8 \text{ Hz}$ **then**
 $P_{\text{ref}}(t) = P_{\max}$
else if $49.80\text{Hz} < f < 49.99 \text{ Hz}$ **then**
 $P_{\text{ref}}(t) = P_{\max} + (50.80 - f)$
else if $49.99\text{Hz} < f < 50.01\text{Hz}$ **then**
 $P_{\text{ref}}(t) = P_{\max} - P_{\text{FCR}} \quad \triangleright 10\text{mHz deadband}$
else if $50.01\text{Hz} < f < 50.20\text{Hz}$ **then**
 $P_{\text{ref}}(t) = P_{\max}(50.80 - f)$
else if $f > 50.20\text{Hz}$ **then**
 $0.6 P_{\max}$
end if

section presents the results of these simulations in the form of 4 case studies:

- I. FCR provision with oscillating grid frequency
- II. FCR provision with realistic grid frequency
- III. FCR provision in turbulent wind
- IV. FFR provision of Types A, B and C

3.6.1 Case I: FCR provision with oscillating grid frequency

In case study I, the wind turbine is subjected to steady wind fields of 7 m/s and 12 m/s respectively. An artificial grid frequency dataset is generated which contains sinusoidally varying ripples, as presented in Section 3.4.1. Although such an oscillating grid frequency does not occur in practice, it is used here to achieve a clear understanding of how FCR provision dynamically impacts the wake. This will provide the required insight to study the dynamic impact of FCR on the wake for realistic grid frequency in case study II.

A series of 12 simulations with varying period of input grid frequency as presented in Figure 3.2 have been performed. The artificial sinusoidal frequency dataset is simulated to study how the dynamics in FCR propagate into the wake dynamics. To analyse the wake behaviour, several different points are chosen.

Figure 3.8 and Figure 3.9 present the results from the simulation where the

period of input grid frequency is 250 s for the cases with steady wind of 7 m/s and 12 m/s respectively. In these figures, there are 4 blue curves corresponding to the left y-axis. These curves represent the wind speed at distances 25 m, 50 m, 75 m and 100 m horizontally behind the rotor center-line respectively. These distances are selected for the FCR simulations as beyond these distances a rather minimal impact of FCR provision on the wake is observed. The grid frequency is shown on the right y-axis. A very clear observation from these results is that the oscillations in the grid frequency are replicated in the wake behind the wind turbine. It can also be observed that the wind speed is most deteriorated at the point closest to the wind turbine and the effect gradually decreases as the distance from the wind turbine increases.

A series of 12 simulations with varying period of grid frequency were performed with the aim to observe the changing magnitude of wake with slow as well as fast variations in the grid frequency and thereby observing the varying magnitude of propagation in the wake. Figure 3.10 and Figure 3.11 present these results at 5 different points for the steady wind cases of 7 m/s and 12 m/s respectively. The x-axis shows the different periods of oscillations for which the simulations are performed. The y-axis shows the magnitude of oscillations in the wind speed at the specified points. A common observation drawn from these figures is that for a fast changing grid frequency with period ≤ 5 s, the oscillations are not replicated in the wake behaviour and no similar sinusoidal pattern is observed. As the period of oscillations increases, the input grid frequency behaviour starts to replicate in the wake. It can be seen in Figure 3.10 that there is a continuous increasing trend in the magnitude of wake for the frequencies with longer periods. However, the increment in magnitude is not continuously linear. On the other hand for the case of high wind speed, in Figure 3.11, a different pattern is observed. The curves start with a steep slope and then gradually declines to a more stable wake magnitude.

3.6.2 Case II: FCR provision with realistic grid frequency

To simulate a realistic scenario, real grid frequency data as shown in Figure 3.3 are used. In this case the wind turbine is subjected to steady wind profiles of 7 m/s and 12 m/s, as presented in Section 3.4.2.1. In order to study the wake effect in a realistic grid frequency condition, several physical points behind the rotor center-line have been chosen. These points are located at distances of 25 m, 50 m, 75 m, 100 m and 125 m behind the rotor. Figure 3.12 presents three different graphs resulting from simulations with a steady wind speed of 7 m/s. The first graph shows the output power with

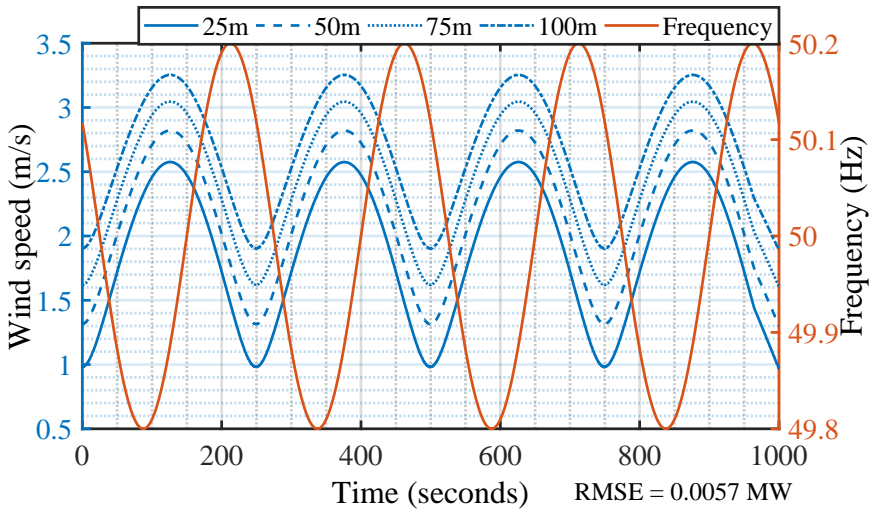


Figure 3.8: Wind speed at different points behind the rotor for 7 m/s simulations

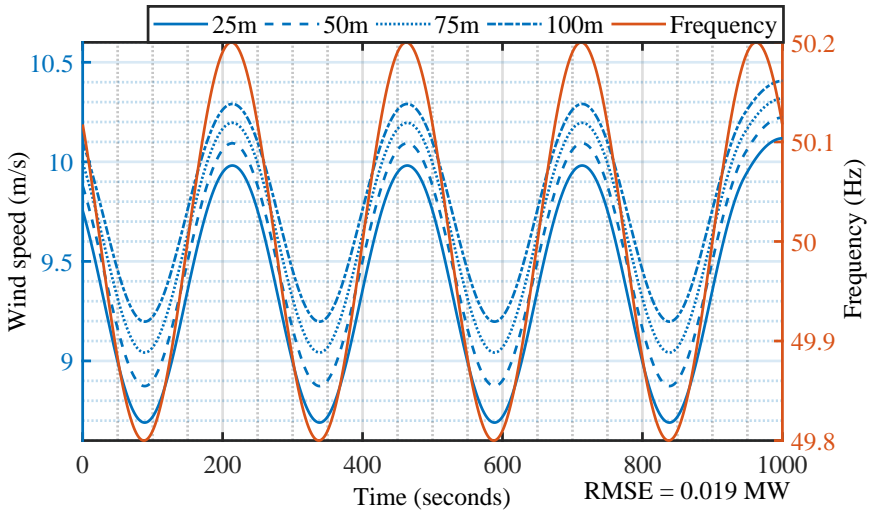


Figure 3.9: Wind speed at different points behind the rotor for 12 m/s simulations

the varying grid frequency. The second graph shows the thrust coefficient C_t and the rotor speed. The third graph shows the wind speed at different points behind the rotor. During the extreme grid event, the grid frequency drops to 49.8 Hz. In response to this frequency dip, the controller generated a reference power to match the contracted FCR bid. The resulting control

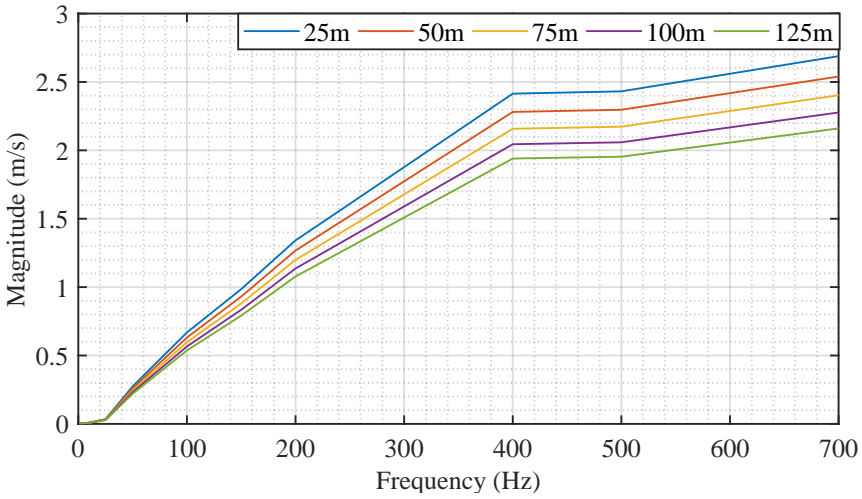


Figure 3.10: Magnitude of wake oscillations with period varying grid frequency for 7 m/s simulations

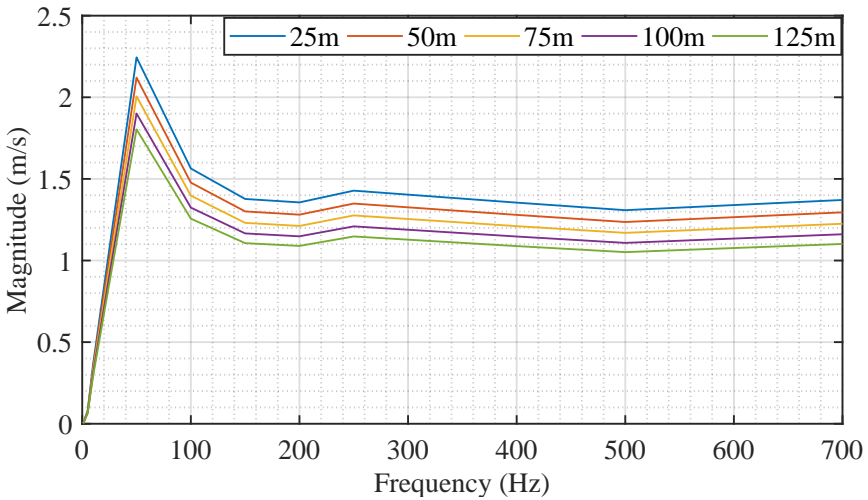


Figure 3.11: Magnitude of wake oscillations with period varying grid frequency for 12 m/s simulations

can be observed by comparing the blue and red curve. It can also be seen that the C_t and the rotor speed also drop at this point. The effect of this event can be seen on the wind speed at different points behind the rotor. At ≈ 400 s, an increase in the wind speed can be observed at each of these points.

Figure 3.13 present the graphs for the case where a steady wind speed of 12 m/s is used. The plot design and placement is similar to Figure 3.12. Here, the control response is again reflected on the output power. The rotor speed in this case sees little variation during this event. This is attributed to the pitch control action that was not active in the case of 7 m/s simulations. However, due to the control action, a changing wind speed at the points of observation is noticed. This change in the wind speed due to the wake behaviour although clearly noticeable, is rather minimal.

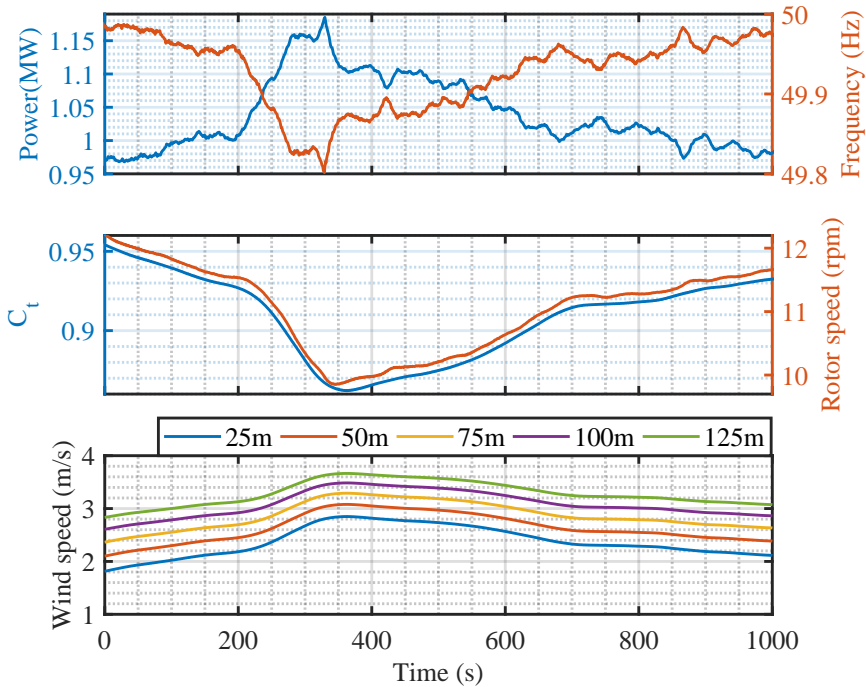


Figure 3.12: Grid frequency and influenced outputs with changing control action for a wind speed of 7 m/s

3.6.3 Case III: FCR provision in turbulent wind

Case III studies the frequency support service in a turbulent wind field. The turbulent wind profile presented in Section 3.4.2.2 is used for these simulations. An 800 s simulation is performed for two different sub-cases. The first case is where the wind turbine operates with FCR based control. A percentage control is used such that the wind turbine provides a linear frequency support of 20% of its total capacity of 5 MW within the range of

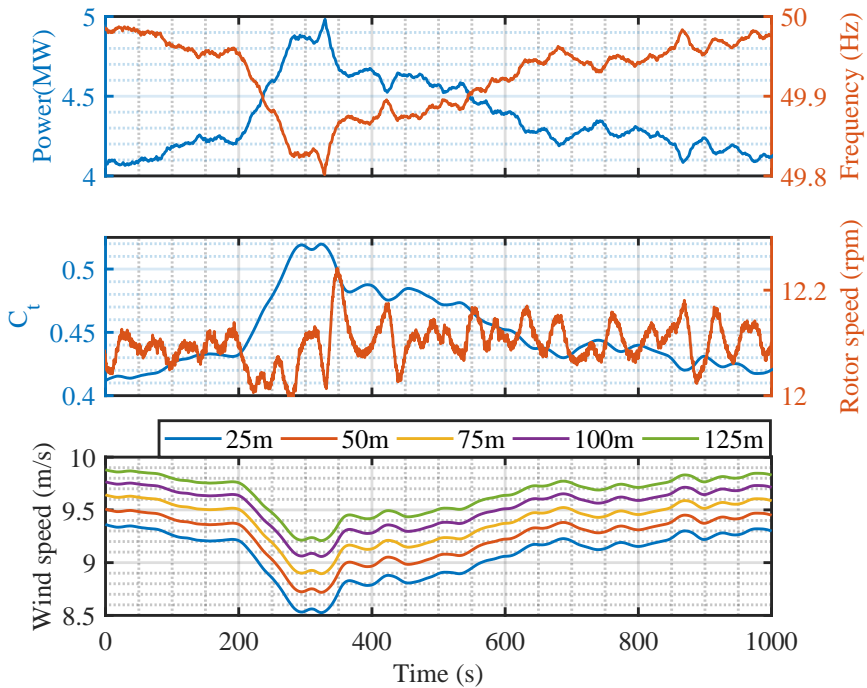


Figure 3.13: Grid frequency and influenced outputs with changing control action for a wind speed of 12 m/s

49.8 Hz - 50 Hz. The second sub-case is without FCR and represents normal operation as a reference. The grid frequency is designed in a step form and ranges from 49.8-50 Hz within the span of the total simulation time. The first graph in Figure 3.14 is the grid frequency that is used to calculate the reference power. The following 3 graphs consist of 2 curves. The FCR case is represented by a *blue* curve and the non-FCR case is represented by a *red* curve. It can be seen in the second graph that during this turbulent wind scenario, for the non-FCR case, the controller tries to follow the reference power of 5 MW. The root mean square error (RMSE) of the power reference tracking for this case is 0.0275 MW. On the other hand, the *blue* curve that represents the FCR power tries to follow the input frequency. The RMSE in this case is 0.0625 MW expectantly higher than the former case due to the increased control action. The third graph shows the C_t for two case. The C_t for both cases is identical, except for the duration in which the wind turbine provides FCR support. The fourth curve shows V_s , the wind speed for the two cases at a distance of 25 m behind and in centre-line of the rotor. The two wind speeds appear to differ slightly within the frequency

support duration. To analyse this in more detail, the final graph shows the difference between the two wind speeds, $V_{S_{FCR}} - V_{S_{NoFCR}}$ i.e. . It is evident that the wake effect indeed differs in the two cases.

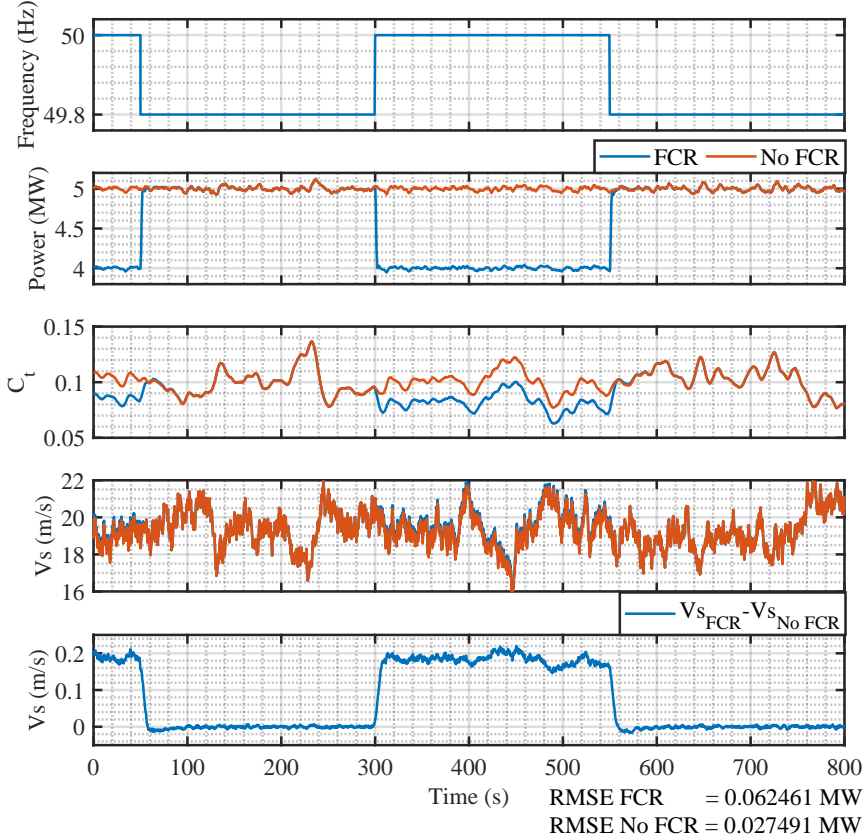


Figure 3.14: Case III: FCR provision in turbulent wind

3.6.4 Case IV: FFR provision of Types A, B and C

The prequalification test for FFR is designed such that all three types of services presented in Table 1.1 can be implemented. Initially there is a sequential step decrease in grid frequency to simulate a situation where all three types of services need to be activated. After this the services are individually activated from a stable grid frequency of 50 Hz. All the services are tested for a long duration support (> 30 s). The purpose of this test is to analyse the capacity of the wind turbine and control system to provide the

FFR service. This test is presented in Figure 3.15.

The wind turbine provides 0.5 MW of FFR for Type A service and 0.25 MW each for Type B and Type C service. The red curve indicates the grid frequency. The frequency starts at a stable 50 Hz for the first 50 seconds, during this time, after the initial transient the wind turbine generates 4 MW of power retaining 1 MW for the FFR services. At time $t = 50$ s the frequency drops to 49.7 Hz and the Type A FFR service is activated and continues for the next 50 seconds. During this time the wind turbine generates 4.5 MW power. At time $t = 100$ s there is a further drop in the grid frequency to 49.6 Hz. At this moment the Type B service is activated and the total power output is increased by 0.25 MW to 4.75 MW. At time $t = 150$ s, Type C service is activated when the frequency drops to 49.5 Hz. The power output at this point is equal to the maximum power output of 5 MW. At time $t = 200$ s, the frequency is stabilised again at 50 Hz. At time $t = 250$ s the frequency drops again to 49.6 Hz, hence activating the Type B service. At time $t = 350$ s the frequency drops to 49.5 Hz and Type C service is activated. Figure 3.16, Figure 3.17 and Figure 3.18 show the zoomed version of activation of all three services. From Figure 3.16 it can be seen that the Type A service is activated at $t = 50$ s and the FFR level of 0.5 MW is activated within 0.5 seconds.

Figure 3.17 shows the activation of the Type B service. In this case the FFR reserve of 0.25 MW is activated within the time limit of 1 second. At the instant of $t = 150$ s, the frequency drops to 49.5 Hz at this point the last 0.25 MW of reserve power is to be activated. However as can be seen in Figure 3.18, the controller was not able to activate the Type C service within the given time limit of 0.7 seconds. A possible reason for this is that at this instant the wind turbine is reaching the upper limit of its power output. A solution to this problem could be to reduce the reserve capacity of Type C service. D1, D2 and D3 are three points located behind and in the centre-line of rotor at distances 373 m, 499 m and 625 m respectively. These distances are equivalent to three, four and five times the distances of the wind turbine rotor diameter, respectively. Greater distances are chosen for FFR simulations compared to the FCR simulations. This is due to the observations made that the impact of FFR provision extends to greater distances. Figure 3.19 shows the changing wind speed at these points due the frequency support based control strategy. A change in the wind speeds at these points can be noticed a few seconds after the instances of frequency change. The change is smaller in the initial 200 s due to the small changes in grid frequency. However, at time $t = 200$ s, 250 s, 350 s and 400 s, the effect is evident.

In Figure 3.20, three point at heights of 90 m, 120 m and 150 m are chosen

to observe the change in wind speed due to the changing grid speed. Like the previous case, a similar pattern of changing wind speed is observed. These results clearly establish the changing wake effect of a wind turbine providing FFR services.

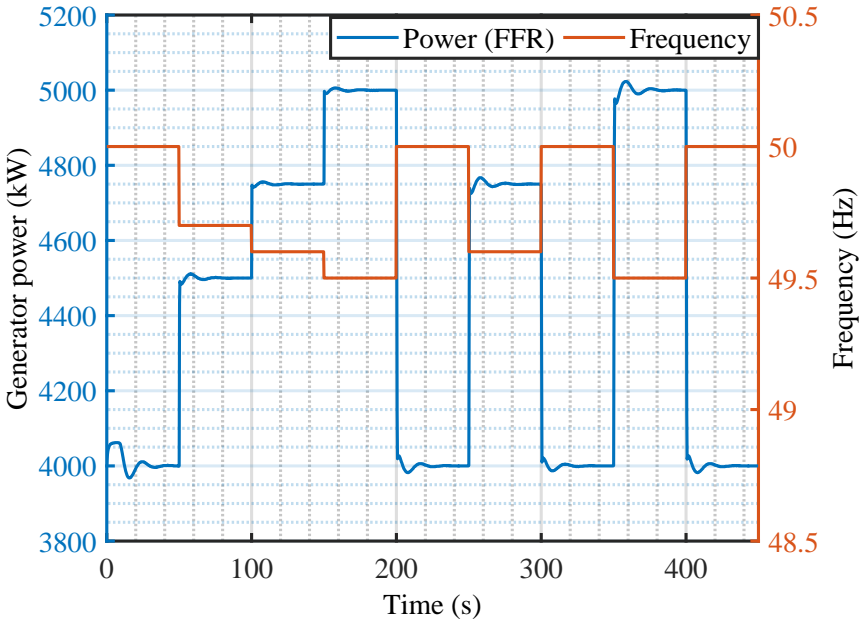


Figure 3.15: FFR power output and frequency

3.7 Conclusion

To study the behaviour of the wake behind a wind turbine providing frequency support services, a series of tests are simulated. The NREL 5 MW wind turbine coupled with a PMSG, torque and pitch controller are used to perform these simulations. A modified Jensen wake model that was deemed robust and needful to the simulation designs is used to model the wake behaviour. The simulations are performed for two benchmark ancillary services, i.e., 200 mHz symmetrical FCR and FFR, as defined in the ENTSO-E directives. The first frequency dataset used in the analysis is a synthetic sinusoidally varying frequency with varying oscillation periods. This data is used to study the frequency oscillation’s replication in the wake behaviour. Secondly, real grid frequency data from an extreme incidence is used to perform a realistic simulation where the effect of changing grid frequency

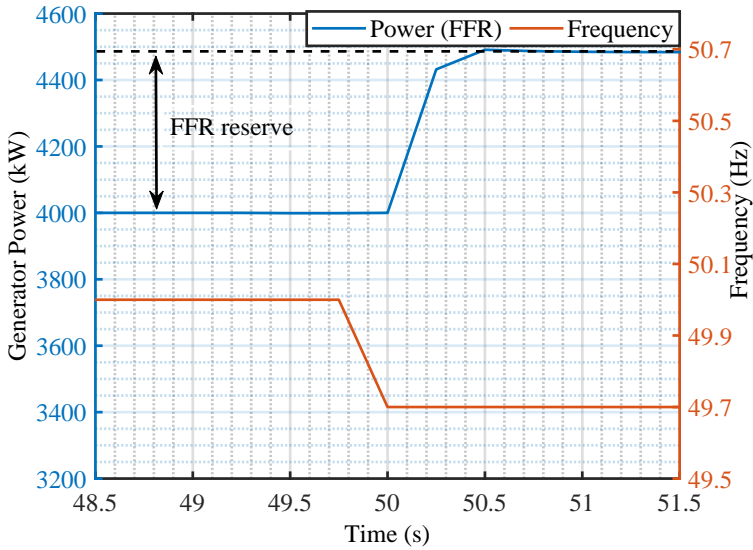


Figure 3.16: FFR Type A service

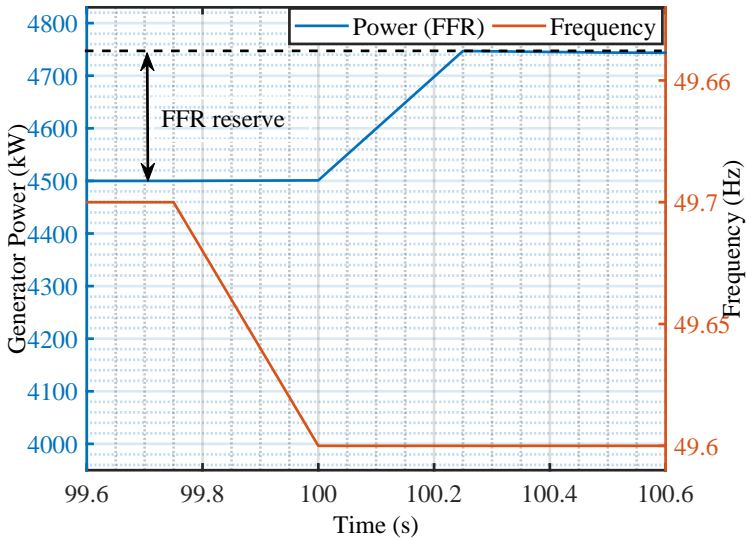


Figure 3.17: FFR Type B service

on the wake can be clearly observable. The simulations are performed for both steady and turbulent wind conditions. The torque control used in the models is designed such that it is capable of following MPPT, PLC as well

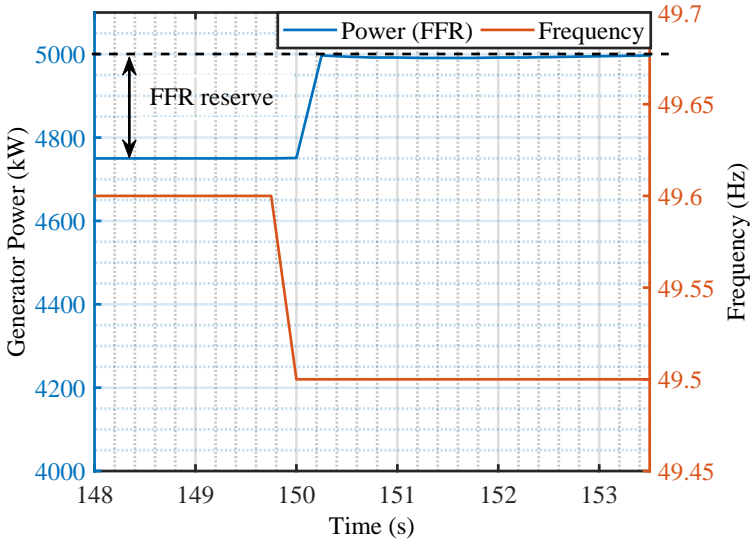


Figure 3.18: FFR Type C service

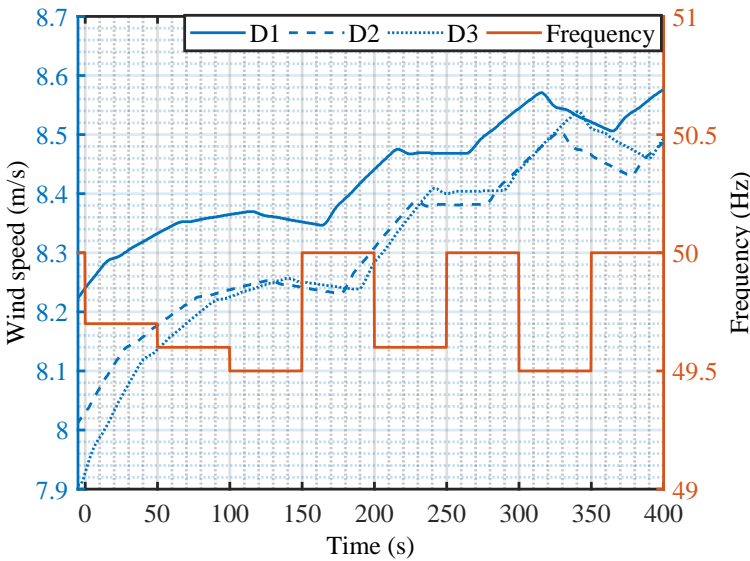


Figure 3.19: Wind speed behind the rotor at 3 different points

as grid frequency based deloaded control. The controller is shown to operate with a high tracking performance. Since the simulations include higher wind speed regions, a pitch control system with gain scheduling is also

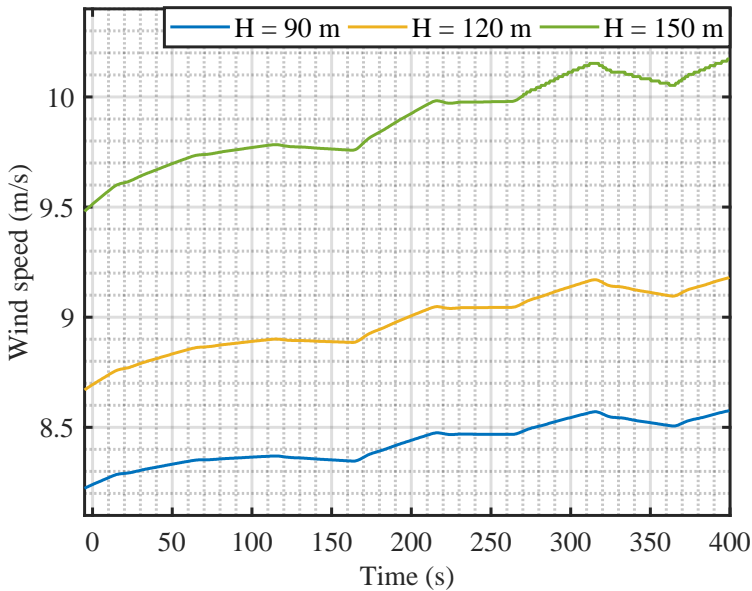


Figure 3.20: Wind speed at different heights behind the rotor

used.

The controller tests performed have strengthened the possibility of an active participation of wind turbines in primary reserve ancillary services. It is clear that the limitations of the wind turbines quick response to the changing grid frequency can be addressed through the development of fast and efficient controllers.

The major topic investigated in this research is to analyse the changes in wake effect of a wind turbine providing frequency support services. The wake effect has been analysed at several locations downwind of the wind turbine. The impact of a changing grid frequency on the nature of the wake is demonstrated. The oscillations in the grid frequency are seen to replicate in the wake behaviour, showing there is a dynamic interaction. Also, changes in the intensity of this effect are clearly visible with the changing distances behind the wind turbine. It is also observed that the magnitude of frequency support offered by the wind turbine and the slope of the changing grid frequency are also active variables that affect the wake.

The tests presented in this research are performed for a single wind turbine. Therefore, the changes observed in the wake are not extreme. A clear effect of changing grid frequency is however observed. This effect is likely to increase in a high capacity density wind farm where a collective wake

effect is generated by several wind turbines. Hence, the main conclusion of this research is that dynamic wake interactions should be taken into account when high density wind farms are to be used to provide dynamic frequency support services such as FCR and FFR.

References

- [1] N. Singh, J. De Kooning, and L. Vandeveldel, "Dynamic wake analysis of a wind turbine providing frequency support services," IET Renewable Power Generation, 2022, doi: 10.1049/rpg2.12455
- [2] "Capacity Densities of European Offshore Wind Farms", 2018. <https://vasab.org/document/capacity-densities-of-european-offshore-wind-farms/>. Deutsche WindGuard GmbH.
- [3] J.K. Lundquist, K.K. DuVivier, D. Kaffine, et al. "Costs and consequences of wind turbine wake effects arising from uncoordinated wind energy development." 2019. doi: 10.1038/s41560-018-0281-2
- [4] N. Baker, A. Stanley, J. Thomas, A. Ning, and K. Dykes (2019). "Best Practices for Wake Model and Optimization Algorithm Selection in Wind Farm Layout Optimization" Preprint. [online] Available at: <https://www.nrel.gov/docs/fy19osti/72935.pdf>
- [5] M. F. Howland, S. K. Lele, and J. O. Dabiri, "Wind Farm Power Optimization through Wake Steering," Proceedings of the National Academy of Sciences, 2019. doi:10.1073/pnas.1903680116
- [6] S. Kuenzel, L. Kunjumammed, B. Pal and I. Erlich, "Impact of wakes on wind farm inertial response," 2014 IEEE PES General Meeting | Conference & Exposition, National Harbor, MD, 2014.
- [7] N. O. Jensen, "A note on wind generator interaction". Risø National Laboratory. Risø, 1983.
- [8] I. Katic, Højstrup, J., & Jensen, N. O. (1987). "A Simple Model for Cluster Efficiency". In W. Palz, & E. Sesto (Eds.), EWEC'86. Proceedings.
- [9] "Elia: grid data overview". Available at: <https://www.elia.be/en/grid-data> [Accessed: September 2023]
- [10] ENTSO-E technical report on the January 2019 significant frequency deviations in Continental Europe. [online] Available at: <https://www.entsoe.eu/news/2019/05/28/entso-e-technical-report-on-the-january-2019-significant-frequency-deviations-in-continental-europe/>
- [11] J. Højstrup "Velocity Spectra in the Unstable Planetary Boundary Layer." Journal of the Atmospheric Sciences, October 1982.

- [12] H.R. Olesen, S.E. Larsen, J. Højstrup. "Modeling Velocity Spectra in the Lower Part of the Planetary Boundary Layer." *Boundary-Layer Meteorology*, July 1984.

4

Wind Turbine Main Bearing Lifetime

In the previous chapters, the capability of wind turbine to provide ancillary services and the subsequent impact on the wake are discussed. The impact of ancillary services provision is also expected on the loads of the wind turbine components. The components of an operational wind turbine are continuously impacted by both static and dynamic loads. Regular inspections and maintenance are required to keep these components healthy. The main bearing of a wind turbine is one such component that experiences heavy loading forces during the operation. These forces depend on various parameters such as wind speed, operating regime and control actions. When a wind turbine provides FCR to support the grid frequency, the forces acting upon the main bearing are also expected to exhibit more dynamic variations. These forces have a direct impact on the lifetime of the main bearing. With an increasing trend of wind turbines participating in the frequency ancillary services market, an analysis of these dynamic forces becomes necessary. To this end, this study assesses the effect of FCR based control on the main bearing lifetime of the wind turbine. Firstly, a control algorithm is implemented such that the output power of the wind turbine is regulated as a function of grid frequency and the amount of FCR. Simulations are performed for a range of FCR to study the changing behaviour of dynamical

forces acting on the main bearing with respect to the amount of FCR provided. Then, based on the outputs from these simulations and using 2 years of LiDAR wind data, the lifetime of the main bearing of the wind turbine is calculated and compared for each of the cases. Finally, based on the results obtained from this study, the impact of FCR provision on the main bearing lifetime is quantified and recommendations are made, that could be taken into account in the operation strategy of a wind farm.

The rest of this chapter is structured as follows: Section 4.1 details reviews the literature and presents the novelty of this chapter to cover the research gap. In Section 4.2, the wind turbine, main bearing and the generator models are presented. Additionally, the torque control algorithm, pitch control system and wind field design used in this study are presented. Section 4.3, presents the methodology to calculate the load and lifetime of the wind turbine main bearing. In Section 4.4, the results and discussion are presented. Finally, the conclusion is drawn in Section 4.5. The content of this chapter has been published in [1].

4.1 Introduction

With the increasing share of wind energy in the energy mix and an increased participation of wind farms in ancillary service markets, there is a growing concern about the structural health and maintenance of wind turbine components. As a wind turbine or a wind farm gets older, the overall performance is reduced. An age based performance of a wind farm is investigated in [2]. A survey of failures of Swedish wind farms is presented in [3]. Reliability analysis and probabilistic methods for wind farm performance are presented in [4]- [5]. Methods to quantify the availability of wind farms are proposed in [6]. An extensive data study presented in [7] has found that wind turbines lose around 1.6% of their nominal output per year due to aging. It has also been seen that some wind turbine components fail before their expected lifetime [8]. To fill this gap, several studies have been conducted that explore new methods of wind turbine monitoring and maintenance. A deep learning approach is explored to predict the remaining useful life of rotating components in [9]. A cost-effective condition monitoring for wind turbines is proposed in [10]. Different methods of wind turbine maintenance management are suggested in [11] and [12]. The approach for a remote condition monitoring system is explored in [13]. Wind turbine failure detection and condition based maintenance strategies are presented in [14] and [15] respectively. In terms of overall optimization of a wind farm, a study exploring wind farm layout optimization is presented in [16].

These studies are focused on overall wind farms or single turbines as a whole. However, specific studies based on important wind turbine components individually are rare. A crucial component of the wind turbine is its main bearing. A downtime due to a main bearing failure can cause a significant loss of revenue in addition to a high replacement cost. There are several factors that affect the health of a bearing. Foremost, the manufacturing quality of the bearing is critical to a long service life. Logistics of storage, application and mounting also play an important role. Also, it is crucial for the bearing to be well lubricated. The lubrication specifications and lubrication change intervals are specific to the application and help ensure a smooth and healthy bearing operation [17]. According to SKF, the leading causes of bearing damage are lubrication (36%), contamination (23%), application (18%), interface (8%), handling (8%), electrical (5%) and fatigue (2%). A few studies have been conducted regarding the health of the wind turbine main bearing. In [18] a novel prognostic approach to predict the remaining useful lifetime of bearings in a wind turbine gearbox is proposed. The study relies on artificial neural networks to

predict the short-term tendencies. The data-driven approach is specific to the bearings in the wind turbine gearbox. Another data driven approach to analyse bearing faults is discussed in [19], where data mining is applied to identify bearing faults in a wind turbine. The research relies on a neural network algorithm using the data collected from several wind turbines. The results from this study are the prediction of over-temperature events ahead of the fault occurrence. A study about the prediction and diagnosis of wind turbine faults is presented in [20]. The temperature parameters of SCADA data such as bearing temperature are used for fault detection. A long-term fault prediction framework is discussed in [21]. This study also utilises SCADA data and secondary measurements from 108 wind turbines with main-bearing failures. Historic wind turbine data for run-to-failure and non-run-to-failure wind turbines is utilized to predict the remaining power generation before failure in [22]. All these studies are data-based and are focused on main bearing related issues such as prediction of time to failure, over-temperature events prediction and remaining power generation before failure. However, there is no study that uses detailed wind turbine models to study the lifetime of the main bearing of the wind turbine. The impact of the provision of ancillary services on the health of the wind turbine main bearing remains unknown. The main bearings of the wind turbine are subjected to dynamically varying forces during its operation. The forces are significantly more dynamic when providing ancillary services such as FCR. This originates from the control algorithms implemented to provide frequency control, which change the radial and axial forces acting upon the main bearing, and hence affect the overall health of the main bearing. A study of these forces and their impact on the lifetime of the main bearing of the wind turbine is important in times when wind turbines are expected to provide ancillary services. A study of the lifetime of the main bearing is also specially relevant as it is a comparatively expensive equipment with high replacement cost and a significant downtime for replacement. To this end, this study analyzes and quantifies the effect of providing ancillary services on the lifetime and health of the wind turbine main bearing.

4.2 Models and data

The models used in this study include the wind turbine rotor and the PMSG, as presented in Section 2.2. The control system presented in Section 2.3 is used. In the following subsection, the main bearing model, control design specific to the study and the wind field design and data processing are presented.

4.2.1 Main bearing

The original wind turbine model developed by NREL does not consider the detailed features of the main bearing. However, since the wind turbine is largely based on the REpower 5M machine, the available literature and data about the bearing design and its properties are used. The schematic of the main bearing positioning in the wind turbine is shown in Figure 4.1. The bearing used in this machine is a spherical roller bearing weighing 3320 kg [23].

Since a detailed datasheet of the turbine main bearing is not publicly available, some assumptions and estimates are made about the bearing properties. The main property of the bearing that is required to calculate the lifetime is its basic dynamic load rating C in Newton, which represents the maximum load that a bearing can be subjected to for a rating life of one million revolutions. In order to estimate the C rating of the bearing, data from similar bearing types available through SKF are used in curve fitting. As a double check, simulations were performed to calculate the load on the main bearing of the wind turbine to make sure that the load is always lower than the bearing rating.

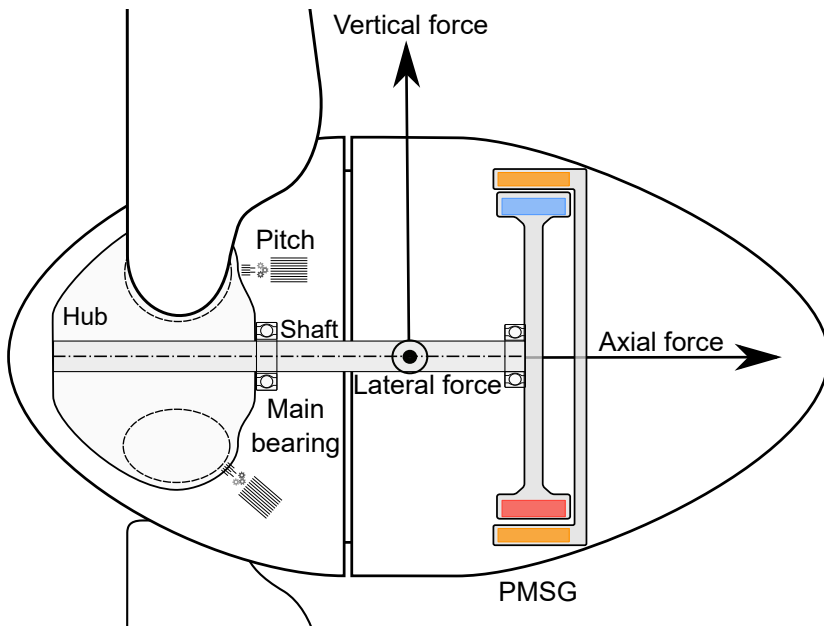


Figure 4.1: Main bearing position

4.2.2 Torque control

The simulations have been performed for 4 different cases. In the first case no FCR is provided, i.e., the wind turbine operates in MPPT mode. In the second case, the wind turbine is deloaded by 20%, i.e., the turbine operates at 80% of the maximum power curve. In the third and fourth case 20% and 40% FCR is provided, i.e., 20% and 40% of the available power is reserved for FCR, respectively. For the 20% FCR case, the wind turbine control design is as shown in Figure 4.2. In Figure 4.2 and Figure 4.3, the blue and red curves represent the upper and lower bound of output power. The black curve represents the base power. The shaded area demonstrates the area of operation, i.e., the reference power at any given point lies within this area based on the grid frequency. The reference power for these cases is calculated by using Algorithm 2. The algorithm is designed such that a symmetrical 200 mHz frequency support is provided. A frequency response dead-band of 10 mHz centered at nominal frequency (50 Hz) is present to reduce excessive control activities and turbine mechanical wear for normal power system frequency variations. Here, P_{UB} and P_{LB} are upper and lower bound powers respectively as presented in Figure 4.2 and Figure 4.3. The reference power P_{ref} is calculated as the sum of base power P_{base} and a time varying term $P_{freq}(t)$. $P_{freq}(t)$ is calculated using β which is proportional to the percentage of FCR provided, p_{FCR} . k is the proportionality constant with the value 0.25. β is defined as follows:

$$\beta = k \cdot p_{FCR} \quad (4.1)$$

P_{base} is defined according to the black curve in Figure 4.2 and Figure 4.3 for the 20% FCR and 40% FCR case respectively. Furthermore, $P_{freq}(t)$ is based on the varying grid frequency f and the contracted FCR bid P_{FCR} , i.e., 20% or 40%.

4.2.3 Wind field design and data processing

The wind data used for the simulations in this research work are from the publicly available data repository of meteorological data provided by Ørsted. The data are available for several offshore meteorological stations [24]. The LiDAR data are 10 minute statistics for wind measurements from LiDARs installed at an offshore wind farm. A total of 2 years data sampled at 10 minutes is used. In order to fit the data to the operating range of the wind turbine, the data were processed to fit the requirements. Firstly, only the data within the range of wind velocities between 3-25 m/s were retained. The wind data are then rounded off to the nearest integer. These data

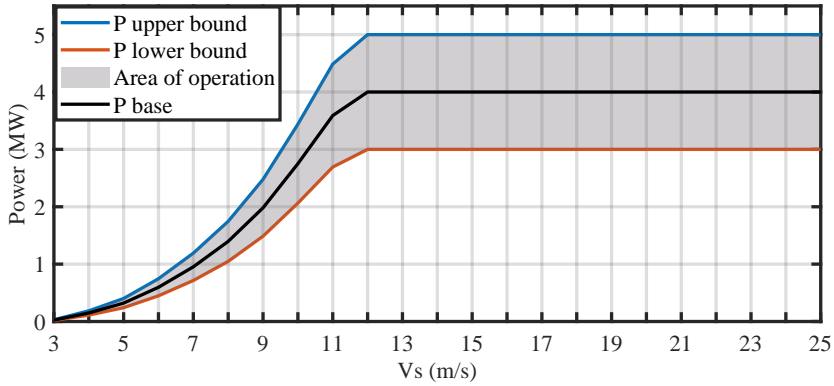


Figure 4.2: Control design for 20% FCR

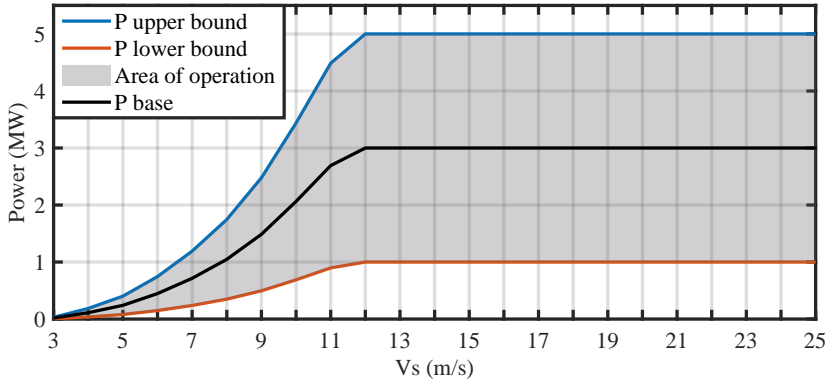


Figure 4.3: Control design for 40% FCR

can be visualised in graphical form as presented in Figure 4.4. Figure 4.4 shows the probability of occurrence of different levels of wind speed within the operating range of the wind turbine. The simulations are performed for each of these wind levels, and their probability of occurrences is used to deduce the final results.

4.3 Methodology

Different outputs from these simulations are analysed and used for the calculation of bearing loads and lifetime. These parameters are presented in the following subsections.

Algorithm 2 Reference power decision

Require: $P_{\text{ref}} \leq P_{\text{UB}}$

if $f \leq 49.8 \text{ Hz}$ **then**

$P_{\text{ref}}(t) = P_{\text{UB}}$

else if $49.80 \text{ Hz} < f < 49.99 \text{ Hz}$ **then**

$P_{\text{ref}}(t) = P_{\text{base}} + P_{\text{freq}}$ $\triangleright P_{\text{freq}} = \beta(50-f)$

else if $49.99 \text{ Hz} < f < 50.01 \text{ Hz}$ **then**

$P_{\text{ref}}(t) = P_{\text{base}}$ $\triangleright 10 \text{ mHz deadband}$

else if $50.01 \text{ Hz} < f < 50.20 \text{ Hz}$ **then**

$P_{\text{ref}}(t) = P_{\text{base}} + P_{\text{freq}}$ $\triangleright P_{\text{freq}} = \beta(50-f)$

else if $f \geq 50.20 \text{ Hz}$ **then**

$P_{\text{ref}}(t) = P_{\text{LB}}$

end if \triangleright all powers given in MW

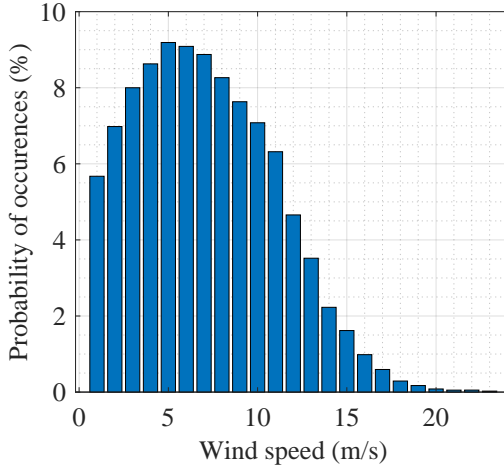


Figure 4.4: Wind speed percentage occurrences

4.3.1 Dynamic equivalent force

There are different forces acting on the blade root of the wind turbine and hence on the main bearing. The axial, vertical and lateral forces are shown in Figure 4.1. These forces are used to calculate the dynamic equivalent force. The axial force is measured at the root of each blade. The 3 individual blade forces are then averaged as shown in (4.2). Here, F_{b1} , F_{b2} and F_{b3} represent the axial forces, F_a (in Newton) at the three blades of the wind turbine.

The radial force on the other hand is given as a resultant of the lateral

force F_l and the vertical force F_v acting on the blade root, as shown in Figure 4.1. The equation is given in (4.3).

$$F_a = \frac{F_{b1} + F_{b2} + F_{b3}}{3} \quad (4.2)$$

$$F_r = \sqrt{F_l^2 + F_v^2} \quad (4.3)$$

The dynamic equivalent force P_d in Newton is defined in (4.4), where b_x and b_y are the dimensionless empirical factors for the specific spherical roller bearing. The SKF catalogue for rolling bearings [25] suggests that the mean force, F_m (in Newton) should be calculated considering their minimum and maximum values. Therefore, the mean values of radial and axial forces are calculated using (4.5). Where F_{\min} and F_{\max} represent the minimum and maximum values of the forces within the steady period of the entire simulation time.

$$P_d = b_x F_r + b_y F_a \quad (4.4)$$

$$F_m = \frac{F_{\min} + 2F_{\max}}{3} \quad (4.5)$$

4.3.2 Lifetime

The linear fatigue damage accumulation method used in this study is based on [26]. The method incorporates the weightage and dynamic equivalent force of each load level. Hence, providing a good estimate of the bearing lifetime. In this method, firstly L_i is defined as the number of revolutions spent at a given wind speed by the main bearing. L_i is calculated as in (4.6). Here, t_i is the number of hours of load level i . Ω is the speed in *rpm* for load level i .

$$L_i = t_i \Omega_i 60 \quad (4.6)$$

Next, the basic rating life L_{10_i} is defined as the life required for 10 % of bearing samples to fail, for an identical group of bearings at a given load level i . L_{10_i} is calculated as given in (4.7). Here, p is a bearing specific value, which is equal to 10/3 for roller bearings as per SKF.

$$L_{10_i} = 10^6 \left(\frac{C}{P_d} \right)^p \quad (4.7)$$

Thereafter, f_i is a fraction of the level i , defined to assign weightage to individual load levels (1 to m). f_i is calculated as in (4.8).

$$f_i = \frac{L_i}{\sum_{i=1}^m L_i} \quad (4.8)$$

The combined lifetime (in years) including all load levels is determined by (4.9). Here a_1 , a_2 and a_3 represent the life modification factors. a_1 is set equal to 0.21 which corresponds to a 99% reliability of the main bearing surviving the estimated lifetime. The factors a_2 and a_3 correspond to the material of the bearing and lubrication conditions and these are set equal to 1.

$$L_M = \frac{1}{\sum_{i=1}^m \left(\frac{f_i}{L_{10_i}} \right)} \frac{a_1 a_2 a_3}{10^6} \quad (4.9)$$

4.4 Results and discussion

For this study, 4 different cases have been designed. For each case, 23 simulations are performed. These 23 simulations are designed such that for each integer wind speed within the operating range (3-25 m/s) of the wind turbine, a simulation is conducted. In this manner, the entire operating range of the wind turbine is included in the study. The main outputs from these simulations, namely axial, radial and dynamic equivalent forces are then used to calculate the lifetime of the main bearing of the wind turbine. These simulations consider the forces once the wind turbine has reached a steady operation.

These 4 cases differ from each other in the type of control applied. Case 1 is where the wind turbine operates to provide maximum available power. Therefore, no margin in the active power is retained to provide an FCR service. The wind turbine operates on either MPPT or power limiting control, based on the wind speed. In Case 2, the control is such that the reference power is deloaded by 20%. Apart from the deloading the operation of the wind turbine remains similar to Case 1, no FCR is provided. Figure 4.5 presents the reference power for curves for Case 1 and Case 2. The blue curve presents Case 1 and the red presents Case 2. It can be seen here that for each individual wind speed load level, a different reference power is set for the 2 cases.

Case 3 and Case 4 are comparative cases that are simulated to observe the effect of providing FCR on the main bearing of the wind turbine. In these cases the wind turbine control systems based on Algorithm 2 are used.

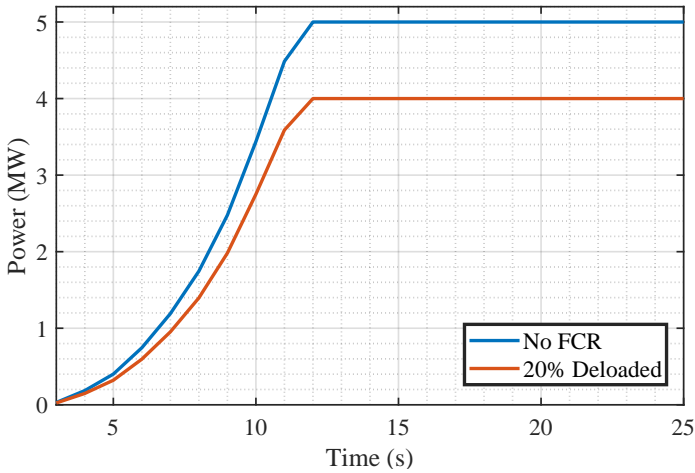


Figure 4.5: Power reference for No FCR and 20% deloaded cases

Figure 4.6 consists of 3 different curves. The red curve corresponding to the right y-axis represents the grid frequency. The first blue curve on the top, corresponding to the left y-axis represents Case 3 where the wind turbine provides 20% FCR. The second blue curve at the bottom represents Case 4 where the wind turbine provides 40% FCR. It can be observed from Figure 4.6 that the reference power changes to accommodate the real-time changes in FCR requirements based on the grid frequency.

Figure 4.7 presents 9 different graphs to present the dynamic axial, radial and equivalent forces acting on the main bearing. The load levels presented in Figure 4.7 correspond to the wind speed of 4 m/s, 12 m/s and 25 m/s. These levels are chosen such that the forces in low, medium and high wind speed ranges can be presented. However, it should be noted that the simulations are performed for each load level from 3 to 25 m/s.

In Figure 4.7 each graph consists of 4 curves, representing the 4 cases, i.e.: No FCR, 20% deloaded, 20% FCR and 40% FCR. Figure 4.7 (a), Figure 4.7 (b) and Figure 4.7 (c) present the axial forces for the 3 load levels. It can be seen that the first 2 curves corresponding to No FCR and 20% deloaded tests, even though oscillating (for $V_s=12$ m/s and $V_s=25$ m/s), are relatively steady compared to the last 2 curves, where FCR is provided. With the varying grid frequency, the power output is changed through torque and pitch control, resulting in a varying axial force.

Figure 4.7 (d), Figure 4.7 (e) and Figure 4.7 (f) present the radial forces for the 3 load levels. The radial forces for each of these cases is relatively lower compared to the axial forces. For the low wind speed of 4 m/s, in

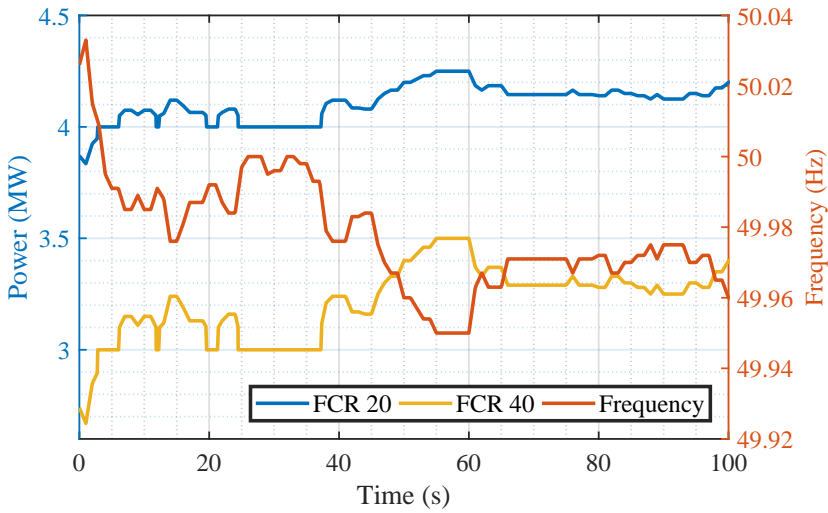


Figure 4.6: Power reference for 20% FCR and 40% FCR cases

Figure 4.7 (d) the radial forces are close for these cases. A clear effect of providing FCR on the radial forces can be observed in Figure 4.7 (e).

Figure 4.7 (g), Figure 4.7 (h) and Figure 4.7 (i) present the dynamic equivalent force. The dynamic equivalent force is calculated as explained in Section 4.3.1. A combined effect of both axial and radial forces can be observed here. The impact of these two forces on the calculated P_d is dependent on the empirical factors b_x and b_y . The lifetime of the main bearing of the wind turbine is directly related to its basic dynamic load rating C . The value of C varies based on the strength of the bearing. In order to study the loading and lifetime depending on different design choices, the range of $0.75C$ to $1.25C$ is used in the simulations, where C is as defined in Section 4.2.1.

The results of bearing lifetime are presented in Table 4.1. The results show that the highest lifetime is in the case of No FCR for all C values. It can be observed that the difference in lifetime as compared to the other 3 cases is higher for higher C values and lower for lower C values. It can also be observed that the values for 20% deloaded and 20% FCR cases are close. The least lifetime is observed for the 40% FCR case. The presented results, firstly point to the effect of higher C rating on the bearing lifetime. A higher C consistently gives a higher lifetime estimate for the main bearing. Secondly, it can be noted that a lifetime reduction for the main bearing is associated with providing FCR. Figure 4.8 presents a graph of the changing lifetime with increasing β , where β represents the amount of provided

FCR. The different curves in Figure 4.8 represent the lifetime for different C ratings that correspond to the basic dynamic load rating values. It is observed that the main bearing lifetime reduces with the increasing β . However, for higher C rating cases, it is seen that the lifetime is higher than the average lifetime of the studied wind turbine, i.e., 20 years. An informed decision can be made based on this research and the economics of wind turbine operation, such that if the cost of using a high C rated main bearing can be compensated by the revenue generated from the provision of FCR, then it is indeed an advantage to provide FCR with a wind turbine. On the other hand, if the C rating of the main bearing is low, it is not advisable to provide FCR due to its detrimental impact on lifetime.

C	No FCR	20% deloaded	20% FCR	40% FCR
0.75	13.88	8.88	9.02	8.1
0.8	17.21	11.01	11.19	10.02
0.85	21.06	13.48	13.7	12.26
0.9	25.49	16.31	16.57	14.84
0.95	30.52	19.53	19.84	17.77
1	36.21	23.17	23.54	21.08
1.05	42.6	27.27	27.7	24.81
1.1	49.75	31.84	32.35	28.97
1.15	57.69	36.92	37.51	33.6
1.2	66.49	42.55	43.23	38.71
1.25	76.18	48.75	49.53	44.36

Table 4.1: Bearing life in years

4.5 Conclusion

In this study, the bearing lifetime of a wind turbine primary shaft has been studied. The importance of this study lies in the fact that there is an increasing participation of wind turbines in the ancillary services market. This participation is expected to grow in the coming years as a result of high penetration of wind power in the energy mix. In such a scenario, it is crucial to conduct research on the impact of providing ancillary services on the wind turbine components. The scope of this study is about a specific component of the wind turbine, its main bearing. The choice of the component is based on the relative cost and downtime associated with the maintenance and replacement of this component. The study explored several different cases and methods of FCR control. A common observation from this study is a clear impact of providing FCR on the lifetime of the main bearing of

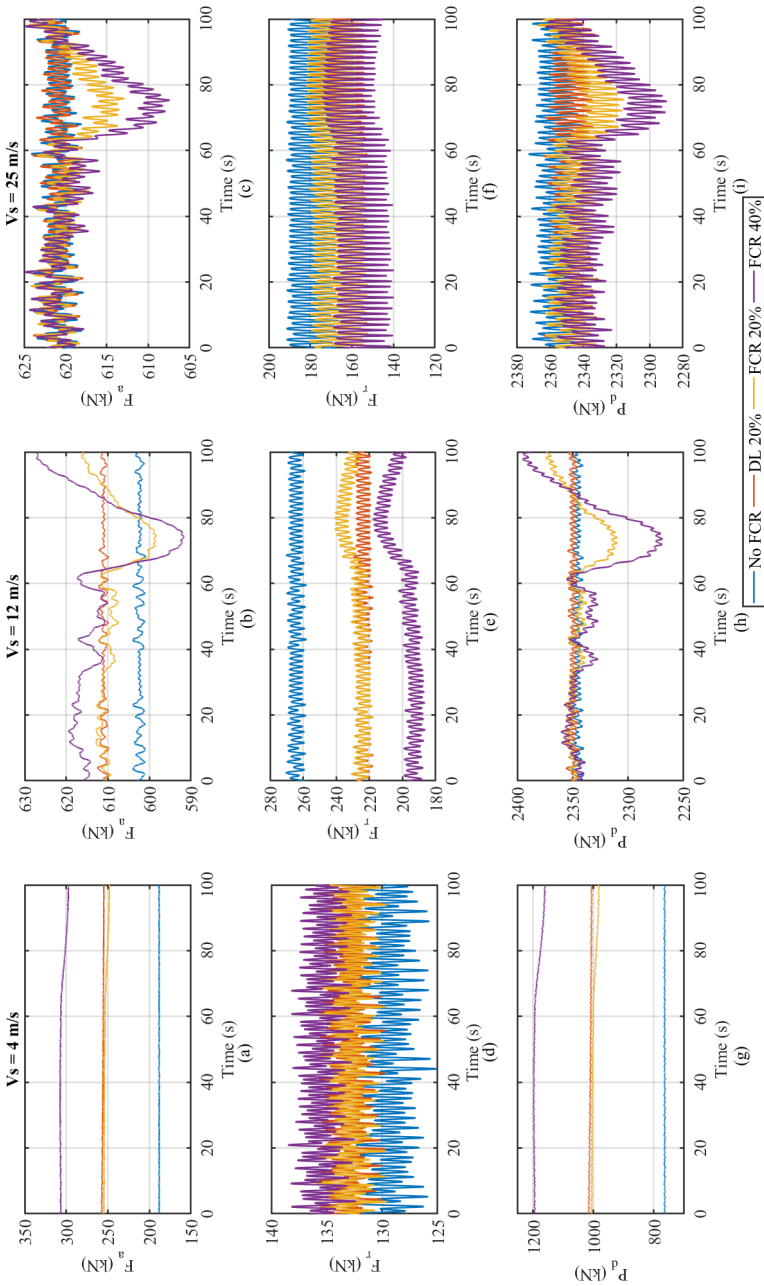


Figure 4.7: Dynamic forces acting on the wind turbine main bearing

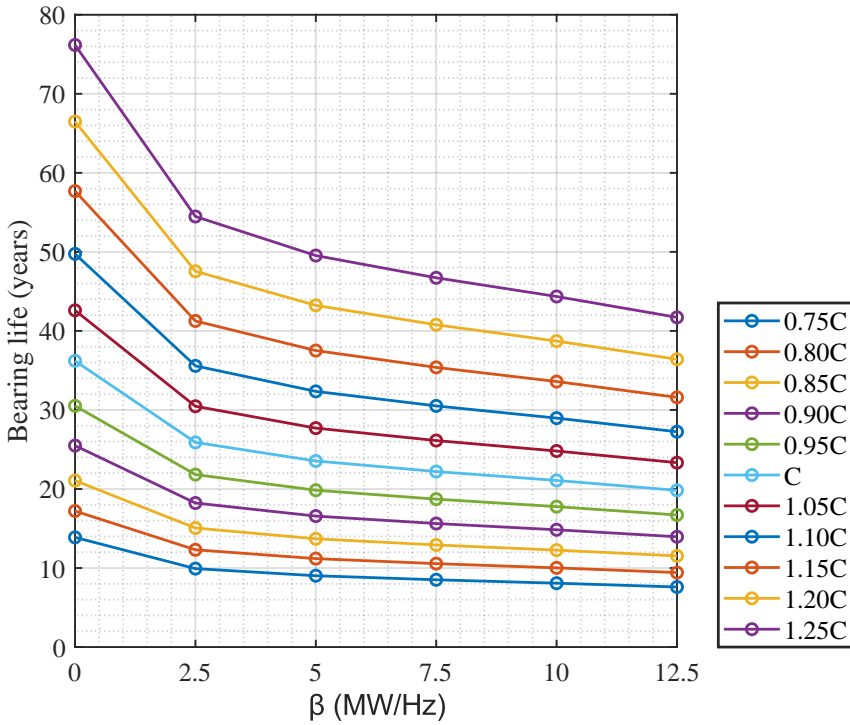


Figure 4.8: Bearing life versus β for different basic dynamic load rating values

the wind turbine. The study concludes that the impact of FCR provision on the lifetime of the main bearing is subjective to the amount of FCR provided and the C rating of the bearing. Considering the No FCR case as the base case, a lifetime reduction of 36% is observed for the case when the wind turbine operates 20% deloaded. A lifetime reduction of 35% and 41.8% is observed for the cases of 20% FCR and 40% FCR, respectively. This trend holds for the entire range of C rating simulated in this study. It is also observed that to achieve the same bearing lifetime as the No FCR case, an oversizing of approximately 15% and 20% in the C rating is required for the 20% FCR and 40% FCR cases, respectively. Based on this study a higher FCR provision can be suggested for a wind turbine consisting of bearings with higher basic dynamic load rating.

References

- [1] N. Singh, D. Boruah, J. De Kooning, W. De Waele, and L. Van-develde, "Impact assessment of dynamic loading induced by the provision of frequency containment reserve on the main bearing lifetime of a wind turbine," *Energies*, vol. 16, no. 6, 2023, doi: 10.3390/en16062851
- [2] G. Hughes, *The performance of wind farms in the United Kingdom and Denmark* Renewable Energy Foundation, London (2012), <https://tinyurl.com/cn5qnqg>
- [3] J. Ribrant and L. Bertling, "Survey of Failures in Wind Power Systems With Focus on Swedish Wind Power Plants During 1997–2005", *IEEE Transactions on Energy Conversion*, 2007. doi: 10.1109/tec.2006.889614.
- [4] P. Tavner, J. Xiang and F. Spinato, "Reliability analysis for wind turbines", *Wind Energy*, 2007. doi: 10.1002/we.204.
- [5] S. Arwade, M. Lackner and M. Grigoriu, "Probabilistic Models for Wind Turbine and Wind Farm Performance", *Journal of Solar Energy Engineering*. 2011, doi: 10.1115/1.4004273.
- [6] N. Conroy, J. Deane and B. Ó Gallachóir, "Wind turbine availability: Should it be time or energy based? – A case study in Ireland", *Renewable Energy*. 2011, doi: 10.1016/j.renene.2011.03.044.
- [7] I. Staffell, R. Green, How does wind farm performance decline with age?, *Renewable Energy*, 2014, <https://doi.org/10.1016/j.renene.2013.10.041>.
- [8] *Managing the wind: Reducing kilowatt-hour costs with condition monitoring*, *Refocus*, Volume 6, Issue 3, 2005, doi: 10.1016/S1471-0846(05)70402-9.
- [9] J. Deutsch and D. He, "Using Deep Learning-Based Approach to Predict Remaining Useful Life of Rotating Components," in *IEEE Transactions on Systems, Man, and Cybernetics: Systems*, Jan. 2018, doi: 10.1109/TSMC.2017.2697842.
- [10] W. Yang, P. J. Tavner, C. J. Crabtree and M. Wilkinson, "Cost-Effective Condition Monitoring for Wind Turbines," in *IEEE Transactions on Industrial Electronics*, vol. 57, no. 1, pp. 263–271, Jan. 2010, doi: 10.1109/TIE.2009.2032202.

- [11] D. Pedregal, F. García and C. Roberts, "An algorithmic approach for maintenance management based on advanced state space systems and harmonic regressions", *Annals of Operations Research*, 2008. doi: 10.1007/s10479-008-0403-5 [Accessed 6 May 2022].
- [12] A. Raouf, (2004), "Maintenance Excellence: Optimizing Equipment Lifecycle Decision", *Journal of Quality in Maintenance Engineering*. doi: 10.1108/13552510410526893
- [13] F. P. G. Marquez, "An Approach to Remote Condition Monitoring Systems Management," 2006 IET International Conference On Railway Condition Monitoring, 2006.
- [14] F. P. García, D. J. Pedregal, C. Roberts, Time series methods applied to failure prediction and detection, *Reliability Engineering & System Safety*, 2009, doi: 10.1016/j.ress.2009.10.009.
- [15] E. Byon and Y. Ding, "Season-Dependent Condition-Based Maintenance for a Wind Turbine Using a Partially Observed Markov Decision Process," in *IEEE Transactions on Power Systems*, Nov. 2010, doi: 10.1109/TPWRS.2010.2043269.
- [16] M. Yeghikian et al., "Wind Farm Layout Optimization with Different Hub Heights in Manjil Wind Farm Using Particle Swarm Optimization," *Applied Sciences*, vol. 11, no. 20, p. 9746, Oct. 2021, doi: 10.3390/app11209746.
- [17] Bearing damage and failure analysis. rep. Available at: <https://www.skf.com> (Accessed: March 3, 2023).
- [18] Teng W, Zhang X, Liu Y, Kusiak A, Ma Z. Prognosis of the Remaining Useful Life of Bearings in a Wind Turbine Gearbox. *Energies*. 2017; 10(1):32. doi: 10.3390/en10010032
- [19] A. Kusiak, A. Verma, Analyzing bearing faults in wind turbines: A data-mining approach, *Renewable Energy*, Volume 48, 2012, doi: 10.1016/j.renene.2012.04.020.
- [20] A. Kusiak, W. Li, The prediction and diagnosis of wind turbine faults, *Renewable Energy*, Volume 36, Issue 1, 2011, doi: 10.1016/j.renene.2010.05.014.
- [21] J. Herp, N. Pedersen and E. Nadimi, "A Novel Probabilistic Long-Term Fault Prediction Framework Beyond SCADA Data - With Applications in Main Bearing Failure", *Journal of Physics: Conference Series*, 2019, doi: 10.1088/1742-6596/1222/1/012043.

-
- [22] B. Wiese, N. Pedersen, E. Nadimi and J. Herp, "Estimating the Remaining Power Generation of Wind Turbines—An Exploratory Study for Main Bearing Failures", *Energies*, vol. 13, no. 13, p. 3406, 2020, doi: 10.3390/en13133406.
- [23] "The great power", 2005. Available: <https://evolution.skf.com/the-great-power-3/>. [Accessed 1 September 2022].
- [24] "Offshore wind data", Orsted.com, 2022. [Online]. Available: <https://orsted.com/en/our-business/offshore-wind/wind-data>. [Accessed: 01- Sep- 2022].
- [25] SKF, "Rolling bearings", 2018.
- [26] E. Zaretsky, "A. Palmgren Revisited: A Basis For Bearing Life Prediction", National Aeronautics and space administration, 1997. [Accessed 1 September 2022].

5

Prediction-based Wind Turbine Operation for Active Participation in the Day-Ahead and Reserve Markets

In the previous chapters the topics of wind turbine capability to provide ancillary services and its physical impacts such as wake and component loads are addressed. The techno-economic aspect related with wind turbine participation in day-ahead and reserve markets are presented in this chapter. Electricity markets around the world are opening up to a greater contribution from wind power producers (WPPs). In this regard, WPPs are incentivised to participate in both energy and reserve market floors while being responsible for real-time deviations from their submitted bids. Therefore, despite uncertainties in wind speed and system frequency, effective control systems should be developed to enable WPPs to respond reliably concerning their committed day-ahead bids, as flexible conventional power plants do. However, designing a control system for WPP to regulate their capacity margin and output power as per the offered reserve bid is challenging, as a fast response with respect to the offered balancing service is required. This study proposes an effective control system that allows WPP to regulate their set-points so as to provide the

committed reserve power while considering the real-time wind variations. A machine-learning algorithm based on the Adaptive Neuro-Fuzzy Inference System (ANFIS) is used to predict the wind speed of the following instances, to be used as input to the control system. Several wind profiles are generated to simulate a practical case study, including real and predicted cases with varying levels of turbulence. Finally, the effectiveness of proposed control strategies on the WPP's profit is evaluated.

The rest of this chapter is structured as follows: Section 5.1 presents the introduction to the study. The models related to the study and their specifications are presented in Section 5.2. The wind profile design and prediction method is presented in Section 5.3. The control and the proposed operation strategies are presented in Section 5.4. The results with illustrative examples and techno-economic analysis is presented in Section 5.5. Finally, Section 5.6 draws the conclusions. The content of this chapter has been published in [1].

5.1 Introduction

The participation of wind energy in the ancillary services market is a matter of concern due to the inherent uncertainty and intermittent nature of wind power. The increasing participation of renewable energy in electricity markets tends to create a degradation of the frequency response. A possible solution to this problem and a way to increase WPP's profit, is increased participation of WPPs in the reserve market [2]. Studies have shown the feasibility of wind turbines in providing ancillary services such as primary reserve [3]. Also, the electricity markets around the world are increasingly offering shorter procurement periods for reserve power. These developments have incentivised a sustained research in this field. However, for active participation in the joint day-ahead energy and reserve market (JERM) a fast response control system is required. There are several methods for the control of a direct-driven wind turbine [4]- [6]. A generator control method that uses interior permanent magnet synchronous generator (PMSG) controlled by a direct torque control scheme is presented in [7]. An improved direct torque control method for smooth power injection and short circuit protection is presented in [8]. These control strategies are widely used for variable-speed generation and for extracting the maximum power available in the wind. However, the control system proposed in this study aims to explore the wind turbine control design that is capable of following not only the grid frequency but also the fast-varying wind speed in order to adjust the power output in real-time and maximise the WPP's profit. The proposed control system is validated with several tests for different control designs and wind profiles with different turbulence intensity levels (TIL). These wind profiles are then processed using a machine learning algorithm based on ANFIS to predict the wind speed data. The real and predicted wind profiles are then used in different case studies to analyse the control response. Finally, the results from the different operation strategies are evaluated focusing on the WPP's profit in the electricity market. The key contribution of this study is proposing an advanced control strategy for reserve provision as well as evaluating the financial outcomes of such strategy for a WPP participating in JERM.

5.2 Model

The simulation setup consists a wind turbine model in FAST, a generator model in MATLAB Simulink as presented in Section 2.2. Additionally, a machine learning algorithm for wind speed prediction. These models are interconnected for a co-simulation with loop communications at each time-

step of the simulation.

5.3 Wind profile design and prediction

TurbSim, an open source tool is used to generate the primary wind field used in the simulations. The IEC Kaimal turbulence model is used to generate several wind profiles with different TIL. This study also uses a machine-learning algorithm based on ANFIS to predict the time-series wind speed data. It involves building a fuzzy-based neural network that learns historical wind information and uses it to observe future sequences [9]. Fortunately, high-quality offshore wind profile measurements are now possible using LIDAR technology, which provides a full 3D spatial mapping of the wind field at multiple heights [10]. The time-series prediction represents a model that uses past values to predict future values. Historical time-stamped wind data are entered into the ANFIS structure as inputs, and the predicted future data will be expected as an output. In general, a non-linear autoregressive model represents this prediction, obtained by the following equation:

$$x(k + t) = f[x(k), x(k - 1), x(k - 2), \dots, x(k - n - 1)] \quad (5.1)$$

where, the function f can find the nonlinear relationship of past, present, and future values of the x over a set period t . In this study, the FIS structure is generated using fuzzy c -means clustering. The Gaussian distribution is considered for membership functions. For training the network, 750,000 data samples are obtained from an hour wind simulation, in which 70% of the data points are randomly chosen for training the network and 30% of the data points are used for test and validation. The training and testing results are shown in Figure 5.1.

5.4 Control and operation strategy

In what follows, the control system and different operation strategies will be described. The operation strategies determine the power set-point, which is tracked by the control system.

5.4.1 Control system

The control system developed for this research aims to track the maximum power point as well as time-varying deloaded power set-points, in order to track the grid frequency and wind speed as per the bids offered in the energy and reserve markets. The controller at its base is a field oriented control, as

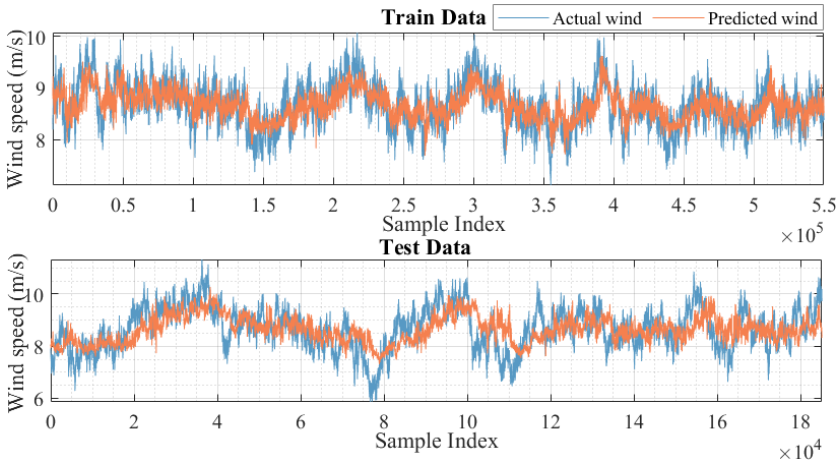


Figure 5.1: Train and test datasets for ANFIS model (60-min).

presented in Section 2.3. The control design is based on the 200 mHz symmetrical ancillary service as defined in Section 1.3. Figure 1.12 shows a graphical representation of this service. The frequency based time-varying reference power P_{ref} is defined in (5.2). For a WPP participating in the reserve market with a bid of P_{RM} must maintain P_{ref} as the sum of base power P_{base} and frequency based power $P_f(t)$. $P_f(t)$ is a time varying quantity proportional to the grid frequency. $P_f(t)$ varies linearly between $-P_{RM}$ and $+P_{RM}$ for the grid frequency of 50.2 Hz and 49.8 Hz respectively. A controller following such service must be capable to follow these downwards and upwards ramps within the specified time. However, for the research presented in this chapter only the frequency range within 49.8 Hz - 50 Hz is considered, as this range requires power up-regulation which is a more complex control implementation.

$$P_{ref} = P_{base} + P_f(t) \tag{5.2}$$

For the operation strategy that uses wind speed to determine the maximum available power, a lookup table based on the power curve of the wind turbine is used. The power curve of the wind turbine is presented in Figure 2.5. For the performance analysis of the controller, a test as presented in Figure 5.2 is simulated. Two cases with a highly turbulent wind speed are simulated. The grid frequency in the two cases is on the margins of the 200 mHz symmetrical service, i.e., 49.8 Hz and 50.2 Hz respectively. A 5 MW wind turbine offering 1 MW of FCR for such a service will need to maintain a base power of 4 MW and a ramp-up and ramp-down of the

power output within the range of 3-5 MW, based on the grid frequency. The controller shows an efficient performance and the maximum error in both these cases does not exceed 1%.

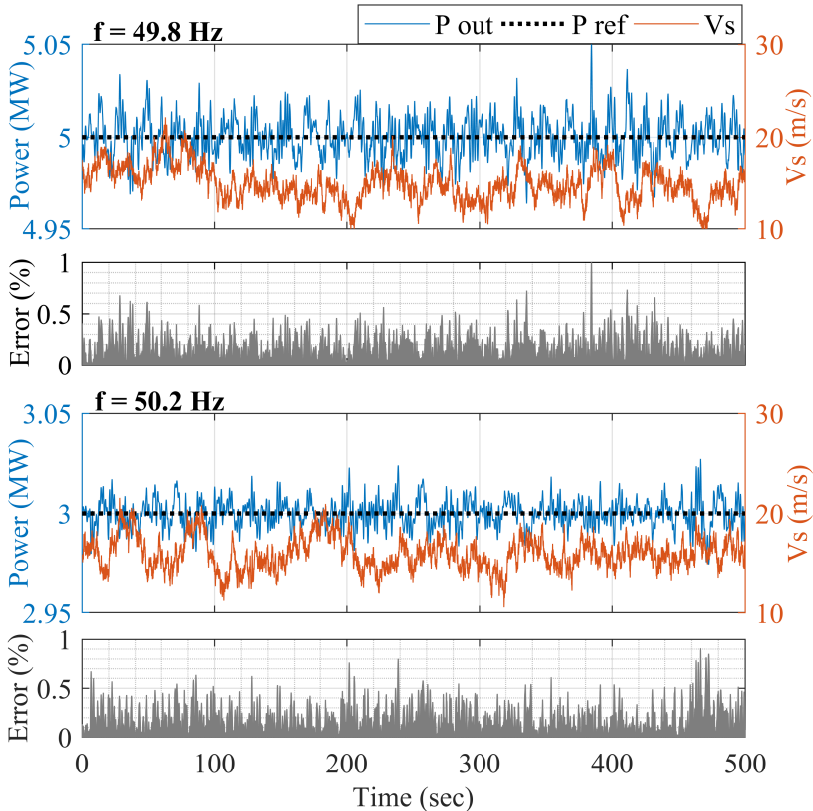


Figure 5.2: Controller performance

5.4.2 Operation strategy

The optimal decisions framework, developed in [11], is considered for the participation of the WPP in JERM. The market incentives in the day-ahead market for energy and reserve floors are 33 €/MWh and 34 €/MW, respectively. Also, the market rate regarding energy imbalance settlement (EIS) for deficit and surplus of generations are, 35 €/MWh and 30 €/MWh, respectively. Finally, the balancing stage penalty rate regarding the unavailability of the offered FCR in real-time is 45 €/MW. The employed decision tool considers wind uncertainty and market incentives to return the opti-

mal share of power assigned to energy and reserve market floors, thereby maximizing the WPP's profit. In this regard, the optimal decisions concerning the day-ahead energy P_{EM} and reserve bids P_{RM} are respectively, 0.5 MWh and 1.78 MW. Hence, the fixed day-ahead revenue of WPP in the day-ahead energy and reserve market is € 16.49 and € 60.72, respectively. Additionally, the employed decision tool considers financial compensations regarding real-time energy and reserve power bids deviations.

In Figure 5.3, three operation strategies are introduced to evaluate the effectiveness of the proposed control system. Notably, the evaluation is performed based on wind speed profiles with medium and high TIL (5% and 10%, respectively), for a duration of 1 hour. At first, an illustrative case, using two wind profiles, is presented to observe the advantages of the proposed method.

5.4.2.1 Operation strategy 1

Operation Strategy 1 (OS-1) uses an advanced control strategy where the reference power of the control system is not only based on system frequency and the day-ahead optimal bids but also based on the actual wind speed. This ideal strategy assumes that the real-time wind speed is known. Therefore, the control is designed such that if the maximum available power P_{max} in the wind is greater than P_{RM} , the reference power P_{ref} is equivalent to $P_{max} - P_{RM}$. Whereas, if P_{max} is less than P_{RM} , P_{ref} is maintained at 0. In this way, the reserve market bid is given priority.

5.4.2.2 Operation strategy 2

Operation Strategy 2 (OS-2) is a naive strategy which merely employs a static reference power along with system frequency to adjust the wind turbine's output so as to maintain the scheduled reserve capacity margin. The controller is designed to linearly operate to generate P_{ref} equal to set-points 2.28 MW and 0.5 MW for the two frequency cases of 49.8 Hz and 50 Hz, respectively. The wind dynamics are disregarded in this strategy. These fixed set-points correspond to the power quantities regarding the energy and reserve markets obtained by the optimal decision tool.

5.4.2.3 Operation strategy 3

Operation Strategy 3 (OS-3) is an operable implementation of the advanced variable reference control strategy based on a predicted wind speed and the day-ahead optimal bids. Since the actual wind speed for the next time-step is unknown to the control system, in order to implement OS-1, a prediction

of wind speed at the next time-step is required. Therefore, in OS-3, a prediction model cfr. § 5.3, is utilized to predict the wind speed. P_{ref} , in this strategy is determined using both, real wind V_{real} and predicted wind V_{pred} values such that the upper bound of P_{ref} is limited by V_{real} based P_{max} . To implement this, V_{pred} is compared to V_{real} at each time-step. If V_{pred} is greater than V_{real} , then P_{ref} is based on V_{real} . Else, P_{ref} is based on V_{pred} .

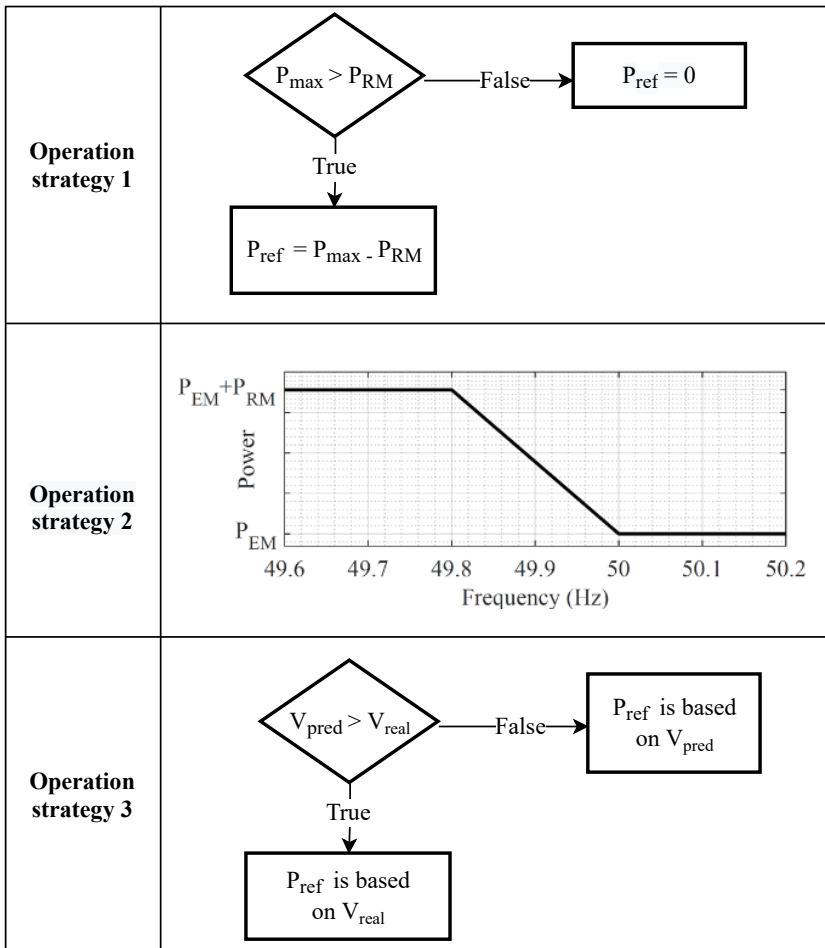


Figure 5.3: Operation strategies

5.5 Results

5.5.1 Illustrative example

Figure 5.4 shows the real-time power submitted to the energy-only market (blue lines). In this case, the system frequency during the 1-hour dynamical ex-post simulation is set to 50 Hz, thus the reserve capacity is not activated. On the other hand, the red lines show the wind turbine output power for a system frequency below 49.8 Hz. In this case, the output power is the summation of the activated reserve capacity and the power submitted to the energy market. Importantly, the area between these 2 curves shows the power that is potentially kept as reserve capacity. Figure 5.4 (a) - (b) shows the harvested wind power using the ideal strategy, OS-1, for wind profiles with both 5% and 10% TIL. The average output power to the energy market for 5% and 10% TIL is respectively, 0.438 MW and 0.545 MW. Moreover, the wind turbine's mean output power for full reserve power activation is 2.215 MW and 2.261 MW, respectively. This can be interpreted as leaving a capacity margin of 1.778 MW and 1.716 MW regarding the 5% and 10% TIL. With this approach, WPP can stay around its submitted day-ahead energy and reserve bids in real-time. The naive strategy, OS-2, submits an average power of 0.5 MW to the energy market regardless of the TIL. Also, the total average submitted power to the network when the reserve is fully activated for TIL 5% and 10% is, respectively, 2.116 MW and 2.010 MW. Thus, the maintained mean capacity margin is 1.616 MW and 1.510 MW for the medium and high TILs, respectively. Note that, as seen in Figure 5.4 (c) - (d), while the average area between the two curves is still fairly close to P_{RM} , there are several periods with power deficits concerning the scheduled reserve power. On the other hand, as seen in Figure 5.4 (e), the total power submitted to the energy market using the proposed strategy, OS-3, is 0.418 MW and 0.447 MW, for 5% and 10% TIL, respectively. Also, as shown Figure 5.4 (f), for a system frequency less than 49.8 Hz, OS-3, returns a mean output power of 2.108 MW and 2.033 MW for TIL of 5% and 10%, respectively. It means that OS-3, on average, is able to keep a reserve capacity of 1.5861 MW and 1.6896 MW concerning the wind profiles with 5% and 10% TIL, respectively. Remarkably, while the average reserve power in OS-3 is lower than the naive strategy, OS-2, the periods with a high deficit of reserve power availability are lower than OS-2 (this is seen in Figure 5.4 (c) - (d) and is further verified in the next subsection by comparing the real-time market penalties). Accordingly, the average reserve capacity margin kept in real-time, and well as the average submitted power to the energy market is not only close to the day-ahead bids, but also similar to the one obtained by the ideal strategy, OS-1 as compared to OS-2.

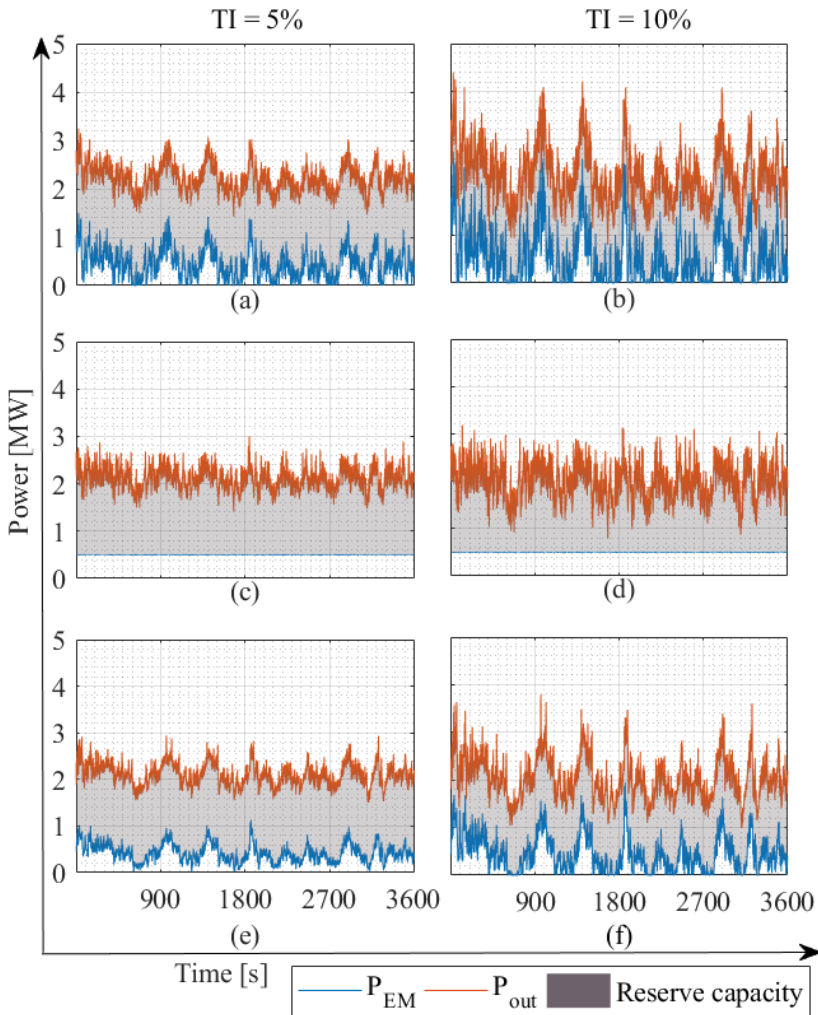


Figure 5.4: Power outputs and reserve margin

5.5.2 Out-of-sample analysis

While observing the overall effectiveness of the proposed control strategy using the illustrative example, an out-of-sample analysis is performed (see Table 5.1). In this way, we are able to correctly evaluate the advantages of the proposed control strategy with respect to the expected in-sample results (obtained by the bidding model as reported in the last column of Table 5.1) and other strategies. The expected market revenue streams, i.e., contribu-

Table 5.1: Revenue (€)

	OS-1		OS-2		OS-3		Expected
	5%	10%	5%	10%	5%	10%	
TI	5%	10%	5%	10%	5%	10%	-
Π^{E+}	0	2.02	0	0	0	0.2	3.69
Π^{E-}	-2.17	-0.78	0	0	-2.86	-2.08	-5.85
Π^{R-}	-2.13	-5.97	-9.1028	-14.69	-4.759	-9.628	-0.57
Π	72.91	72.48	68.10	62.52	69.591	65.702	74.49

tion regarding EIS for deficit Π^{E-} and surplus Π^{E+} of generation, as well as the balancing stage penalty Π^{R-} , will be compared to three operation strategies in order to evaluate their performance. As seen in Table 5.1, the penalty paid by WPP using the ideal control strategy, OS-1, is close to the expected revenue streams. Specifically, in this case, the total revenue of the WPP (Π) for 5% and 10% TILs are, respectively, € 72.91 and € 72.48 (which is close to the corresponding expected value € 74.49). On the other hand, the naive model, OS-2, is unable to provide the reserve power for many periods, thus paying a high penalty at the balancing stage (i.e., € -9.1028 and € -14.69 regarding 5% and 10% TIL, respectively). Therefore, the overall revenue is greatly lower than the expected values (€ 68.10 and € 62.52 respectively, for TIL of 10% and 5%). Finally, it is seen that the total revenue obtained by the practical realization of the ideal strategy, OS-3, acquires a higher profit than the OS-2 (i.e., € 69.591 and € 65.702 for 5% and 10% TILs). That is since the penalty paid by WPP due to the inability to activate the committed reserve is lower than OS-2.

5.6 Conclusion

An operation strategy is developed that allows WPPs to participate in the JERM. The proposed control strategy not only takes system frequency and scheduled bids as input but also predicts the wind speed of the next time-step to properly adjust the reference power, thus providing the reserve power. The controller is validated with an efficient performance for several cases with varying level of TILs. The effectiveness of the proposed control strategy is also validated ex-post, based on the optimal WPP bidding decisions.

References

- [1] N. Singh et al., "Prediction-based wind turbine operation for active participation in the day-ahead and reserve markets," in 2022 IEEE Power & Energy Society General Meeting (PESGM), Denver, Colorado, 2022.
- [2] Hosseini, S. A.; Toubeau, J.-F.; Singh, N.; De Kooning, J. D. M.; Kayedpour, N.; Crevecoeur, G.; De Grève, Z.; Vallée, ; Vandeveldel, L.: 'Impact of fast wind fluctuations on the profit of a wind power producer jointly trading in energy and reserve market', IET Conference Proceedings, 2021, DOI: 10.1049/icp.2021.1386.
- [3] N. Singh, J. D. M. De Kooning and L. Vandeveldel, "Simulation of the Primary Frequency Control Pre-Qualification Test for a 5MW Wind Turbine," 2020 IEEE/PES Transmission and Distribution Conference and Exposition (T&D), 2020, doi: 10.1109/TD39804.2020.9299921.
- [4] S. Li, T. A. Haskew, R. P. Swatloski and W. Gathings, "Optimal and Direct-Current Vector Control of Direct-Driven PMSG Wind Turbines," in IEEE Transactions on Power Electronics, May 2012
- [5] X. Zeng, T. Liu, S. Wang, Y. Dong and Z. Chen, "Comprehensive Coordinated Control Strategy of PMSG-Based Wind Turbine for Providing Frequency Regulation Services," in IEEE Access, 2019.
- [6] Z. Zhang, Y. Zhao, W. Qiao and L. Qu, "A Discrete-Time Direct Torque Control for Direct-Drive PMSG-Based Wind Energy Conversion Systems," in IEEE Transactions on Industry Applications. 2015.
- [7] Y. Inoue, S. Morimoto and M. Sanada, "Control method for direct torque controlled PMSG in wind power generation system," 2009 IEEE International Electric Machines and Drives Conference, 2009, doi: 10.1109/IEMDC.2009.5075360.
- [8] Abdolghani, Nazanin, Jafar Milimonfared and Gevork Babamalek Gharehpetian. "A Direct Torque Control Method for CSC Based PMSG Wind Energy Conversion Systems." Renewable energy & power quality journal (2012).
- [9] Khosravi, Ali, Luiz Machado, and R. O. Nunes. "Time-series prediction of wind speed using machine learning algorithms: A case study Osorio wind farm, Brazil." Applied Energy (2018).

- [10] Mikkelsen, Torben, et al. "A spinner-integrated wind lidar for enhanced wind turbine control." *Wind Energy* (2013).
- [11] Seyyed Ahmad Hosseini, Jean-François Toubreau, Zacharie De Grève, François Vallée, An advanced day-ahead bidding strategy for wind power producers considering confidence level on the real-time reserve provision, *Applied Energy*, <https://doi.org/10.1016/j.apenergy.2020.115973>.

6

Wind Turbine Load Aware Operation

In Chapter 4, it was established that the provision of ancillary services impact the load and lifetime of the wind turbine main bearing. The study presented in this chapter takes all the major loads on the wind turbine into account. This loading on different parts of the wind turbine can possibly result in sub-optimal performance leading to a reduced net power output or even a faster degradation of the wind turbine. On the other hand, no or low participation of a wind turbine in ancillary services market will lead to a lesser revenue on a long term. Moreover, low participation of wind turbines in the ancillary market will eventually limit the amount of wind power, since the ancillary services are needed to stabilise the grid and must then be provided by other energy sources. Addressing this challenge requires a holistic method to gauge both load and revenue for wind power producers (WPP), thus enabling them to make informed decisions. This study firstly presents a method of calculating major loads on the wind turbine. Then, a load-aware optimisation method of wind power scheduling in JERM is proposed that provides WPPs, an ability to strike a balance between revenue and the physical loading of wind turbine.

The rest of this chapter is organised as follows: Section 6.1 presents an introduction to the study. Section 6.2 describes

the model and data used in this study. Section 6.3 presents the methodology used to calculate the loads on the wind turbine as well as the optimisation strategy. In Section 6.4, results from this study are discussed. The conclusion of this study is derived in Section 6.5.

6.1 Introduction

The participation of wind farms in JERM is a lucrative avenue for the WPPs. Studies point to an increase in the revenue of WPPs as a result of participating in the ancillary service market. A study exploring the advanced bidding strategy dedicated to optimal dispatch of WPP in the JERM is presented in [1]. The revenue generated using this technique has shown an increase in the revenue of WPP. A data-driven probabilistic energy and reserve bidding approach for wind turbines participating in reserve market has also concluded similar results [2].

Although the ancillary services market is a lucrative avenue for the WPPs, the physical loading of the wind turbine may be affected by these control techniques. There has been some research regarding the physical loading of the wind turbine. The impact of loads on composite wind turbine blades is studied in [3]. Loads on wind turbine blades are studied by using finite element analysis in [4]. Load identification of a wind turbine tower using Kalman filtering techniques is presented in [5]. Dynamic analysis of offshore wind turbine tower subjected to wind and wave loading is shown in [6]. There are also studies that explore the global physical loading of the wind turbine [7], [8] and [9]. Amidst all these studies, there exists limited literature on the effect of ancillary services provision on the loading of the wind turbine components. A study presented in [10] studies the effect of such loading although it is confined to the main bearings of the wind turbine. Wind turbines face a range of issues during their operation such as malfunctioning components, misalignment of bearings, unbalanced rotor, blade erosion and icing, etc. to name a few. There is a need to quantify the overall major loads on a wind turbine and moreover to study the impact of ancillary service provision on these loads.

To this end, this study proposes a load-aware optimisation method of wind power bidding in the JERM. The purpose of the developed method is not only to maximise the profit of the WPP but also to create an optimal balance between the net market revenue and the physical loads on the wind turbine. Firstly, a methodology is developed to calculate the physical loading on different components of the wind turbine, namely, the main bearing, the blades, the shaft and the tower. These loads are calculated for different reserve market bids. These loads are then used as an input into an optimisation problem that generates energy and reserve market bids for profit maximisation of the WPP while taking into account the wind turbine loading.

This chapter is organised as follows: Section 6.2 describes the model and data used in this study. Section 6.3 presents the methodology used to

calculate the loads on the wind turbine as well as the optimisation strategy. In Section 6.4, results from this study are discussed. The conclusion of this study is derived in Section 6.5.

6.2 Models and data

The models used in the study include the wind turbine, the permanent magnet synchronous generator and the control systems used for torque and pitch control of the wind turbine. These models are as presented in Section 2.2 and Section 2.3. The torque and pitch control design used for this study are as presented in Section 2.3. The wind data used for the simulations in this research work are generated by using TurbSim [11]. The mean wind speed is 6 m/s with a turbulence intensity of 5 %, as presented in Figure 6.1.

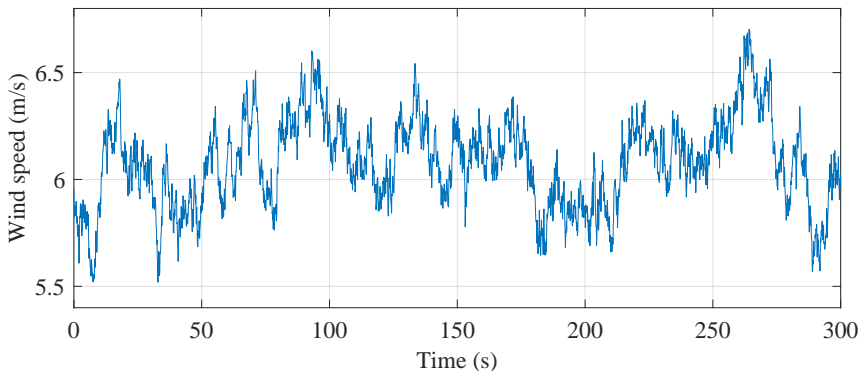


Figure 6.1: Wind profile used for the simulations

6.3 Methodology

The methodology used in this study is developed for a wind turbine participating in JERM, where bids are submitted day-ahead for energy and reserve markets by the WPP. The methodology is outlined in Figure 6.2.

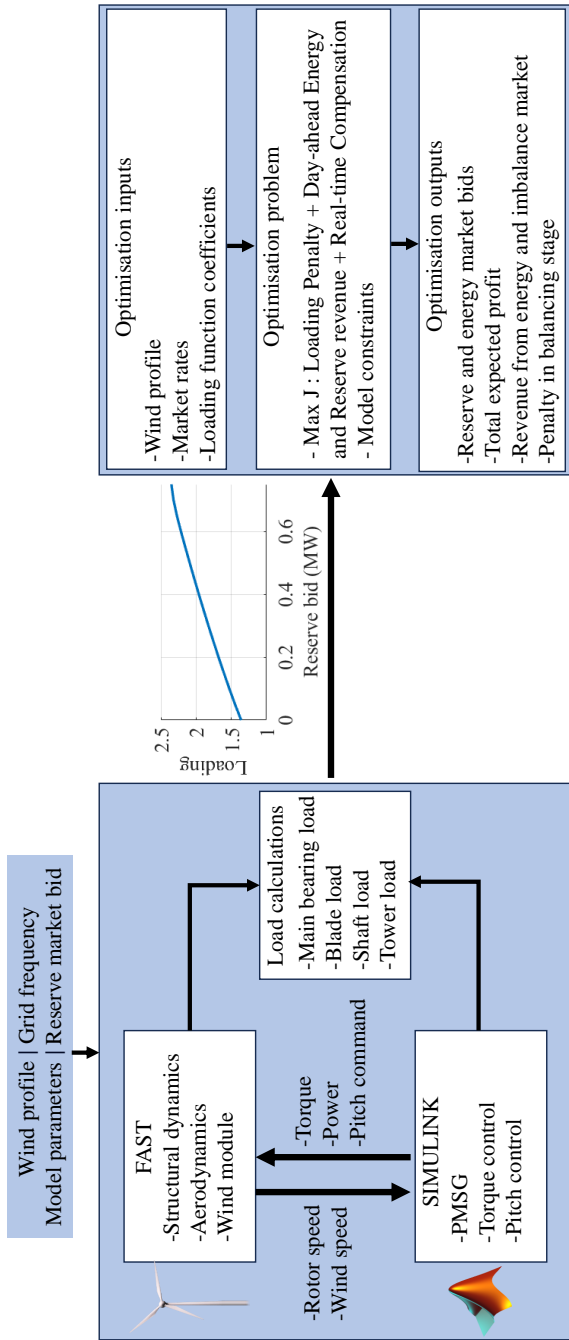


Figure 6.2: Methodology

With the inputs of wind profile, grid frequency, model parameters and the reserve market bid, software-in-the-loop simulations are performed to calculate the loads on different sections of the wind turbine. As an output from these simulations a mapping between the reserve bid and total loading is achieved. Incorporating the derived loading map as a penalty term into the WPP's scheduling objective function, our proposed model strategically optimizes the WPP profit while mitigating wind turbine loads. The optimal decision variables of the model yield reserve and energy market bids. Additionally, the revenues and real-time compensations are also calculated. The following subsections present the calculation methods in detail.

6.3.1 Load calculation

The total load on the wind turbine, referred to as L consists of 4 different loads. The *RMS* values of these loads from simulations for a time period of 300 s for each case are used. These loads associated with the main bearing, blades, shaft and the tower are presented in the following subsections.

6.3.1.1 Bearing load

The bearing load calculations are performed based on the method presented in [10]. The forces acting on the main bearing of the wind turbine are, axial force F_a (in N), lateral force F_v and vertical force F_l . Figure 6.3 shows these three forces acting on the wind turbine. F_a is calculated as the average of the 3 blade root forces F_{b1} , F_{b2} and F_{b3} as in (6.1). The radial force F_r (in N) is calculated using F_l and F_v as in (6.2). The root mean square (RMS) of the two forces are then used to calculate the dynamic equivalent force L_{br} acting on the main bearing as in (6.3). Here, t and T represent the time variable and the total duration of the simulation, respectively. b_x and b_y are dimensionless empirical factors for load calculations in a spherical roller bearing.

$$F_a = \frac{F_{b1} + F_{b2} + F_{b3}}{3} \quad (6.1)$$

$$F_r = \sqrt{F_l^2 + F_v^2} \quad (6.2)$$

$$L_{br} = \sqrt{\frac{1}{T} \int_0^T [b_x F_r(t) + b_y F_a(t)]^2 dt} \quad (6.3)$$

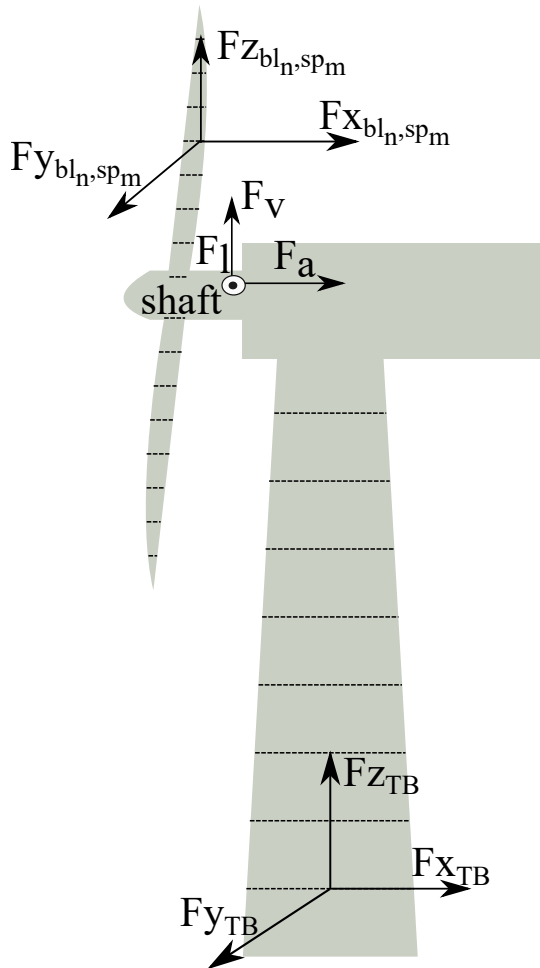


Figure 6.3: Forces acting on the wind turbine

6.3.1.2 Blade load

In the wind turbine model used for the simulations, each of the three blades are divided into 9 spans along the length of the blade. Each of these spans are subjected to forces directed along x, y and z axis. These forces and the division of the wind turbine blade in 9 spans is represented in Figure 6.3. The equivalent of the 3 forces on each span is calculated as per (6.4), where n is the number of blade (from 1 to 3) and m is the number of the span (from 1 to 9). The total blade load L_{bl} is then calculated as the RMS of the individual forces on each span of each blade as in (6.5). Note that the time

dependence (t) is omitted to not overload the equations.

$$F_{bl_n,sp_m} = \sqrt{Fx_{bl_n,sp_m}^2 + Fy_{bl_n,sp_m}^2 + Fz_{bl_n,sp_m}^2} \quad (6.4)$$

$$L_{bl} = \sqrt{\frac{1}{T} \int_0^T \left(\sum_{m=1}^9 F_{bl_1,sp_m} + F_{bl_2,sp_m} + F_{bl_3,sp_m} \right)^2 dt} \quad (6.5)$$

6.3.1.3 Shaft load

The shaft load comprises of rotating shaft bending moment at the shaft's strain gauge along y and z axis (in Nm). The bending moments are then divided by the distance from rotor apex to calculate the two equivalent forces Fy_{sh} and Fz_{sh} (in N) along y and z axis, respectively. These coordinates follow the similar plane as F_l and F_v , as shown in Figure 6.3. Finally, the total shaft load L_{sh} is calculated using the RMS of the equivalent forces as shown in (6.6).

$$L_{sh} = \sqrt{\frac{1}{T} \int_0^T [Fy_{sh}^2(t) + Fz_{sh}^2(t)] dt} \quad (6.6)$$

6.3.1.4 Tower load

The tower loads are divided into two categories, the loads associated with the main structure of the tower L_{TM} and the loads at the base of the tower L_{TB} . For the calculation of L_{TM} , the tower is divided into 9 sections. Each section of the tower is subjected to forces Fx_{TM} , Fy_{TM} and Fz_{TM} along x, y and z axis, respectively. The section of the wind turbine tower and associated forces are presented in Figure 6.3. The equivalent force at each of the sections is calculated as in (6.7), where k represents the section of the tower from 1 to 9. L_{TM} is then calculated as the sum of loads on each of the section as in (6.8). The tower base loads Fx_{TB} , Fy_{TB} and Fz_{TB} (in N) are directed along x, y and z axis respectively. The equivalent load on the tower base, L_{TB} is calculated as in (6.9). Finally, the total tower load L_{twr} is calculated as the sum of tower main and base loads as in (6.10).

$$L_{TM}(k) = \sqrt{Fx_{TM}^2(k) + Fy_{TM}^2(k) + Fz_{TM}^2(k)} \quad (6.7)$$

$$L_{TM} = \sqrt{\frac{1}{T} \int_0^T \left(\sum_{k=1}^9 L_{TM}(k, t) \right)^2 dt} \quad (6.8)$$

$$L_{TB} = \sqrt{\frac{1}{T} \int_0^T \left[Fx_{TB}^2(t) + Fy_{TB}^2(t) + Fz_{TB}^2(t) \right] dt} \quad (6.9)$$

$$L_{twr} = L_{TM} + L_{TB} \quad (6.10)$$

6.3.1.5 Equivalent load metric

The equivalent load metric, L is calculated as weighted sum of the four individually calculated loads as in (6.11). Here L does not symbolise the physical load on the wind turbine quantitatively. Rather, the physical loading is converted into a cost term L as equivalent load metric using the weight factors a , b , c and d . To determine the values of these weight factors, informed by their economic implications, a base case simulation is conducted over a duration of 3000 s. The weight factors based on the base case are setup such that each individual term on the right hand side of (6.11) is equivalent to 0.25. Hence, making the base value of L equal to 1. This arbitrary choice is made to demonstrate the functioning of the methodology. However, these are adjustable factors and can be tuned by the wind farm operator based on the economic costs associated with each of these components.

$$L = aL_{br} + bL_{bl} + cL_{sh} + dL_{twr} \quad (6.11)$$

6.3.2 Optimisation

The optimisation strategy presented in [1] proposed a wind power scheduling framework that accounts for the revenue stream from both day ahead and real-time stages of the energy and reserve markets. However, in this strategy the loads acting on the wind turbine due to the optimal bids in JERM are not accounted for. For this study, the optimisation strategy has been improved to include the effect of wind turbine loading. The optimisation is performed in Matlab, using the Gurobi optimiser [12]. Based on the optimisation, optimal decisions are made to maximise the revenue of the WPP while taking the wind turbine physical loading into account. The objective function is stated in (6.12). Here, L as defined in (6.11) is the factor based on the mapping generated from the load calculations. The day-ahead bids related to the energy and reserve markets are, respectively, shown by Em_{bid} and Rm_{bid} . α is a dimensionless variable weight factor associated with the load L . λ_{sp} and λ_{cap} are the spot market and the reserve capacity prices, respectively. λ_{BU} and λ_{BD} are imbalance prices for surplus and

deficit, respectively. λ_{cp} is the unavailability penalty price for the reserve. π_ω is the probability of occurrence of the scenario. δ_t is the market time unit equal to 1 hour. Ω/ω represents the scenario index/set. $\Delta P_{u\omega}$, $\Delta P_{d\omega}$ are the positive and negative deviation of injected power at scenario ω . $\Delta R_{d\omega}$ is the deviation of available capacity margin from the offered bid at scenario ω .

$$J = -\alpha L + \lambda_{sp} E m_{bid} \Delta_t + \lambda_{cap} R m_{bid} + \sum_{\omega \in \Omega} \pi_\omega \{ \Delta_t (\lambda_{BU} \Delta P_{u\omega} - \lambda_{BD} \Delta P_{d\omega} - \lambda_{cp} \Delta R_{d\omega}) \} \quad (6.12)$$

The loading constraint used for the optimisation is shown in the following equation. This constraint takes into account the impact of increasing $R m_{bid}$ on the overall loading of the wind turbine. The choice of using only reserve market bid is based on the fact that the most influential factor of the wind turbine loading is the amount of reserve power provided since it has to be injected to the network dynamically thus affecting the load on the wind turbine. The values of p_1 and p_2 are calculated as shown in (6.14) and (6.15).

$$L = p_1 R m_{bid} + p_2 \quad (6.13)$$

$$p_1 = \frac{n \sum_{i=1}^n (R m_{bid_i} L_i) - (\sum_{i=1}^n R m_{bid_i}) (\sum_{i=1}^n L_i)}{n \sum_{i=1}^n R m_{bid_i}^2 - (\sum_{i=1}^n R m_{bid_i})^2} \quad (6.14)$$

$$p_2 = \frac{\sum_{i=1}^n L_i - p_1 \sum_{i=1}^n R m_{bid_i}}{n} \quad (6.15)$$

The other constraints associated with the optimisation are listed in the following equations. Here, Q_c is the amount of the offered bids for the day-ahead market. P_ω , R_ω and Q_ω are the delivered power to the energy market, available reserve power and the total available wind power at scenario ω . M is a large positive constant for mixed integer programming. δ is the binary variable associated with the sufficient power capacity.

$$Em_{bid} + Rm_{bid} = Q_c \quad (6.16)$$

$$P_\omega + R_\omega = Q_\omega \quad (6.17)$$

$$Em_{bid} - P_\omega = \Delta P_{d\omega} - \Delta P_{u\omega} \quad (6.18)$$

$$Rm_{bid} - R_\omega \leq \Delta R_{d\omega} \quad (6.19)$$

$$Q_\omega - Rm_{bid} - M\delta \leq 0 \quad (6.20)$$

$$Q_\omega - Rm_{bid} + M(1 - \delta) \geq 0 \quad (6.21)$$

$$R_\omega \leq Rm_{bid} \quad (6.22)$$

$$R_\omega \leq Q_\omega \quad (6.23)$$

$$R_\omega \geq Rm_{bid} - M(1 - \delta) \quad (6.24)$$

$$R_\omega \geq Q_\omega - M\delta \quad (6.25)$$

6.3.3 Revenue calculation

The revenue calculations for a wind turbine participating in JERM are presented in this section. The total revenue consists of energy and reserve market revenues. All the revenue calculations are performed for a duration of 1 hour. The combined revenue from energy market and imbalance settlement, R_{EI} is calculated as shown in the following equation. It accounts for the spot market price, the optimal reserve power bid, the positive and negative deviations of injected power and the respective imbalance prices for surplus and deficit.

$$R_{EI} = \lambda_{sp} Em_{bid} \Delta t + \sum_{\omega \in \Omega} \pi_\omega \Delta t (\lambda_{BU} \Delta P_{u\omega} - \lambda_{BD} \Delta P_{d\omega}) \quad (6.26)$$

The revenue generated by WPP in the day-ahead reserve market, R_{DR} is determined by multiplying the reserve capacity price by the optimal reserve power bid, as shown in the following equation.

$$R_{DR} = \lambda_{cap} Rm_{bid} \quad (6.27)$$

The following equation uses unavailability penalty price for the reserve and deviation of available capacity margin from the offered bid to calculate R_{PB} , the penalty incurred by WPP during the balancing stage.

$$R_{PB} = \sum_{\omega \in \Omega} \pi_\omega \Delta t (-\lambda_{cp} \Delta R_{d\omega}) \quad (6.28)$$

The total revenue from participating in the reserve market and balancing stage, R_{RB} encompasses both the reserve capacity price and penalties. It

takes into account the optimal reserve power bid, the unavailability penalty price, and the deviation of available capacity margin from the offered bid.

$$R_{RB} = \lambda_{cap} R_{m_{bid}} + \sum_{\omega \in \Omega} \pi_{\omega} \Delta_t (-\lambda_{cp} \Delta R_{d\omega}) \quad (6.29)$$

The overall profit R is the sum of various revenue components, including revenue from the energy market, reserve market, and imbalance settlement as shown in the following equation.

$$R = \lambda_{sp} E_{m_{bid}} \Delta_t + \lambda_{cap} R_{m_{bid}} + \sum_{\omega \in \Omega} \pi_{\omega} \Delta_t (\lambda_{BU} \Delta P_{u\omega} - \lambda_{BD} \Delta P_{d\omega} - \lambda_{cp} \Delta R_{d\omega}) \quad (6.30)$$

6.4 Results and discussion

A first set of simulations are performed to find a mapping function between the reserve market bid and the loading of the wind turbine. The reserve bid is varied in the range of 0 MW to 0.75 MW in steps of 0.05 MW. These simulations are performed with a 6 m/s wind profile with 5 % turbulence as shown in Section 6.2. The other inputs to the coupled model of wind turbine and generator are, grid frequency, model parameters and the reserve market bid, as presented in Figure 6.2. For each of these simulations, the loads on different parts of the wind turbine are analysed. Figure 6.4 shows the forces in the base case which is simulated to define the base values of the weight factors associated with each of the 4 loads, as explained in Section 6.3.1.5. This simulation is performed for a duration of 3000 s. Figure 6.4 (a) and (b) show the axial and radial forces on the wind turbine bearing. Figure 6.4 (c) and (d) show the loads on the span 1 and span 9 of the blade. Figure 6.4 (e) and (f) show the load on shaft along the y and z axis. Figure 6.4 (g) and (h) show the main load and base load of the tower.

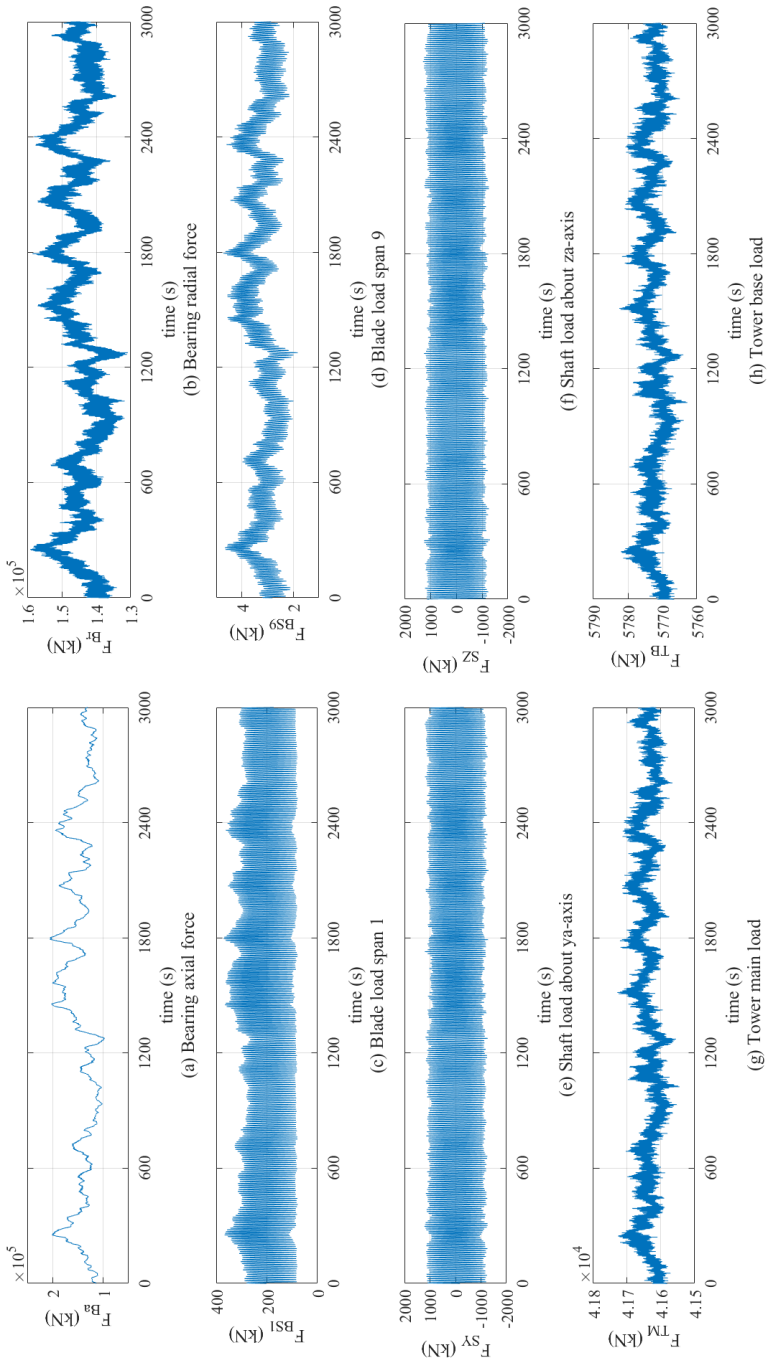


Figure 6.4: Forces acting of different wind turbine components

Table 6.1 presents the results from the simulations in terms of the normalised loading, L_{br} , L_{bl} , L_{sh} , L_{twr} and L representing the bearing, blades, shaft, tower and the total loading respectively. The data in Table 6.1, while demonstrating a clear increasing trend in loading with respect to Rm_{bid} , also reveals a predominantly linear characteristic. This validates our decision to employ linear regression as detailed in Section 6.3.2, through (6.13) - (6.15). As Rm_{bid} increases from 0 to 0.75, there is a noticeable rise in each of the loading terms. L_{br} exhibits a consistent increasing progression with its value increasing from 0.471 for no reserve bid to 1.027 for the highest reserve bid in the range. Similarly, L_{bl} shows a consistent increment from 0.403 to 0.828 as Rm_{bid} increases. In contrast, L_{sh} and L_{twr} demonstrate a relatively marginal increase from 0.236 to 0.246 and 0.25 to 0.251 across the same Rm_{bid} range, respectively. Notably, L_{sh} stabilises from Rm_{bid} value of 0.25 MW onwards. With the maximum influence coming from L_{br} and L_{bl} , L_{total} shows a consistent upward trend. The increased L is due to the increased control action that in turn effects the forces acting on different components of the wind turbine. This dataset establishes the relationship between Rm_{bid} and the corresponding load variations, indicating a trend of load increases with the rise in Rm_{bid} . A corresponding graph between the cumulative L and Rm_{bid} is shown in Figure 6.5.

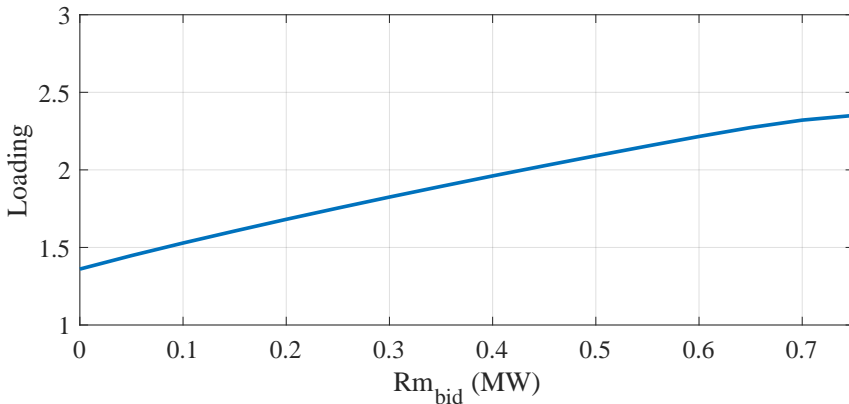


Figure 6.5: Reserve market bid versus Loading

$R_{m_{bid}}$ Loading	0	0.05	0.10	0.15	0.20	0.25	0.30	0.35	0.40	0.45	0.50	0.55	0.60	0.65	0.70	0.75
L_{br}	0.471	0.522	0.568	0.611	0.654	0.695	0.735	0.773	0.811	0.847	0.883	0.918	0.952	0.984	1.010	1.027
L_{bl}	0.403	0.440	0.474	0.507	0.539	0.570	0.601	0.630	0.659	0.687	0.715	0.742	0.769	0.794	0.815	0.828
L_{sh}	0.236	0.236	0.237	0.238	0.238	0.239	0.240	0.241	0.242	0.242	0.243	0.244	0.245	0.245	0.245	0.246
L_{twr}	0.250	0.250	0.250	0.250	0.250	0.251	0.251	0.251	0.251	0.251	0.251	0.251	0.251	0.251	0.251	0.251
L_{total}	1.361	1.447	1.528	1.606	1.681	1.754	1.825	1.894	1.961	2.027	2.091	2.154	2.215	2.273	2.321	2.351

Table 6.1: Normalised loading associated with the changing $R_{m_{bid}}$ [MW]

The next set of simulations are performed by the optimisation model (6.12)-(6.25), to evaluate the optimal market bids in order to balance the wind turbine loads and the WPP's revenue. The values of λ_{sp} , λ_{cap} , λ_{BU} , λ_{BD} and λ_{cp} for revenue related calculations are € 33, € 34, € 30, € 35 and € 45, respectively. In these simulations of a time period of 1 hour each, different scenarios are studied in terms of α , which is the weight factor associated with L . The intent is to analyse the impact of weightage (α) of L on the revenue and the optimised bids. Table 6.2 presents a synopsis of the reserve market bids and expected revenue from JERM. An examination of the data shows the impact of changing α on the optimal bid and various presented revenues. Firstly, it is evident that $R_{m_{bid}}$ decreases with the increasing α . The maximum reserve bid of 0.60 MW is offered when α is zero, which means that the effect of L is not taken into account for the optimisation. As the value of α gradually increases, a decreasing trend is observed in the $R_{m_{bid}}$. Eventually, for α values 75 and higher, the corresponding $R_{m_{bid}}$ is zero.

The revenues associated with each scenario and the total profit are presented in Table 6.2. The revenue from energy market and imbalance settlements, R_{EI} shows proportionate changes to the values of α . The value of R_{EI} rises from € 5.02 to € 24.52, as α increases up to 75. The growth indicates that the increasing values of α positively influence the revenue from energy market. This is because with higher values of α , a greater portion of energy is designated for $E_{m_{bid}}$, while a lower amount is set aside for $R_{m_{bid}}$. This occurs due to the negative term L in the objective function being directly influenced by $R_{m_{bid}}$. Expanding on this, it can be observed that the revenue for the reserve market, R_{RB} is highest for the lower values of α and gradually decreases as the value of α increases. R_{RB} is a combined sum of the revenue in the reserve market R_{DR} and the penalty in balancing stage R_{PB} . R_{DR} is bound with α and thereby by $R_{m_{bid}}$. Similar is the case for R_{PB} . As α grows, the amount of reserve offered reduces. As a result, due to the lower WPP's deviations from the planned capacities, lower penalties are incurred. The overall profit of the wind turbine participation in JERM, the total revenue, R is also presented in Table 6.2. The values of R include the revenues from energy and reserve markets along with the penalties due to the unavailability. It can be seen here that the maximum profit is earned when the value of α is zero, indicating that the impact of loading, L is not taken into account. The least revenue is observed for the higher values of α .

Another key observation is made by identifying the knee point in the data trend. This is achieved by calculating the difference between consecutive data points of $R_{m_{bid}}$ and R . The allocated reserve bid $R_{m_{bid}}$ and

total revenue R , as presented in Table 6.2, pinpoint a knee point at the α value of 75, as illustrated in Figure 6.6 and Figure 6.7. This suggests that decision-makers can prioritize the loading of the wind turbine over a broad range without sacrificing profit, up to an α value of 75. However, if the emphasis on the wind turbine loading becomes significantly pronounced, the rate of change in revenue (or the potential for revenue loss) becomes steeper, rather than gradual. It should be noted that the values presented here are for a single wind turbine, for 1 hour and for a low wind speed scenario. The cumulative difference in the profit for a longer duration and for an entire farm can be highly significant in the interest of WPPs.

α	$R_{m_{bid}}$ [MW]	R_{EI} [€]	R_{RB} [€]	R_{DR} [€]	R_{PB} [€]	R [€]
0	0.60	5.02	20.04	20.29	-0.25	25.06
5	0.59	5.15	19.91	20.15	-0.24	25.06
10	0.59	5.31	19.75	19.97	-0.22	25.06
15	0.58	5.47	19.59	19.78	-0.19	25.06
20	0.57	5.70	19.36	19.53	-0.17	25.06
25	0.57	5.83	19.23	19.38	-0.16	25.05
30	0.56	6.05	19.00	19.14	-0.14	25.05
35	0.56	6.26	18.79	18.91	-0.12	25.05
40	0.55	6.45	18.59	18.70	-0.10	25.05
45	0.54	6.73	18.31	18.40	-0.09	25.04
50	0.53	6.99	18.05	18.12	-0.08	25.04
55	0.52	7.53	17.50	17.55	-0.05	25.02
60	0.49	8.25	16.75	16.79	-0.03	25.01
65	0.46	9.19	15.79	15.81	-0.01	24.98
70	0.44	10.16	14.79	14.80	0.00	24.95
75	0.00	24.52	0.00	0.00	0.00	24.52
80	0.00	24.52	0.00	0.00	0.00	24.52

Table 6.2: Revenues as a function of α

6.5 Conclusion

This study presents a novel method of wind turbine participation in JERM using a load-aware profit maximising approach. A methodology is developed to aggregate the major loads of the wind turbine and present it as a

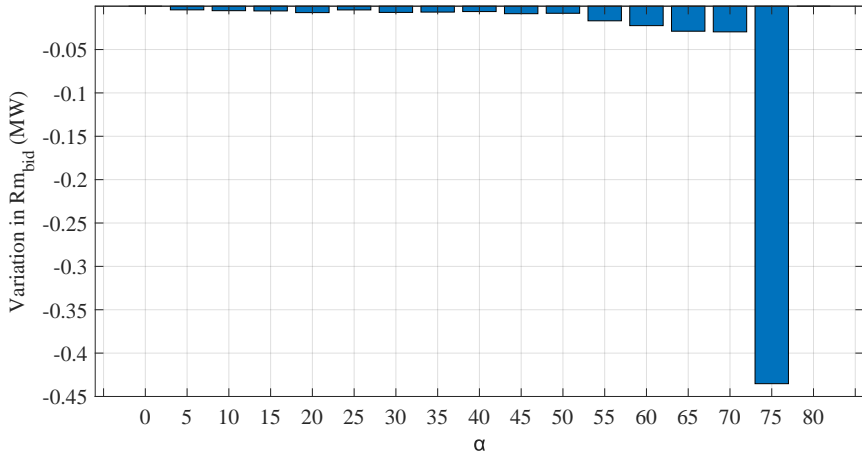


Figure 6.6: Variation in R_{m_bid} with respect to α

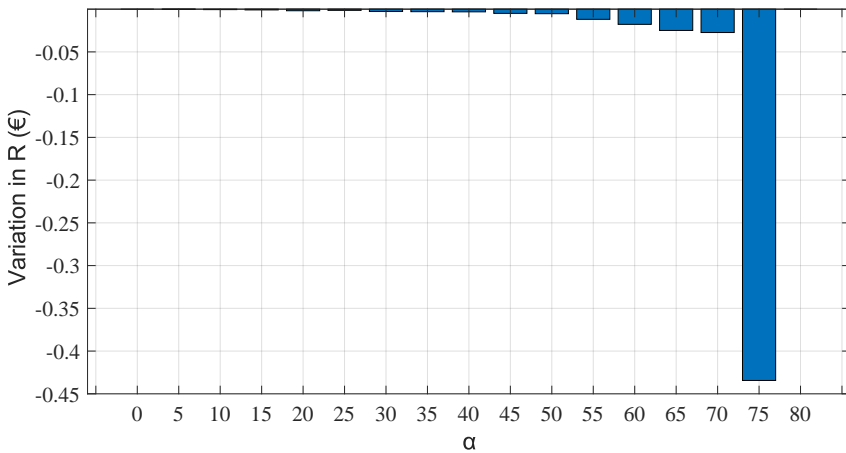


Figure 6.7: Variation in R with respect to α

single unit. The loading factor generated from this methodology acknowledges the loads on the blade, main bearing, shaft and the tower of the wind turbine. The aggregate loading is then used as an input to the optimisation problem that, given the constraints, maximises the WPP's profit while minimising the physical loading of the wind turbine. The results of this study indicate that the physical loading of the wind turbine can be effectively modeled as a function of the reserve bid. It is observed that when considering the wind turbine loading in wind power scheduling, a lower reserve bid is achieved as the loading weight increases. Similarly, as the

loading weight rises, the market revenue decreases. This is because, unlike traditional scheduling models that overlook the wind turbine loading and its hidden costs, our model implicitly accounts for the costs associated with the wind turbine physical health. Another crucial consideration for decision-makers is that the profit and loss remains minimal across a broad range of loading weights before experiencing a significant drop with only a slight change in loading weight. Therefore, decision-makers should identify the knee point in their data, as demonstrated in this study, to ensure a profit that does not compromise turbine health significantly. The weight factors a , b , c and d associated with the loads as defined in the study, provide the WPP a useful tool at their disposal. These factors can be tuned as per the costs and condition of these wind turbine components. Additionally, the factor α associated with the physical loading in the bidding optimisation is an adjustable factor that can be tuned to balance the revenue and the loading as per the requirement of the WPP. In this way the WPPs always have a trade-off option to create a balance between the physical load on the wind turbine and the monetary benefit.

References

- [1] S. A. Hosseini, J. F. Toubeau, Z. De Grève and F. Vallée, "An advanced day-ahead bidding strategy for wind power producers considering confidence level on the real-time reserve provision", Volume 280, 2020, 115973, ISSN 0306-2619, Applied Energy, doi:10.1016/j.apenergy.2020.115973.
- [2] S. A. Hosseini, J. -F. Toubeau, N. Amjady and F. Vallée, "Day-Ahead Wind Power Temporal Distribution Forecasting With High Resolution," in IEEE Transactions on Power Systems, doi: 10.1109/TPWRS.2023.3295915.
- [3] A. S. Verma, J. Y., W. Hu, Z. Jiang, W. Shi and J.J.E. Teuwen, "A review of impact loads on composite wind turbine blades: Impact threats and classification", Renewable and Sustainable Energy Reviews, 2023, doi:10.1016/j.rser.2023.113261.
- [4] R. P. Tavares, V. Bouwman and W. Van Paepegem, "Finite element analysis of wind turbine blades subjected to torsional loads: Shell vs solid elements", Composite Structures, 2022, doi:10.1016/j.compstruct.2021.114905.
- [5] D. Wei, D. Li, T. Jiang, P. Lyu, X. Song, Load identification of a 2.5 MW wind turbine tower using Kalman filtering techniques and BDS data, Engineering Structures, 2023, <https://doi.org/10.1016/j.engstruct.2023.115763>.
- [6] Y. Hu, J. Yang, C. Baniotopoulos, X. Wang and X. Deng, "Dynamic analysis of offshore steel wind turbine towers subjected to wind, wave and current loading during construction", Ocean Engineering, 2020, doi:10.1016/j.oceaneng.2020.108084.
- [7] S. Wang, T. Moan and Z. Gao, "Methodology for global structural load effect analysis of the semi-submersible hull of floating wind turbines under still water, wind, and wave loads", Marine Structures, 2023, doi:10.1016/j.marstruc.2023.103463.
- [8] S. Wang, Y. Xing, R. Balakrishna, W. Shi and X. Xu, "Design, local structural stress, and global dynamic response analysis of a steel semi-submersible hull for a 10-MW floating wind turbine", Engineering Structures, 2023, doi:10.1016/j.engstruct.2023.116474.

-
- [9] N. Beganovic, J. Njiri, and D. Söffker, "Reduction of Structural Loads in Wind Turbines Based on an Adapted Control Strategy Concerning Online Fatigue Damage Evaluation Models," *Energies*, vol. 11, no. 12, p. 3429, Dec. 2018, doi: 10.3390/en11123429.
- [10] N. Singh, D. Boruah, J. D. M. De Kooning, W. De Waele, and L. Vandeveldel, "Impact Assessment of Dynamic Loading Induced by the Provision of Frequency Containment Reserve on the Main Bearing Lifetime of a Wind Turbine," *Energies*, vol. 16, no. 6, p. 2851, Mar. 2023, doi: 10.3390/en16062851.
- [11] 'TubSim'. NREL.
Available at: <https://www.nrel.gov/wind/nwtc/turbsim.html>.
- [12] Gurobi Optimization, LLC. "Gurobi Optimizer Reference Manual," 2023. [Online]. Available: <https://www.gurobi.com>

7

Conclusions & future work

This chapter offers a summary of the conclusions drawn from the preceding individual chapters. Additionally, the discussions concerning potential future extensions and applications derived from this work is presented in the subsequent sections.

7.1 Conclusions

The growth of wind energy in the recent past has been remarkable. Wind turbines have emerged as a clean, cost efficient and environment friendly alternative to the conventional power sources. In the global effort to mitigate greenhouse gases, the role of wind energy is indispensable. Wind energy is advancing its step in major power systems around the world. On the other hand, for the remote areas that face isolation from the power grid, wind power is an excellent solution. In addition to its environmental benefits, the wind energy sector also contributes to the economy by creating jobs.

Despite all the advantages, due to its discontinuous availability, wind energy is considered an intermittent source of energy. Depending on the amount of wind energy in the power mix, this variability leads to fluctuations in the power grid that can potentially cause voltage and frequency deviations effecting the reliability of the power grid. Also, most wind farms currently do not participate in ancillary services provision. Ancillary services such as frequency control, reactive power and voltage control are essential for maintaining a reliable power system. With the growing share of wind energy, the current framework of power system is not feasible. An increased participation of wind energy in the ancillary service market is the need of hour. The advancements in wind forecast have come to an aid, providing the tools to have a more seamless and planned integration of wind energy in the grid. This provides the wind farm owners to have a strong dispatch plan. By offering these ancillary services, wind energy not only provides an overall stability and efficiency to the grid but also opens additional revenue stream for the wind farm owners. This dual role of wind power, as both a clean energy source and a provider of ancillary services is crucial to the green transition towards a more sustainable landscape. The work presented in this dissertation addresses the issues related to ancillary services provision from wind turbines. The research results are as follows:

Chapter-2 is the starting point of the research presented in this thesis. Here, a fast acting, grid frequency following control system is developed. In order to assess the capability the wind turbine to provide frequency support ancillary services, the TSO established pre-qualification test is conducted on the developed control system. Wind profiles with different turbulent intensity are used to evaluate the control system performance in different scenarios. The test was focused on 200 mHz symmetrical FCR service providing frequency support within the grid frequency range of 49.8 Hz-50.2 Hz. The test requires the FCR provider to ramp up and down the power output within a given time range, based on the real-time grid frequency. From the results, it is observed that the control error increases with the turbulence

intensity of the wind. However, the control system is able to follow the pre-qualification test under each of the tested scenarios. The control system served as the foundational control framework that was further developed and used in further studies presented in the following chapters.

In Chapter-3, wake studies are performed to analyse the effect of ancillary services provision on the wake behind a wind turbine. The torque control based system is power regulated to provide FFR and FCR based on 200 mHz symmetrical service. The robust Jensen wake model is used to assess the behaviour of the wake. The results of this study showed the replication of grid frequency in the wake behaviour at several radial and axial points downwind of the wind turbine. The wake behaviour is observed to be varying with the axial and radial distances from the wind turbine. A higher effect is observed at closer points. A clear impact of the changing grid frequency was observed on the wake. It is also observed that the magnitude of frequency support offered by the wind turbine and the slope of the changing grid frequency are also active variables that affect the wake. The results of this study can be useful to optimise the ancillary services participation as well as to design wind farms such that the effect of wakes can be mitigated and maximum power can be derived from the wind farm.

In Chapter-4, the effect of varying load on the lifetime of the main bearing of a wind turbine due to provision of FCR are studied. Main bearing is one of the most important components of the wind turbine and is subjected to varying loads due the changes in wind turbine control actions. The results point to a considerable reduction in lifetime due to the provision of FCR. It is also observed that the impact of FCR provision on the lifetime of the main bearing is subjective to the amount of FCR provided and the C rating of the bearing. Based on this study a higher FCR provision can be suggested for a wind turbine consisting of bearings with higher basic dynamic load rating.

In Chapter-5, an optimisation strategy is developed that allows WPPs to participate in JERM by taking grid frequency, scheduled bids and the wind speed into the account. The study compared the traditional approach of market participation to the proposed strategy. It is observed that the proposed strategy generated higher profit for the WPP.

In Chapter-6, a novel method of wind turbine participation in JERM using a load-aware profit maximising approach is proposed. The developed methodology aggregates all the major loads on the wind turbine such as the blade, the main bearing, the shaft and the tower loads into a single unit. The aggregate loading is then used as an input to the optimisation problem that, given the constraints, maximises the WPP's profit while minimising the physical loading of the wind turbine. The study shows that a wind

turbine's physical loading is linked to the extent of its participation in the reserve market. Increasing the weight of loading in the optimisation algorithm has shown to lower reserve bids, impacting the overall revenue. With the adjustable loading factors, this study has provided a tool for wind farm owners to create a balance between the physical load on the wind turbine and the monetary benefit.

7.2 Future work

The research work presented in this dissertation explores various areas related to ancillary services provision from wind turbine and its resulting effects. This research work makes valuable contributions to enhance a fine integration of wind energy in the power system. The prospective future works that can be built up on the current research are summarised in the following sections.

7.2.1 Wind turbine ageing

As one of the major contributors of energy, wind farms are increasingly participating in the joint day-ahead energy and reserve market (JERM). Here, the wind turbines actively provide ancillary services such as FCR. However, the provision of ancillary services is known to effect the physical loading on a wind turbine. This loading also depends on the age of the wind turbine as the components of a wind turbine gradually wear over time. Due to the ageing, a sub-optimal performance of the wind turbine is observed which is reflected on the net power output of the wind turbine. A study that investigated the ageing issue in 282 wind farms across UK has found that the wind turbines lose around 1.6% of their output each year [1]. Based on this data, the declining power curve of the wind turbine with the age can be estimated as shown in Figure 7.1. It is also feasible to model the power curve into a high-fidelity model. However, care needs to be taken to implement the ageing impact on all the major components of the wind turbine including the blades, the tower, the bearings, the shaft and the generator. These loads also need to be studied for varying participation of wind turbines in JERM. As has been shown in Chapter-6, the loads on the wind turbine are directly effected by the amount of the offered reserved bid.

A primitive model developed in this direction has shown that the *Loading* on a wind turbine, as defined in Chapter-6 is directly effected by the amount of offered reserve market bid. This effect is consistent throughout the lifetime of the wind turbine. Figure 7.2 shows the variation of *Loading* with the increasing amount of reserve market bid.

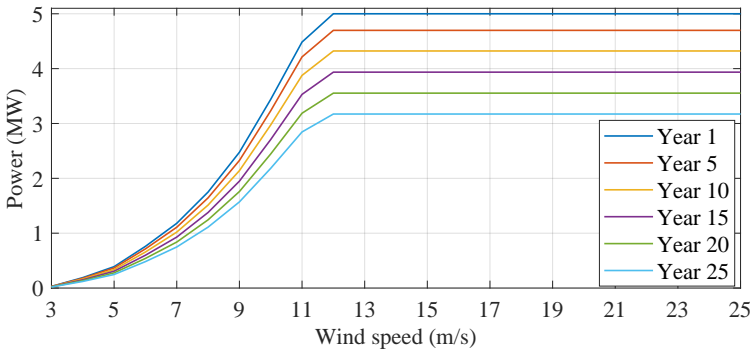


Figure 7.1: Power curve of a 5 MW wind turbine with years

The topic of imminent wind turbine ageing is a pressing issue for wind farms and perhaps the most economically challenging one. A large part of the world’s turbine fleet will come to the end of its operational life over the next 10-15 years [2]. 14 GW of Europe’s existing wind farms are now over 20 years old. Another 38 GW and 78 GW will join them in the next 4 years and 8 years respectively [3]. The existing models of wind turbines can be adapted to accurately simulate the ageing scenarios. The benefits of such models can help the entire wind energy industry. Such models have the potential to be used for realistic performance prediction, maintenance planning, component lifetime assessment, technological improvement and energy forecasting, to name a few. Moreover, these models can be beneficial in development of new wind turbine models as well as in optimising the existing wind turbines operations.

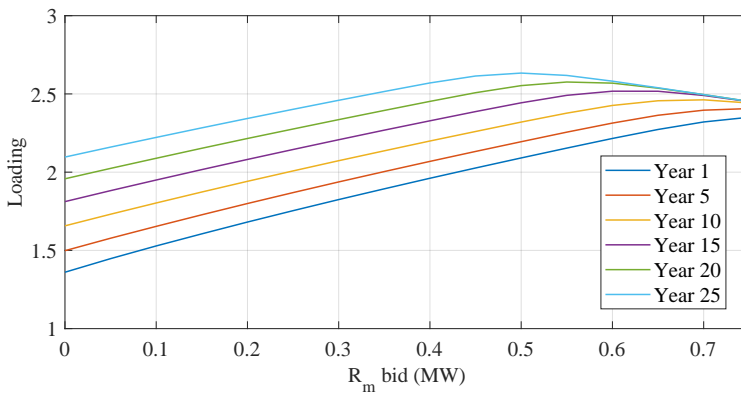


Figure 7.2: Reserve market bid versus Loading

7.2.2 Wind farm load informed reserve dispatch

In Chapter 4 the effects of reserve provision on the main bearing of a wind turbine are studied. In Chapter 6 all the major loads on a wind turbine are studied. From these studies it is concluded that the provision of ancillary services, such as FCR have a clear impact on the loads and lifetime of a wind turbine. A methodology for WPPs to create a balance between the physical load on the wind turbine and the monetary benefit is also presented in the Chapter 6.

In a wind farm, there exist wind turbines with different physical conditions. The physical conditions and the impact of ageing on these wind turbines can be assessed by the means of the studies presented in this dissertation and the ageing method proposed in the previous section. For a wind farm participating in the reserve market, this information can be crucial. By means of an optimisation method, the reserve participation power can be divided amongst the wind turbines of the wind farm. In this manner, the WPP has the informed option to load a wind turbine that has a higher load bearing capacity. Therefore, minimising the physical loads on the more vulnerable wind turbines.

References

- [1] I. Staffell and R. Green, "How does wind farm performance decline with age?", *Renewable Energy*, 2014. Available: 10.1016/j.renene.2013.10.041 [Accessed: 25- Apr- 2023].
- [2] WindEurope's Annual End of Life Issues & Strategies Seminar - EoLIS 2022", *EoLIS 2022*, 2022. [Online]. Available: <https://windeurope.org/eolis2022/>. [Accessed: 25- Apr- 2023].
- [3] WindEurope EoLIS 2021 - End-of-Life Issues & Strategies Seminar, *EoLIS 2021*, 2022. [Online]. Available: <https://windeurope.org/eolis2021/>. [Accessed: 25- Apr- 2023].

Author bibliography

- [1] **N. Singh**, S. A. Hosseini, J. De Kooning and L. Vandeveldel. *Load-aware operation strategy for wind turbines participating in the joint day-ahead energy and reserve market*. Submitted to IEEE Access Sept 2023.
- [2] **N. Singh**, D. Boruah, J. De Kooning, W. De Waele, and L. Vandeveldel. *Impact assessment of dynamic loading induced by the provision of frequency containment reserve on the main bearing lifetime of a wind turbine*. Energies, 2023. doi:10.3390/en16062851.
- [3] **N. Singh**, J. D. De Kooning, and L. Vandeveldel, *Dynamic wake analysis of a wind turbine providing frequency support services*, IET Renewable Power Generation, 2022. doi:10.1049/rpg2.12455
- [4] **N. Singh** et al., *Prediction-based Wind Turbine Operation for Active Participation in the Day-Ahead and Reserve Markets*, 2022 IEEE Power & Energy Society General Meeting (PESGM), Denver, CO, USA, 2022, doi: 10.1109/PESGM48719.2022.9917213.
- [5] **N. Singh**, J. De Kooning and L. Vandeveldel, *Dynamic Wake Analysis of a Wind Turbine Providing Frequency Containment Reserve in High Wind Speeds*, The 9th Renewable Power Generation Conference (RPG Dublin Online 2021), Online Conference, 2021, doi: 10.1049/icp.2021.1364.
- [6] **N. Singh**, J. D. M. De Kooning and L. Vandeveldel, *Simulation of the Primary Frequency Control Pre-Qualification Test for a 5MW Wind Turbine*, 2020 IEEE/PES Transmission and Distribution Conference and Exposition (T&D), Chicago, IL, USA, 2020, doi: 10.1109/TD39804.2020.9299921.
- [7] **N. Singh**, D. Boruah, W. De Waele, J. De Kooning, and L. Vandeveldel, *Impact of the provision of frequency containment reserve on*

- the main bearing lifetime of a wind turbine*. in Flanders Make Scientific Conference 2023, Abstracts, Antwerp, Belgium, 2023.
- [8] A. E. Samani, J. D. De Kooning, N. Kayedpour, **N. Singh**, and L. Vandevelde, *The impact of pitch-to-stall and pitch-to-feather control on the structural loads and the pitch mechanism of a wind turbine*, *Energies*, 2020. doi:10.3390/en13174503
- [9] N. Kayedpour, **N. Singh**, J. D. M. De Kooning, L. Vandevelde and G. Crevecoeur, *An optimal wind farm control strategy for grid frequency support using particle swarm optimization*, 11th International Conference on Renewable Power Generation - Meeting net zero carbon (RPG 2022), Hybrid Conference, London, UK, 2022, doi: 10.1049/icp.2022.1675.
- [10] S. A. Hosseini, J.-F. Toubreau, **N. Singh**, J. D. M. De Kooning, N. Kayedpour, G. Crevecoeur, Z. De Grève, Vallée, L. Vandevelde. *Impact of fast wind fluctuations on the profit of a wind power producer jointly trading in energy and reserve markets*. in The 9th Renewable Power Generation Conference (RPG Dublin Online 2021), Dublin, Ireland (Online), 2021, doi: 10.1049/icp.2021.1386.
- [11] N. Kayedpour, A. Ebneali Samani, **N. Singh**, J. De Kooning, , L. Vandevelde, G. Crevecoeur. *An optimal control strategy to maximize power in an offshore wind farm by reducing wake interaction*. in 16th EAWC PhD seminar on Wind Energy, Proceedings, Porto, 2020.
- [12] N. Kayedpour, **N. Singh**, J. De Kooning, L. Vandevelde, and G. Crevecoeur, *An optimal operational strategy for wind farms*. in Flanders Make Conference on Machines, Vehicles and Production Technology (CMVPT) 2022, Abstracts, Ghent, Belgium, 2022.
- [13] N. Kayedpour, A. Ebneali Samani, S. Asiaban, **N. Singh**, J. De Kooning, L. Vandevelde, and G. Crevecoeur, *Wind turbine anomaly detection using surrogate models*. in 18th EAWC PhD Seminar, Abstracts, Bruges, Belgium, 2022.
- [14] N. Kayedpour, **N. Singh**, A. Ebneali Samani, J. De Kooning, G. Crevecoeur, and L. Vandevelde, *Deep learning time series prediction of wind speed using group method of data handling*. in BERA PhD day on Wind Energy, Abstracts, Ghent, Belgium, 2020.
- [15] N. Kayedpour, **N. Singh**, J. De Kooning, G. Crevecoeur, and L. Vandevelde, *Beowind: offshore wind farms as an ancillary service provider*. in Seanergy 2019: posters, Dunkerque, France, 2019.

In the end, I would like to thank those who financially supported this thesis.

The BEOWIND project funded by the Energy Transition Fund of the Belgian federal government managed by the FPS Economy.





Wind energy supporting the electric power grid.